

# Beyond Poisson-Boltzmann: Strong Correlations and Extreme Confinement in Ionic Fluids

by

Amir Levy

B.Sc., Tel Aviv University (2007)

M.Sc., Tel Aviv University (2013)

Submitted to the Department of Physics  
in partial fulfillment of the requirements for the degree of

Doctor of Philosophy

at the

MASSACHUSETTS INSTITUTE OF TECHNOLOGY

February 2020

© Massachusetts Institute of Technology 2020. All rights reserved.

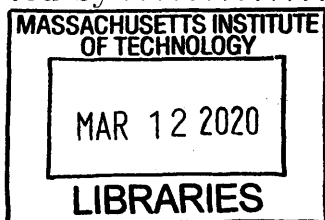
Author ... **Signature redacted** .....  
Department of Physics

.....  
December 11, 2019  
Certified by ..... **Signature redacted** .....  
Martin Z. Bazant

E. G. Roos (1944) Professor and Executive Officer of Chemical  
Engineering  
Professor of Mathematics  
Thesis Supervisor

Certified by ..... **Signature redacted** .....  
Mehran Kardar  
Francis Friedman Professor of Physics  
Thesis Supervisor

Accepted by ..... **Signature redacted** .....  
Negris Mavalvala  
Associate Department Head of Physics



ARCHIVES



77 Massachusetts Avenue  
Cambridge, MA 02139  
<http://libraries.mit.edu/ask>

## **DISCLAIMER NOTICE**

Due to the condition of the original material, there are unavoidable flaws in this reproduction. We have made every effort possible to provide you with the best copy available.

Thank you.

**The images contained in this document are of the best quality available.**



# Beyond Poisson-Boltzmann: Strong Correlations and Extreme Confinement in Ionic Fluids

by

Amir Levy

Submitted to the Department of Physics  
on December 11, 2019, in partial fulfillment of the  
requirements for the degree of  
Doctor of Philosophy

## Abstract

Understanding the electrostatic interactions of ions in the bulk and near electrified surfaces has been a fundamental question in physics for over a century since the "Poisson-Boltzmann" theory was first introduced. In this thesis, we study the bulk properties of ionic fluids in two important cases where the "Poisson-Boltzmann" theory fails: extreme confinement and strong ion-ion interactions.

We first ask how ions behave when confined to a long and narrow tube. Recent advances in nanofabrication technology enabled us to make precise measurements in extremely narrow nanopores and revealed critical gaps in our understanding. A striking result of constraining ions to reside along a line is the exponentially long screening length that easily exceeds the macroscopic length of the pore, leading to *electroneutrality breakdown*. Remarkably, this result has not been reported before, despite its fundamental consequences for ion transport and electrokinetic phenomena. We build a general theoretical framework for electroneutrality breakdown in nanopores and show how it provides an elegant interpretation for the peculiar scaling observed in experimental measurements of ionic conductance in carbon nanotubes.

Strong ion-ion correlations arise when the electrostatic interaction between neighboring ions is comparable to or greater than their thermal energy. This is most pronounced in ionic liquids, highly concentrated solvent-free electrolytes. While generally the Poisson-Boltzmann theory predicts monotonically decaying correlation function, ionic liquids have strong charge ordering and long-ranged charge oscillations. In this work, we show that the charges in ionic liquids are forming the optimal structure that minimizes the electrostatic energy, in the presence of strong positional disorder. We develop an approximated minimization scheme based on the Goemans-Williamson Max-Cut algorithm, adapted for a fully-connected graph with Coulombic interactions. We demonstrate how the persistent layering structure exists due to partial ordering, which is maximized in ionic solids but gradually disappears with added solvent. Eventually, by adding solvent molecules or increasing the temperature, the system departs from its ground state and a mean-field description is more suitable.

Finally, we study the regime of intermediate ionic strength using a non-local per-

mittivity operator, which captures two important effects: ion-ion correlations and solvent structure. Our approach is phenomenological and introduces a small number of fitting parameters. We study the activity coefficients of bulk electrolytes in a wide range of ionic solutions and find that our models capture well the experimental data.

Thesis Supervisor: Martin Z. Bazant

Title: E. G. Roos (1944) Professor and Executive Officer of Chemical Engineering  
Professor of Mathematics

Thesis Supervisor: Mehran Kardar

Title: Francis Friedman Professor of Physics

# Acknowledgments

*“Ben Zoma said: Who is wise? He who learns from every man, as it is said: I have gained understanding from all my teachers”* (Pirkei Avot, Chapter 4, Jewish Oral Law).

My journey in the world of research began a decade ago when I started my Master’s thesis. As I am now approaching the end of my doctoral studies, I want to express my deep gratitude to many women and men I have had the privilege of learning from along the way.

First and foremost, I am extremely thankful to my advisor, professor Martin Z. Bazant. Thank you for giving me the opportunity to join your group. Thank you also for giving me the freedom to navigate the research to areas I found interesting and exciting while having the patience to guide me along the way and instilling in me the confidence that at least some of these ideas will bear fruits. And most of all, thank you for an incredible mentorship. I was particularly amazed by the clarity of your scientific vision and your ability to see the governing principles behind technical derivations. I am truly grateful for the opportunity I have had to learn from you.

I am also grateful to my co-advisor, professor Mehran Kardar. From my first days at MIT, more than 6 years ago, his door was always open for me. His help and understanding were vital for me, especially in my first year, and after returning from a two-year leave. Also, his classes were a true inspiration in physics-teaching for me. His way of conveying physical ideas in elegant and beautiful ways had strengthened my admiration for statistical mechanics and inspired me to become a better teaching assistant. I would also like to thank professor Arup Charabortry and professor Ibrahim Cisse for serving in my committee and proving helpful comments and valuable insights.

I am thankful for having the opportunity to work with professor Alexei A. Kornyshev from Imperial College, London, a long-time collaborator of Professor Bazant. The MIT-MITSI fund supported our collaboration and gave me a unique chance to learn from one of the most prominent scientists in this field. His very close and

hands-on guidance had taught me a lot. I would like to take this opportunity and also extend my appreciation to my Master's thesis advisor, prof. David Andelman. Going to MIT would not have been possible if it were not for your mentorship. Your care and compassion for your students are unparalleled, and your guidance during my first steps in the academic world had shaped me as a researcher.

I was extremely fortunate to be a part of the Bazant group. It is not usual for a physics graduate student, especially one who is interested in theory, to be a part of such a large group and to be consistently surrounded by so many brilliant people. The atmosphere of sharing ideas, collaborating and helping others had made my time at MIT enjoyable. I want to thank Emond (Tingtao) Zhou, a fellow physics student in our group, for being a great source of knowledge for me and the immense help with the General Exams. A special thanks go to Mike McEldrew and Pedro de Souza, who taught me that a theoretical work does not have to be a lonely task. I have learned much from our discussions and brainstorming, and I feel that one of the biggest accomplishments as a student was convincing both of you to collaborate with me and to coauthor our papers. I would also like to thank other friends and colleagues in the group: Dan Cogswell, Mohammad Mirzadeh, Amin Amooie, Tao Gao, Neel Nadkarni, Mohammad Alkhadra, Supratim Das, Dimitrios Fragedakis, Huanhuan Tian, Hongbo Zhao, Fan He, Kameron Conforti, Edwin Sze Lun Khoo, and Arash Sayyah.

I would like to thank my parents for their unconditional love and support in the past 34 years of my life, the past 6 years since I started MIT, and especially for their immense help in the past 4 months since the birth of my twin boys, Yonatan and Itamar.

Finally, to my best friend and the love of my life, Moria, thank you for building a home with me in Boston, and I'm looking forward to many more years of exciting adventures.

# Contents

<b>1</b>	<b>Introduction</b>	<b>21</b>
1.1	Derivation of the PB Equation . . . . .	22
1.2	Extensions to PB Theory . . . . .	24
1.2.1	Finite-size Effects . . . . .	25
1.2.2	Ion-ion Correlations . . . . .	26
1.2.3	Ion-solvent Interactions . . . . .	27
1.3	Electrolyte in Confinement . . . . .	28
1.3.1	A Phase Diagram for Confined Electrolyte . . . . .	28
1.4	What are We Still Missing? . . . . .	30
<b>2</b>	<b>Breakdown of electroneutrality in nanopores</b>	<b>33</b>
2.1	Introduction . . . . .	33
2.2	Mean-field Theory of Confined Electrolytes . . . . .	36
2.2.1	General Equations . . . . .	36
2.2.2	Example of a Spherical Cavity . . . . .	38
2.3	Screening Length for Ions Confined to Lower Dimensions . . . . .	39
2.4	Uniform Embedded Pore model . . . . .	43
2.4.1	Derivation . . . . .	44
2.4.2	Cylindrical Nanopore Geometry: a Phase Diagram . . . . .	47
2.4.3	Sub-nanometer Nanopores: Dehydration and Images Forces . . . . .	51
2.5	Mean-field Theory on a One-dimensional Lattice . . . . .	52
2.5.1	A Uniformly Charged 1-d Nanopore . . . . .	54
2.5.2	Charge Distribution around a Central Ion . . . . .	57

2.6	Comparison with Experiments . . . . .	60
2.6.1	Single Digit Nanopores . . . . .	60
2.6.2	Sub-nanometer Channels . . . . .	62
2.7	Conclusions . . . . .	66
<b>3</b>	<b>Transport in nanopores</b>	<b>69</b>
3.1	Equilibrium Density Profile: The Consequence of Electroneutrality Breakdown . . . . .	69
3.1.1	An Exact Solution for Weakly Charged Cylinders . . . . .	71
3.2	The "Electric Leakage" Boundary Condition . . . . .	73
3.2.1	The "Electric Leakage" Boundary Condition in a Spherical Cavity	73
3.2.2	The "Electric Leakage" Boundary Condition in a Nanopore . .	74
3.2.3	Revisiting the Poisson-Boltzmann Equation . . . . .	78
3.3	Transport in Nanopores: Stefan-Maxwell Coupled Fluxes . . . . .	81
3.3.1	Fickian vs Stephan-Maxwell Diffusion . . . . .	82
3.3.2	Electro-osmotic Flow: The Slip Length Approximation . . . . .	84
3.4	Results . . . . .	85
3.5	Discussion . . . . .	87
<b>4</b>	<b>Spin-Glass Charge Ordering in Ionic Liquids</b>	<b>89</b>
4.1	Introduction . . . . .	89
4.2	Theory . . . . .	91
4.3	Results . . . . .	94
4.3.1	Ionic Liquids . . . . .	94
4.3.2	Water-in-Salt Electrolyte . . . . .	97
4.3.3	Molten Salts . . . . .	99
4.3.4	Turbulence in Bacterial Suspensions . . . . .	100
4.4	Discussion . . . . .	102
4.A	MD Simulation Details . . . . .	104

<b>5</b>	<b>Activity Coefficients: Correlations and finite size effect in a BSK model</b>	<b>107</b>
5.1	Model . . . . .	110
5.2	Origins of the 4th Order Term: Correlation Vs. Screening . . . . .	112
5.3	Activity: Charged Shell in BSK Model . . . . .	115
5.3.1	Returning to the Boundary Condition Problem . . . . .	117
5.4	Comparing Results with Experiments . . . . .	119
5.4.1	Temperature Dependence . . . . .	120
5.4.2	Nitrate, Sulfate and Hydroxide: Adding Short-Range Interactions . . . . .	121
5.5	A closer Look at the Correlation Length . . . . .	123
5.6	Conclusions . . . . .	124
5.A	Modified BSK: Short-Range Interaction . . . . .	125
<b>6</b>	<b>Ionic activity in concentrated electrolytes: solvent structure effect revisited</b>	<b>133</b>
6.1	Introduction . . . . .	133
6.2	Model . . . . .	136
6.3	Results . . . . .	141
6.4	Discussion . . . . .	144
<b>7</b>	<b>Future prospects</b>	<b>147</b>
7.1	Linear Electrokinetics of Concentrated Multicomponent Systems in Nanopores . . . . .	147
7.2	Electroneutrality Breakdown for Interacting Pores . . . . .	148
7.3	Validating Electroneutrality Breakdown: Experiments and Simulations	149
7.4	The Hidden Order of Ionic Liquids . . . . .	149
7.4.1	Orientational Order in 2D . . . . .	151
7.4.2	Ring Statistics in 3D . . . . .	151
<b>8</b>	<b>Concluding Remarks</b>	<b>153</b>



# List of Figures

1-1	. Electrostatics under confinement. Different behavior expected for the electrostatic interactions in a nanopore as a function of ionic concentration (c) and pore radius (d). Classical theories (Poisson-Boltzmann) are only appropriate in the bottom right corner. New approaches are needed under extreme confinement and high concentrations. The Bjerrum length, or the characteristic length for electrostatic interactions, determines the extent of ion pairing relative to $r_{nn}$ . Under extreme confinement, $d < r_{nn}$ or $d < \lambda_D$ , 1d correlated transport is expected to dominate. At high concentrations, $\lambda_d < D$ , 3D correlations and ion pairing can play a bigger role. . . . .	29
2-1	Sketch of a confined electrolyte, in chemical equilibrium with a distant external reservoir (in the grand canonical ensemble), as indicated by an ideal "salt bridge," which does not otherwise perturb the system. The governing equation in the inner region ( $\Omega$ ) is the usual Poisson-Boltzmann equation. The outer region has a fixed dielectric constant and is described by a Laplace equation. The surface charge on the boundary layer ( $\partial\Omega$ ) determines the jump in the normal component of the electric field. . . . .	37

2-2	Electroneutrality breakdown for a spherical nanopore in equilibrium with an external reservoir. The surface charge is not fully screened by the confined electrolyte, as electric fields extend into the solid matrix (assumed here to have the same dielectric constant as the pore). Bottom: the accumulated charge inside the sphere, relative to the total surface charge, as a function of the ratio of the radius to the Debye length. Top: an illustration of the electric field intensity for different Debye lengths. As the Debye length decreases, the electric fields are screened from the outer region and are concentrated in a narrow region near the surface of the sphere. . . . .	40
2-3	Illustration of the standard Debye screening in 3d(a), and the extended screening length of 1d(b), according to Eq. 2.8. . . . .	43
2-4	Left: Phase diagram for electroneutrality, as a function of the Gouy-Chapman length ( $\lambda_{GC}$ ) which is related to the surface charge, and Debye screening length ( $\lambda_D$ ), which is related to the bulk ionic concentration. The color intensity indicates the ratio of total accumulated charge inside a nanochannel to the surface charge and is obtained by solving Eq. 2.22. In electroneutral systems, this ratio is 1. The dashed mark the transition to electroneutrality Eq. (2.25-2.26). Right: illustration of the 4 regimes of the phase diagram. The blue circles mark the Debye screening length. . . . .	47
2-5	The total ionic concentration in a nanotube, as a function of concentration for different surface charges. Dashed lines show concentration calculated for electroneutral pores. . . . .	51
2-6	Solution of the 1D-ring equation with uniform surface charge (Eq. 2.37). The solution, $q_i = q_0 + q_1(-1)^i$ , has an average part ( $q_0$ , left figure) that screens the external charge ( $Q$ ) and an oscillatory part ( $q_1$ , right figure). Solutions are presented as a function of the bulk Debye length ( $\lambda_D$ ) and the Gouy-Chapman length ( $\lambda_{GC}$ ). The dashed vertical line is the critical Debye length, calculated by Eq. 2.39. . . . .	54

2-7	<p>Charge distribution around a central ion and the resulting activity coefficient, for different concentrations. (a-f) Charge distribution around a central ion for six different coupling strengths (<math>\chi</math>). For weak coupling, the central ion is screened only by oppositely charged ions (e-f). As the coupling increases, over screening and oscillations are observed. (g) Ionic activity in a nanopore, based on the exact 1D solution for the mean field equation (Eq. 2.45, solid blue line) and the dilute limit approximation (Eq. 2.46, dashed red line). . . . .</p>	55
2-8	<p>Conductance of a KCl solution as a function of concentration, inside CNT with varying surface charge and radii, fitted according to our model (dashed lines). The experimental data (circles) was adapted from [219], where the surface charge was controlled by changing the pH. (a) - A 3.5nm wide pore, fitted barrier energy of <math>4.6k_B T</math> and 4 different surface charges, from bottom to top: <math>-3\text{mC/m}^2</math> (black), <math>-1.6\text{mC/m}^2</math> (red), <math>3.4\text{mC/m}^2</math> (green), <math>5.2\text{mC/m}^2</math> (blue). (b) - A 10nm wide pore, with only one surface charge: <math>12\text{mC/m}^2</math>. (c) - A 14nm wide pore, with 3 different surface charge, fitted to: <math>63\text{mC/m}^2</math> (black), <math>213\text{mC/m}^2</math> (red) and <math>417\text{mC/m}^2</math> (blue). (d)- A 34nm wide pore, with fitted surface charge of: <math>-7\text{mC/m}^2</math> (black), <math>55\text{mC/m}^2</math> (red) and <math>110\text{mC/m}^2</math> (blue). . . . .</p>	60
2-9	<p>Conductance of sub-nanometer pores as a function of ionic concentration. Main figure: Conductance of a <math>3.5\text{\AA}</math> wide CNT porin as a function of KCl concentration (filled squares), adapted from [239] and fitted according to our model (dashed lines). The bottom curve (blue) has pH 3.5, which corresponds to zero charge, while the upper (black) curve has pH 7.5, and is fitted to a surface charge of <math>6\text{mC/m}^2</math>. Inset: conductance in Gramicidin-A channel as a function of NaCl concentration (filled squares, adapted from [83]) and its fit (dashed lines). The fitted surface charge is <math>13\text{mC/m}^2</math>. . . . .</p>	63

2-10 Fitted mobilities. The mobilities of 6 datasets, Gramicidin-A, CNT Porin, and 4 different CNT experiments, were fitted according to Eq. 2.48. Experimental data and fits are shown in Figs. 7-8. Each pH was fitted separately, and within each experiment the bins are ordered from low pH to high. The bulk value for KCl mobility (last column) was taken from [165] . . . . . 65

3-1 Electroneutrality breakdown in nanopores: simulations, exact analytical results and approximated schemes. (a) illustration of the nanopore configuration, a narrow channel connected to two reservoirs, and surrounded by a dielectric matrix with different permittivity. (b-d) Electroneutrality breakdown (ratio of ionic charge to surface charge) calculated for a pore with  $R = 5\text{nm}$ , and  $L = 100\text{nm}$  (b),  $L = 50\text{nm}$  (c) and  $L = 20\text{nm}$  (d). Results are based on the UEP model (2.14), dot-dash black line), solution of the PB equation with "electric leakage" boundary conditions (3.18, dashed red line), exact solution (3.8, solid blue line) and COMSOL simulation (black X). (f) An illustration of COMSOL simulation box. (e) A cross section of the electric field found by the numerical simulation in the nanopore. . . . . 76

3-2 Effect of neutrality breakdown and coupled fluxes on nanopore conductance. Conductance was calculated by Eq. 3.53 with no-slip condition, and by solving the PB equation with boundary conditions from Eq. 3.18. (a) No coupling limit ( $\chi = 0$ ). (b) Intermediate coupling ( $\chi = 10$ ). (c) Strong coupling ( $\chi = 1000$ ). . . . . 86

4-1 Illustration of the reconstruction procedure. 1 - the input is a full MD simulation of the ionic liquids. 2- The first step is to take a single snapshot, calculate the position of each molecule (as an average over its atomic positions), and delete the molecule identity. 3- Based on molecular positions, we construct a connectivity network, by connecting each molecule to its nearest neighbors. 4- Minimizing the spin-glass Hamiltonian for the network yields identities for the molecules, marked by orange and blue in the figure. The minimization is carried for each snapshot separately. . . . . 92

4-2 Order vs. Frustration in Ionic Liquids. **Top-** examples of 2D Ising model, with different degree of order. Red lines mark connections between parallel spins. The more ordered the system (right), more connections are satisfied. **Bottom-** examples of 3D spin-glass with Coulomb interaction. (b)- Charge distribution around a central ion in a Random hard sphere model, for different packing fractions ( $\Phi$ ), ranging from 0 to 0.2 in steps of 0.02. (inset: cumulative charge distribution. Over-screening is defined as the maximum of this curve). (c) - Charge distribution around a central TFSI ion in EMIM-TFSI, based on MD simulation (black line) and the spin-glass reconstruction (dashed red) (inset: a snapshot from the MD simulation). (d) - EMIM-TFSI charge density near a weakly charged surface ( $0.01\text{C}/\text{m}^2$ ), based on MD simulation (black line) and spin-glass reconstruction (dashed red) (inset: a snapshot from the MD simulation). . . . . 95

4-3	LiTFSI in Water- from concentrated electrolyte to WiSE: Charge distribution around a central TFSI ion is shown for different molality (1 mol/kg solvent = 1m), from 2m to 21m. Each graph is plotted with an offset of 1e/nm. Results from MD simulation (solid black line) are compared with random hard-sphere toy model (dashed-dot blue) and the spin-glass reconstruction (dashed red). Snapshots are shown from the LiTFSI MD simulation for 2m(bottom), 7m(middle) and 21m (top). The hard sphere diameter equals 4.12Å. . . . .	98
4-4	Screening cloud around a central TFSI ion is shown for different molality (1 mol/kg solvent = 1m), from 2m to 21m. Results from MD simulation (right blue bars) are compared with random hard-sphere toy model (left red bars). The hard sphere diameter equals 4.12Å. . .	99
4-5	Charge distribution around a central ion in a NaCl-type molten salt and TMA-OTF. Right- comparison of spin-glass reconstruction (dashed red line) vs MD simulation results (solid black line) for a molten salt. Left - testing the reconstruction scheme on a protic ionic liquid, TMA-OTF (dashed red line) with MD simulation results (solid black line). The difference in both cases is less than 1%, as shown in the top figures. The small difference is due to the fact that an overwhelming majority of ions were identified correctly. . . . .	101
4-6	Applying spin-glass reconstruction for swimming bacteria. (a)- snapshot of simulated flow field (adapted from [69] with permission) . (b)- A vortex network constructed by extracting the vortices centers as nodes. The sign of each node, clockwise (red) or counter-clockwise (blue) rotation, was derived from minimizing spin-glass Hamiltonian and matches 19 out of the 23 nodes of the simulation. (c)- Illustration of the reconstructed flow field, based on a superposition of independent LambãÑOseen vortices . . . . .	102

5-1	Activity coefficients for different aqueous solutions. Green lines are fitted according to Eq. 5.30 with $l_c$ as a fitting parameter, the solid blue lines are according to Born approximation, the dashed green lines are based on our model, with $l_c$ fitted to data $< 1.5M$ , and the dash-dot black lines show the result of our model, fitted for the whole range. The black dots are based on experimental data fitted to Bromley formula [42] . . . . .	129
5-2	Activity coefficients for different aqueous solutions. Green lines are fitted according to Eq. 5.30 with usual definition of $\lambda$ , the dash-dot black lines incorporate direct specific interaction term with $\lambda$ defined by Eq. 5.36. The black dots are based on experimental data fitted to Bromley formula [42], and the blue line is according to classic DH approximation . . . . .	130
5-3	Estimated correlation length according to experimental data (solid line) and according to Eq. 5.32 (dashed line), for different ionic solutions . . . . .	131
6-1	The response function $\chi(k)$ as a function of wavelength, for three models of dielectric functions: simple Lorentzian model, over-screening model and a hybrid model. . . . .	141
6-2	The dimensionless electrostatic potential, $e\beta\phi(r)$ , around a spherical ion, for ionic concentrations 1mM, 10mM, 100mM, 0.5M and 2.5M, based on a the non-local dielectric function described by Eq. 6.6. Parameters of the non-local function are given in Table. 1. The ionic diameter used is 3.5Å. Right inset- the dimensionless electrostatic potential in a constant dielectric medium. Left inset- the dimensionless electrostatic potential profile near the surface of the sphere. At larger distances from the ion, as well as at any distances for the case of constant permittivity, the potential decreases with electrolyte concentration, but in the vicinity of the ion the effect is non-monotonic. . . . .	143

6-3	Activity coefficients as a function of ionic concentrations. Left- The activity coefficient for monovalent binary solutions, based on the non-local permittivity model, Eq. 6.12. Three different activity curves are shown, corresponding to three ionic diameters (from bottom to top): 4Å, 3Å and 2Å. The parameters of the pure water dielectric function are summarized in Table. 1, and the smearing parameter was taken to be $\eta = 0.5\text{Å}$ . Left- Experimental data of activity coefficients for three ionic solutions (from bottom to top): KCl, NaCl and LiCl. Data is taken from [42]. . . . .	144
7-1	Charge density in uncharged pores. The concentration profile of anions and cations in a pore connecting reservoirs with different concentrations (1mM and 10mM) . . . . .	148
7-2	Proposed validation of electroneutrality breakdown in experiment and simulation. (a) An illustration of molecular dynamics simulation to test the breakdown of electroneutrality. (b) The net charge of the membrane changes with surface charge in agreement without theory. (c-d) Examples of AAO membranes with different pore density, figures are courtesy of the Elimelech group at Yale. (e-f) Numerical and analytical results of electroneutrality breakdown as a function of pore-pore separation. . . . .	150
7-3	The hidden order in ionic liquids. (a) The ratio of 3-rings to 4-rings for different systems with increasing degree of charge ordering. (b) 2d example: the orientational order parameter $\psi_4$ as a function of temperature in a MC simulation of melting. . . . .	152

# List of Tables

4.1	Force Field Parameters used for model molten salt (representative of NaCl). . . . .	106
5.1	Correlation length and Fitting Errors . . . . .	121
5.2	Correlation length as a function of temperatures . . . . .	121
6.1	Parameters for our hybrid model of pure-water dielectric response (Eq. 6.18). . . . . .	142



# Chapter 1

## Introduction

In 1923, in their seminal paper[61], simply called "The Theory of Electrolyte", Peter Debye and Ernest Hückel were the first to use the "Poisson-Boltzmann" (PB) theory to study bulk properties of electrolytes. Many scientists have followed them and proved the PB theory and its extensions to be invaluable for understanding the ways ions interact with each other or with other charged objects. This thesis is our small contribution to this century-long effort and focuses on extreme conditions of confinement and strong correlations.

In their paper, Debye and Hückel sought to explain the experimentally measured phenomenon of freezing point depression in electrolytes. When a salt is dissolved in water, the freezing point of water is reduced. The freezing temperature decreases with concentration until ion-ion interactions limit these effects. To study ion-ion correlations, Debye and Hückel calculated thermodynamic properties of ions in solution in a "mean-field" manner. The electrostatic potential ( $\phi$ ) around an ion is determined by ions in its vicinity in accordance with the Poisson equation:  $-\epsilon\nabla^2\phi = \rho$ , where  $\epsilon$  is the solvent dielectric constant, and  $\rho = \sum_i q_i c_i$  is the charge density. The charge density itself is given by the Boltzmann distribution, which leads to the Poisson-Boltzmann (PB) equation:

$$\epsilon\nabla^2\phi = 2ec \sinh(\beta e\phi), \quad (1.1)$$

where  $\beta = 1/k_B T$  is the inverse temperature.

The PB equation was first introduced by Gouy in 1910 [96] and later independently by Chapman[53] to explain the screening of charged surfaces by electrolytes. The ionic atmosphere in the bulk is essentially equivalent to the *double layer* structure that ions form near the surface. When considering bulk properties, the amplitude of the electrostatic potential, compared with thermal fluctuations, is usually small, and the hyperbolic sinus function can be approximated well to linear order. This is known as the Debye-Huckel (DH) approximation:

$$\nabla^2\phi = \lambda_D^{-2}\phi, \tag{1.2}$$

where  $\lambda_D = \sqrt{2ce^2/\epsilon k_B T} = \sqrt{1/2cl_B}$  is the well known *Debye screening length*, and  $l_B = e^2/4\pi\epsilon k_B T$  is the Bjerrum length. In their paper they describe this length as "the most essential size of our theory", and this is indeed the single most important size that characterizes the bulk properties of ionic solutions. Interestingly, the nonlinear analysis of the PB equation was omitted from the paper for the sake of brevity.

The linear DH regime was able to accurately explain the experimental observations of the freezing point depression for a variety of salts and ionic strength, with a single fitting parameter- the ionic size. This success was subsequently followed by further investigations of thermodynamic properties, such as activity coefficient, osmotic pressure, heat capacity, and more[61, 118, 107, 208, 48]. The PB equation is not limited to bulk properties and is widely used in biological systems, where ions are interacting with charges on the cell surface or other polyelectrolytes such as proteins or DNA molecules [120, 188, 75, 12]. Finally, both the DH limit, as well as the full nonlinear PB equation, is often used in the design and modeling of electrochemical and energy storage devices[56, 120, 85, 82, 181].

## 1.1 Derivation of the PB Equation

We described the PB equation as a "mean-field" theory, derived self-consistently by combining the Poisson equation and Boltzmann distributions. Let us now sketch a

rigor derivation for the PB equation from a statistical mechanical perspective. This will illustrate the approximations and limitations of the theory and will serve as a starting point for our discussion on the extensions to the theory. We focus our discussion here on symmetric monovalent binary solutions, but the derivation can be extended for different valencies as well. Our derivation here is based on a field-theoretic approach that offers a powerful way of extending the PB equation beyond mean-field[205, 189, 160, 161, 5].

Let us consider a lattice with lattice a constant  $a$ , which roughly corresponds to the size of the ions. We further assume that the solvent is described by a constant dielectric background medium, and allow each lattice site to occupy a single ion, negative or positive. The electrostatic energy of this system is given by a sum over all the pairwise interactions. Working in the grand canonical ensemble, the valance of each lattice site  $i$  can take three values  $z_i = \{-1, 0, 1\}$ . The partition function is:

$$\Xi = \prod_i \sum_{z_i=-1,0,1} \exp \left( \beta\mu \sum_i z_i^2 - \int d\mathbf{r} \int d\mathbf{r}' \frac{\beta\rho(\mathbf{r})\rho(\mathbf{r}')}{4\pi\epsilon|\mathbf{r}_i - \mathbf{r}_j|} \right), \quad (1.3)$$

where  $\mu$  is the chemical potential, the charge density is  $\rho(\mathbf{r}) = \sum_i z_i e\delta(\mathbf{r} - \mathbf{r}_i)$ , and  $\mathbf{r}_i$  is the location of the  $i^{\text{th}}$  lattice site. At this point it is not clear how a Poisson-Boltzmann equation can pop out of this seemingly complicated partition function. To achieve this, we use the Hubbard-Strantovic (HS) transformation[233, 117], and write the partition function in terms of an auxiliary field  $\varphi$  that conjugates the charge density field  $\rho$ . For a general pair-wise interaction  $v(\mathbf{r} - \mathbf{r}')$ , the HS transformation can be viewed as a generalization of the Fourier transform of a multivariate Gaussian to the continuum:

$$\exp \left[ \int d\mathbf{r} \int d\mathbf{r}' \rho(\mathbf{r})v(\mathbf{r} - \mathbf{r}')\rho(\mathbf{r}') \right] = \int \mathcal{D}\varphi(\mathbf{r}) \exp [\varphi(\mathbf{r})v^{-1}(\mathbf{r} - \mathbf{r}')\varphi(\mathbf{r}) - i\rho(\mathbf{r})\varphi(\mathbf{r})] \quad (1.4)$$

For Coulomb interactions, the inverse interaction operator  $v^{-1}(\mathbf{r} - \mathbf{r}')$  is proportional to the Laplace operator. The HS transformation allows us to decouple different lattice sites, and explicitly calculate the summation in the partition function. Eventually,

we get [39]:

$$\Xi = \int \mathcal{D}\varphi \exp \left( -\frac{\beta\varepsilon}{2} \int d\mathbf{r} |\nabla\varphi|^2 + \frac{1}{a^3} \int d\mathbf{r} \ln \{1 + 2\Lambda \cos [e\beta\varphi(\mathbf{r})]\} \right), \quad (1.5)$$

where  $\Lambda = \exp(\beta\mu)$  is the fugacity. We now see that  $\varphi$  is closely related to the electrostatic potential. In the mean-field level, which is the saddle-point approximation of the partition function, the auxiliary field equals  $\varphi = -i\phi$ . The free energy at the saddle point is:

$$\frac{F}{k_B T} = -\ln \Xi = -\frac{\beta\varepsilon}{2} \int d\mathbf{r} |\nabla\phi|^2 - \frac{1}{a^3} \int d\mathbf{r} \ln \{1 + 2\Lambda \cosh[e\beta\phi(\mathbf{r})]\}. \quad (1.6)$$

Minimizing the free energy with respect to  $\phi$ , and taking the dilute limit  $\Lambda \rightarrow 0$  we obtain the PB equation (Eq. 1.1):

$$\frac{\partial F}{\partial \phi} = \beta\varepsilon \nabla^2 \phi - 2e\beta \frac{\Lambda}{a^3} \sinh [e\beta\phi(\mathbf{r})] = 0. \quad (1.7)$$

## 1.2 Extensions to PB Theory

From the statistical mechanical derivation of the PB theory, the main limitations of the PB theory are apparent. First, it is a theory of low packing fractions: the size of the ions, compare to the ion-ion separations, has to be large. More importantly, as a mean-field theory, it will only be applicable if fluctuations beyond mean fields are negligible. The partition function allows us to systematically expand the theory beyond mean-field. Taking the first-order correction, also known as a "one-loop" expansion, we find that it can be negligible if the Bjerrum length,  $l_B$ , is small compared to the average distance between ions[246]. Hence, a mixture of ions, immersed in a dielectric continuum, and interacting only with electrostatic forces are described by the PB theory only if both  $ca^3 \ll 1$  and  $cl_B^3 \ll 1$ .

An electrolyte, however, is not an ideal mixture of ions, nor does it always dilute enough to justify the PB underlying assumptions. The solvent, dipole molecules such as water, can interact with the ions. Ions themselves have different sizes and

shapes, and ion-ion interactions at small distances are complicated and not strictly electrostatic.

Different approaches have been suggested over the past century to handle the limitations of the original theory. Let us briefly discuss some of the prominent ones:

### 1.2.1 Finite-size Effects

Perhaps the largest body of literature is devoted to including finite-size effects to the Poisson-Boltzmann theory. The short-range interactions can either be modeled with van-der Waals forces, a hard-sphere model or even a lattice model.

### Primitive Models and Liquid State Theories

The "primitive models" of electrolytes are defined as ions interacting with a combination of hard-sphere repulsion in addition to the electrostatic interaction:

$$u_{ij}(|\mathbf{r}_i - \mathbf{r}_j|) = \begin{cases} \frac{q_i q_j}{|\mathbf{r}_i - \mathbf{r}_j|} & |\mathbf{r}_i - \mathbf{r}_j| > a \\ \infty & |\mathbf{r}_i - \mathbf{r}_j| < a \end{cases} \quad (1.8)$$

A very useful technique of studying the local structure, or pair-correlation functions, of hard sphere liquids is integral equation[1, 194, 197]. By postulating that the pair-correlation function can be separated to "direct" and "total" correlations functions, the pair correlation function is calculated from the Ornstein Zernike (OZ) equation[1]. Solving the OZ equations requires a closure- an assumption on how the direct correlation function behaves. For the case of electrolytes, some simple closures have been suggested, and showed good agreement with simulations [222, 44, 224]. While usually a numerical scheme is required to solve the integral equations, the mean-spherical approximation[150, 244] has an exact analytical solution.

### Lattice Models

Liquid state theories can be very accurate, but they lack the simple and intuitive picture that makes PB theory so popular. One way of extending the PB and still

maintaining some finite size effects is to write the PB theory on a lattice[20, 40, 26, 130, 144]. In the derivation we presented in the previous section, we approximated the exponent of the partition function to lowest order in the fugacity to obtain the regular PB equation. Alternatively, we could have calculated directly the corresponding mean-field equation and obtain:

$$\nabla^2\phi = \frac{2e}{\varepsilon} \frac{c \sinh(e\beta\phi)}{1 + 2ca^3 \sinh^2(\beta e\phi/2)} \quad (1.9)$$

First introduced by Bikerman in 1942[26], and rediscovered many times since the "modified PB" equation has a maximal density constraint that prevents unphysical charge accumulations. It is especially useful when electrolytes are in contact with large electrified surfaces, where screening charges form a compact layer. Interestingly, within this approximation, one can obtain a closed-form formula for the differential capacitance[40, 130, 144].

The main drawback of the lattice models is its failure to capture density waves at high packing. Much like the standard PB equation, the solution of the electrostatic potential is strictly decaying. This limitation leaves the lattice model applicable only in the very dilute limit, away from charge oscillations and over-screening that characterizes high concentrations.

## 1.2.2 Ion-ion Correlations

We can define "ion-ion correlations" as all the interactions that are not described by the mean-field Poisson-Boltzmann theory. One example is the formation of ion-pairs[28, 84, 6], ions that are so close, they form a stable pair (a dipole). ion-ion correlations can also be short-lasting, but one consequence of it is the formation of density oscillations. The solutions of the PB theory are always decaying, and higher-order statistics is required to capture the oscillatory structures.

A rigor analysis of correlations beyond the mean-field can be carried out by a systematic expansion of the partition function[189]. Alternatively, a phenomenological approach to ion-ion correlations have recently been introduced by Bazant, Storey

and Kornyshev (BSK[21]) who proposed a generalized mean-field theory, known as the BSK equation:

$$(1 - l_c^2 \nabla^2) \nabla^2 \phi = \frac{2ze}{\epsilon} \frac{c \sinh(e\beta\phi)}{1 + 2ca^3 \sinh^2(\beta e\phi/2)}, \quad (1.10)$$

where  $l_c$  is a phenomenological correlation length. Note that the BSK equation captures finite-size effects as well. This simple way of accounting for correlations has been widely used since it first appeared, and successfully explained a wide range of experimental phenomena. Examples include electro-kinetics and transport[231, 151], the electrical double layer structure and capacitance [21, 254], and electrophoresis[232]. Moreover, Molecular Dynamic simulations too showed good agreement with the BSK predictions [125]

### 1.2.3 Ion-solvent Interactions

At the concentrated electrolyte limit, in addition to ion-ion correlations, we have to consider ion-solvent interactions as well. Treating the solvent as a continuous dielectric medium misses the important interplay between the dipoles and the ions. The main consequence of this interplay is the lowering of the dielectric constant, especially at high molalities, as noted by Huckel himself two years after the original DH theory was introduced theory[118].

The PB equation can be extended to include simple point-like dipoles, generalizing the electrolyte to a mixture of both ions and dipoles[3]. However, unlike ions, the solvent molecules are highly concentrated and are strongly interacting[146, 141, 36, 227]. Therefore, while some aspects of solvent-salt interaction can be captured within this framework, the complex local structures are usually beyond the reach of simple theoretical descriptions.

## 1.3 Electrolyte in Confinement

Our discussion was so far limited to cases where the electrolyte extends to all space. Indeed, in many applications, this is a good approximation. The typical length-scales of electrolytes (Bjerrum length, Debye length) are nanometric, while the size of a typical system, biological or electrochemical, is much larger.

Yet, in one important case, this assumption breaks down: ionic channels. Biological ion channels can be as narrow as the size of single molecules[113]. Synthetic channels, such as carbon nanotubes are fast approaching this limit[78, 115, 239]. Ion exchange membranes, such as ones that are used for water filtration, have pores in the nanometer scale as well[236]. Traditionally, modeling an electrolyte under such extreme confinement has taken one of two routes [185]. On the one hand, a single-file transport was described as a chemical reaction, where the channel is a transition state for ions in the process of going from one reservoir to another. This is a popular approach in ion channels that are limited to a handful of ions. A completely different picture utilizes the Poisson-Boltzmann theory, combined with Nernst-Planck diffusion, to characterize the transport of ions through narrow channels. Without explicitly accounting for the 1-d nature of the channels, this approach works best in the "thin" double layer limit: if the size of the double layer is smaller than the size of the channel.

In recent years there has been a growing interest in *Single Digit Nanopores*(SDNs): pores with a diameter less than 10nm[78]. As this regime becomes accessible for precise measurements, the behavior of the SDNs is found to be strikingly different than wider pores. Enhanced slip flow[248, 115], peculiar conductance curves[219], spatial and temporal correlations[87] of ions are some unique characteristics of extreme confinement that are not captured by classical continuum modeling.

### 1.3.1 A Phase Diagram for Confined Electrolyte

Three length-scales dominate the SDN regime: the radius of the channel ( $R$ ), the mean-ionic spacing (average distance to the nearest neighbor,  $r_{nn}$ ) and the Debye

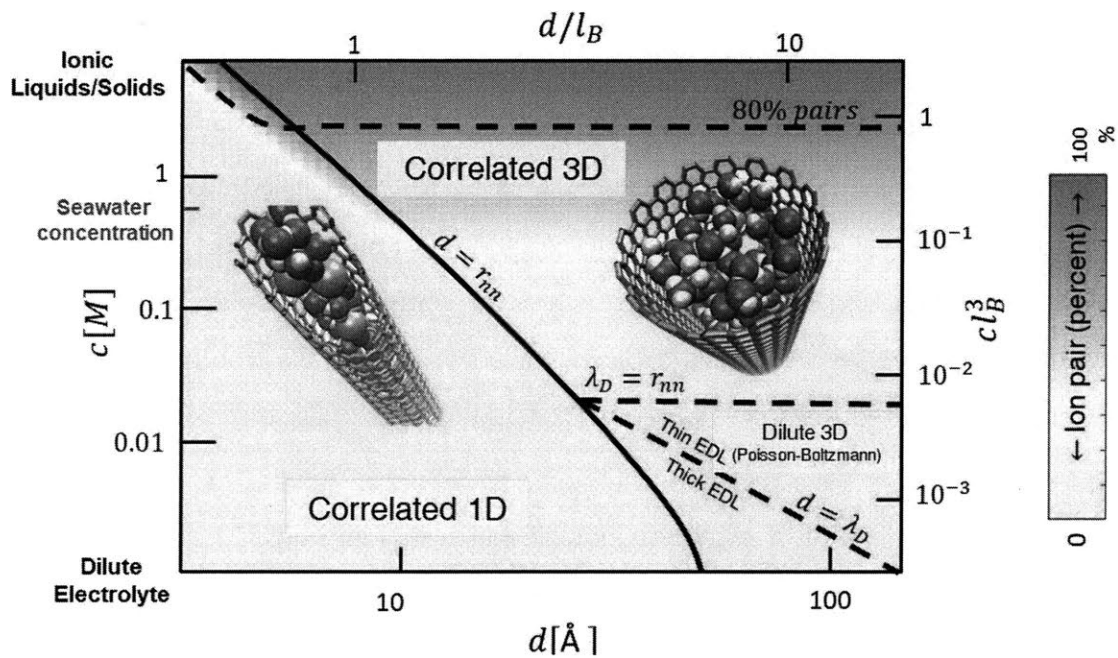


Figure 1-1: . Electrostatics under confinement. Different behavior expected for the electrostatic interactions in a nanopore as a function of ionic concentration ( $c$ ) and pore radius ( $d$ ). Classical theories (Poisson-Boltzmann) are only appropriate in the bottom right corner. New approaches are needed under extreme confinement and high concentrations. The Bjerrum length, or the characteristic length for electrostatic interactions, determines the extent of ion pairing relative to  $r_{nn}$ . Under extreme confinement,  $d < r_{nn}$  or  $d < \lambda_D$ , 1d correlated transport is expected to dominate. At high concentrations,  $\lambda_d < D$ , 3D correlations and ion pairing can play a bigger role.

screening length ( $\lambda_D$ ). Under extreme conditions, other lengths, such as the size of the ions or the solvent, can play an important role. However, in typical experimental setups, the pore is wide enough so they are safely ignored.

The PB theory works best in wide pores ( $R \gg \lambda_D$ ) and dilute concentrations ( $r_{nn} \ll \lambda_D$ ). In concentrated electrolytes, ion-ion correlations can lead to charge inversion inside the channel and result in electroosmotic flow reversals and electrophoretic mobility reversals[201, 25]. Confinement-induced effects lead to unusually strong correlative transport modes, dramatically enhancing mechanisms such as electroosmotic transport and ion concentration polarization[136, 30].

These different regimes are illustrated in Fig. 1-1 (published in Ref. [78]). We consider a channel of radius  $R$ , connected to a reservoir with ionic concentration  $c$ . The color of the plot corresponds to the amount of "ion-pairs", the percent of ions that are separated by less than  $l_B$ , the classical definition of Bjerrum pairs. This serves as a measure for the strength of ion-ion correlations. We assume that ions are uniformly distributed inside the pore and that the nearest neighbor's distance follows a Poisson point process.

The starting point of continuum models in the bottom right corner: the small region where the PB assumptions are satisfied. The extensions described in the previous section allow us to go in the up-word direction and predict the behavior of moderately concentrated wide pores. However, there is a large region of the phase diagram that remains uncharted territory. Can the PB theory serve as a good starting point when ions are so close to each other? Are 3d equations valid when ions form long 1d chains?

## 1.4 What are We Still Missing?

The large interest in the Poisson-Boltzmann theory has led to countless extensions and refinements of the theory. At the same time, technological advances in both fabrication technologies and computer hardware are now giving us new ways of studying electrolytes. New experimental results require us to re-frame old ideas, and powerful

molecular simulations give us a glimpse of the microscopic structure of materials.

It is remarkable that the Debye-Huckel equation, the linearized model of the non-linear PB equation, has such a strong appeal despite its limitations. It demonstrates the power of a simple theory to guide our physical intuition, which is often more useful than providing the most accurate description of reality. Yet, inevitably, at some point, the Debye-Huckel equation breaks down, and it is more instructive to have a different picture in mind. Strong ion-ion correlations and extreme confinement pose such a theoretical challenge: finding simple guiding principles that hold in those regimes. In this thesis address this challenge in three different ways:

We begin (Chapters 2 and 3) by considering ionic channels as 1d electrolytes interacting with a 3d Coulomb interactions. In contrast to 3d bulk electrolyte, we find that an exponentially long screening length replaces the standard Debye length ("the most essential size of our theory"). When the screening length exceeds the length of the pore, we find a surprising breakdown of global neutrality. We explore the significant implications of the electroneutrality breakdown on the density profile and transport properties of ionic channels in these chapters.

In Chapter 4 we study charge ordering in ionic liquids. The strong ion-ion interactions in ionic liquids lead to long-range correlations that are not well understood from a PB-like theory. Using molecular simulations, we show that the charge ordering follows a very simple principle: it exactly minimizes the electrostatic energy in a system of disorder ionic positions. We demonstrate an intimate and overlooked link between the ionic position and charge ordering and show that local positional ordering is required to maintain long-ranged charge ordering.

Finally, in chapters 5 and 6 we show that phenomenological models can be valuable for moderately correlated ions. We study the activity coefficients of highly concentrated ionic solutions in terms of a non-local dielectric constant. The properties of the phenomenological permittivity allow us to retain closed-form approximated expression while capturing important effects such as ion-ion correlations and ion-solvent interactions.



# Chapter 2

## Breakdown of electroneutrality in nanopores

Except for minor edits, the contents of this chapter have been submitted for publication and are currently under review[163].

### 2.1 Introduction

The transport of ions in extreme confinement has applications ranging from physiology to chemical engineering[113, 66, 24, 111, 247, 243, 251, 134, 131, 176, 201, 216]. Whether we consider ions traveling through the protein channels in the cell membrane or through pores in an ion-exchange membrane, the underlying physics shares many similarities[192, 236]. A growing interest in ionic transport through nanopores has emerged in recent years owing to nano-fabrication advances that enable us to study pristine nano-channels at the single-channel level, such as carbon nanotubes, boron-nitride nanotubes or silicon nano-channels[154, 8, 223, 103, 60]. These experiments have revealed that our understanding of even the basic physics is incomplete, and important theoretical knowledge gaps still exists[78].

Classical theories of ion transport were inspired by the membrane technology that was available at that time[229, 102, 77]. The complicated interplay of fluxes and potential gradients (chemical, electrical, and pressure) was naturally modeled

with continuum theories. The so-called “capillary-pore model,” based on the Poisson-Boltzmann (PB) equation for the charge distribution normal to the pore walls under the local equilibrium assumption, with Navier-Stokes and Nernst-Planck equations for the fluid flow and ionic flux, is a continuum linear response theory of transport in charged cylinders[201], which is widely used in different electrochemical applications, from electro-osmotic pumps to energy conversion devices[212, 252, 202, 135, 52, 250]. A competing school of thought, rooted in transition state theory[259], emerged in the biophysical community. Experiments on ion channels show that when open, the transport of the ions is best described by a discrete, single-file reaction model, where ions are attached to specific binding in the channel by a chemical reaction[113, 111, 11, 66, 24, 213].

Evidently, a new theory is required for nanochannels with a pore diameter of less than 10nm (single-digit nanopores, or SDNs[78]), in order to span between the two limiting regimes, from discrete to continuum behavior. While the two traditional pictures have some merit, neither can exactly capture experimentally measured conductivity curves. Unusual scaling behavior of ionic conductance in carbon nanotubes (CNTs), for example, was recently reported by Secchi et al[219] and was subsequently interpreted with a Space-Charge continuum model[25]. The conductance of a narrow CNT porin, in contrast, was fitted to a Michalis-Menten reaction model[239], suitable for a single-file transport mechanism.

In this work, we propose a new theoretical framework for electrolytes in nanopores, consisting of confined ions with three-dimensional (3d) electric fields that extend into the surrounding matrix. In the most interesting and relevant case of SDNs, we construct a truly one-dimensional (1d) mean-field theory of ions confined to a long, thin nanopore in a 3d matrix, in contrast to previous models of ion chains with 1d Coulomb interactions [33-35]. Surprisingly, 1d electrolytes exhibit several interesting behaviors, most notable is the breakdown of global electroneutrality: a system can have a net charge where the total charge of the ionic solution does not exactly cancel out external charges. When the pore diameter is comparable to the spacing between ions, the system essentially behaves like a 1d correlated electrolyte. Ions are not

necessarily restricted to transport in single-file, but the nature of the electrostatic interactions resembles a 1d chain. Despite our interest in transport, this chapter will only focus on the equilibrium properties of ion channels. The equilibrium properties can in turn be used to understand transport properties of the nanotube.

Electroneutrality breakdown in nanopores has been observed in Monte-Carlo simulations [228, 207, 170, 156, 157, 32, 31, 34], and was recently even measured experimentally[173]. However, it was not interpreted as a unique feature of the 1d geometry. Instead, the breakdown was assumed to occur due to an excess screening of charges outside of the pore. This type of local breakdown of charge neutrality is not suited to most transport problems, where the channel is surrounded by a constant dielectric medium.

Without charge neutrality, electric fields leak out of the confined region into the outer substrate. We derive (section II) a mean-field theory of a confined electrolyte by properly accounting for the outer region as well. We then focus on a 1d cylindrical geometry and consider three different models to illustrate how and why electroneutrality is no longer maintained. First (section III), we present a general scaling argument for the enhanced screening length in low dimensions. We show that 1d systems have an exponentially long screening length that can easily exceed the size of the system. In the following (section IV), we consider a uniformly charged pore and solve a self-consistent algebraic mean-field equation for the excess charge. Three length-scales govern the accumulated charge: the Debye screening length (ion-ion interactions), the Gouy-Chapman length (ion-wall interactions) and the pore diameter. Finally (section V), we solve a full 1d lattice mean-field equation and observe the emergence of ion-ion correlations at high concentrations. The breakdown of electroneutrality has profound implications on the transport of ions through nanochannels, and in section VI we show that our model can account for the unusual scaling of conductance in CNT.

## 2.2 Mean-field Theory of Confined Electrolytes

Electroneutrality is often a hidden assumption of continuum models: it hides in the boundary conditions for the Poisson-Boltzmann equation, where the electric fields outside the electrolyte are assumed to vanish. According to Gauss's law, if there is no electric flux emanating from the electrolyte in the pore, it has zero net charge. Electroneutrality relies on the nanometer-scale screening length, which guarantees macroscopic charge fluctuations are negligible. A rigorous analysis requires us to solve the Laplace equation outside the electrolyte, in addition to the PB equation inside.

It is important to note that electroneutrality is not always assumed[171, 172, 173, 55, 216]. As a recent example, Colla et al[55] considered two charged plates immersed in water, with free ions on both sides of each plate, and solved a density functional theory (DFT) in the entire space. Since the screening is not symmetric, especially when the screening length is large, the accumulated charge between the plates can be small. The authors consider this as an example of a local breakdown of electro-neutrality (LEC), and while it shares some similarities with our approach, LEC is fundamentally different from the global electroneutrality breakdown which we discuss, and is not a unique property of a 1d geometry.

### 2.2.1 General Equations

Let us consider the PB equation for a symmetric binary monovalent electrolyte, fixed at a chemical potential that is set by an external reservoir with ionic concentration  $c_0$ , and confined to a small region in space ( $\Omega$ , see Fig. 2-1). We further assume that the electrolyte is embedded in a constant dielectric medium with permittivity  $\epsilon_{\text{out}}$ , and the boundary is charged with a surface charge  $q_s$ . The electrostatic potential ( $\phi$ ) is determined by a set of PB and Laplace equations:

$$\begin{cases} \epsilon_{\text{in}} \nabla^2 \phi_{\text{in}}(\mathbf{r}) = 2c_0 e \sinh [e\beta\phi_{\text{in}}(\mathbf{r})] & \forall \mathbf{r} \in \Omega \\ \epsilon_{\text{out}} \nabla^2 \phi_{\text{out}}(\mathbf{r}) = 0 & \forall \mathbf{r} \notin \Omega. \end{cases} \quad (2.1)$$

where  $e$  is the electron charge,  $\varepsilon_{\text{in}}$  and  $\varepsilon_{\text{out}}$  are the dielectric constants in the solvent and dielectric matrix, respectively, and  $\beta = 1/k_{\text{B}}T$  is the inverse temperature and  $k_{\text{B}}$  is the Boltzmann constant. A similar approach was previously introduced to calculate the effect of image charges on the ionic self energy in confinement[128], and to study the transport of ions through porous media[216], but the resulting electroneutrality breakdown was not emphasized. The boundary conditions for this system are:

$$\begin{aligned} [\phi_{\text{out}}(\mathbf{r}) - \phi_{\text{in}}(\mathbf{r})]_{\forall \mathbf{r} \in \partial\Omega} &= 0 \\ \mathbf{n}(\mathbf{r}) \cdot [\varepsilon_{\text{in}} \nabla \phi_{\text{in}} - \varepsilon_{\text{out}} \nabla \phi_{\text{out}}(\mathbf{r})]_{\forall \mathbf{r} \in \partial\Omega} &= q_s \\ \phi_{\text{out}}(\mathbf{r})|_{r \rightarrow \infty} &= 0, \end{aligned} \quad (2.2)$$

where  $\partial\Omega$  is the electrolyte boundary, and  $\mathbf{n}$  is an outward unit vector normal to the boundary.

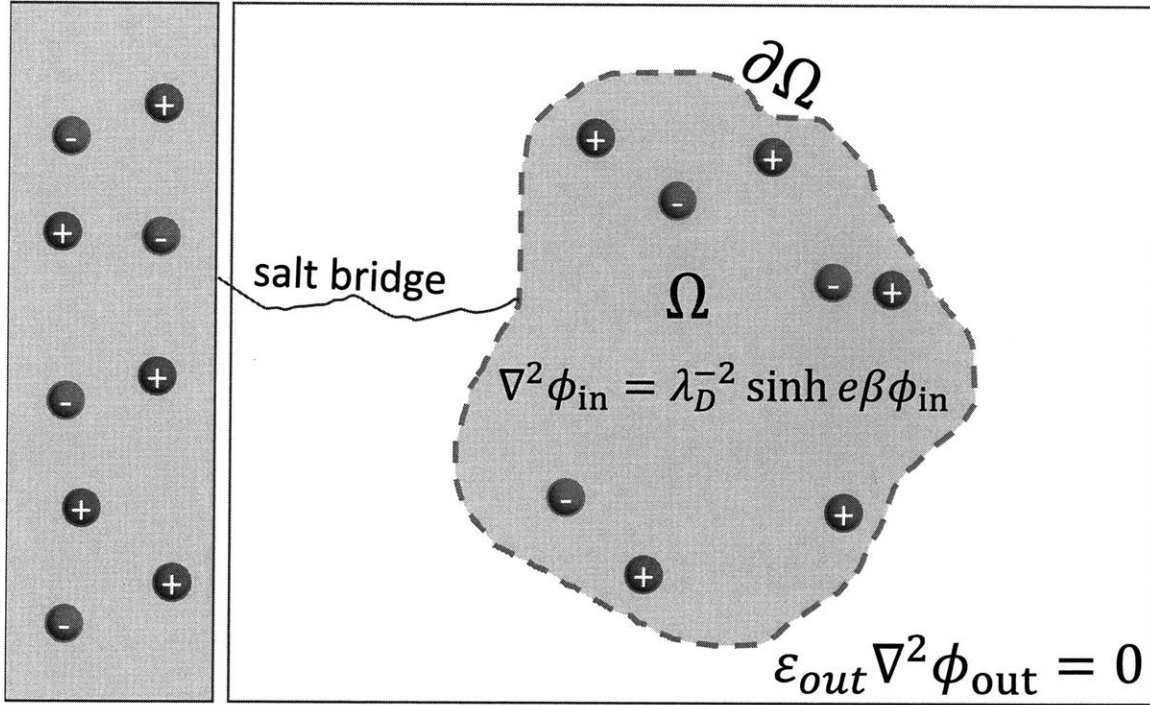


Figure 2-1: Sketch of a confined electrolyte, in chemical equilibrium with a distant external reservoir (in the grand canonical ensemble), as indicated by an ideal “salt bridge,” which does not otherwise perturb the system. The governing equation in the inner region ( $\Omega$ ) is the usual Poisson-Boltzmann equation. The outer region has a fixed dielectric constant and is described by a Laplace equation. The surface charge on the boundary layer ( $\partial\Omega$ ) determines the jump in the normal component of the electric field.

Solving the set of PB/Laplace equations for a finite cylinder can only be done numerically. In many cases, we will find that accounting for outer electric fields is redundant, since the outer electric fields vanish. In other cases, dramatic differences in the charge profile can be observed. In the remaining sections of the paper, we will present simplified models that permit analytical results, which will help us explore the implication of Eq. 2.1. While some of the accuracy of the complete model is lost, we will gain a much better physical understanding, as well as mathematically convenient approximations.

## 2.2.2 Example of a Spherical Cavity

Let us start by considering the pedagogical example of a weakly charged spherical cavity, which allows us to analytically observe the breakdown of charge neutrality. Note that this example only illustrates how net neutrality is achieved, though it has little practical use since spherical cavities will usually not be in chemical equilibrium with the bulk. For weakly charged surfaces, the electrostatic potentials are weak ( $e\beta\phi \ll 1$ ), which allows us to linearize the PB equation ( $\sinh(e\beta\phi) \approx e\beta\phi$ ). We solve the combined PB/Laplace equations for a sphere of radius  $R$  in the linearized Debye-Hückel (DH) regime:

$$\phi(r) = \begin{cases} A \frac{\sinh(\kappa_D r)}{\kappa_D r}, & r < R. \\ \frac{B}{r}, & r > R, \end{cases} \quad (2.3)$$

where  $\kappa_D = \lambda_D^{-1} = \sqrt{2c_0 e^2 \beta / \epsilon_{\text{in}}}$  is the inverse Debye screening length, and  $A$  and  $B$  are coefficients determined by the boundary conditions (Eq. 2.2). The total charge accumulated inside the spherical cavity, in the linear DH regime, reads:

$$\begin{aligned} Q_{\text{in}} &= -2\beta e^2 c_0 \int_0^R 4\pi r^2 \phi(r) dr \\ &= -4\pi R^2 q_s \frac{1 - \frac{\tanh(\kappa_D R)}{\kappa_D R}}{1 + \left(\frac{\epsilon_{\text{out}}}{\epsilon_{\text{in}}} - 1\right) \frac{\tanh(\kappa_D R)}{\kappa_D R}}. \end{aligned} \quad (2.4)$$

For a pore much larger than the Debye length ( $\kappa_D R \gg 1$ ), or equivalently in the thin double-layer limit, the charge inside the sphere is equal and opposite to the total surface charge ( $Q_{\text{ext}} = 4\pi R^2 q_s$ ), regardless of any relative dielectric discontinuity. If the size of the sphere is comparable with the screening length, only partial screening is achieved. Further decreasing the size of the sphere leads to screening of only a small fraction of the surface charge. If the medium has a lower dielectric constant, the accumulated charge is even smaller. However, since we aim to understand the effect of confining ions alone, in the absence of dielectric polarization effects, we restrict our analysis hereafter to a constant permittivity everywhere.

It is not surprising that when the Debye length is much smaller than the size of the spherical cavity, the electrolyte fully screens the surface charge. However, what would happen if only some directions are restricted, as in the cases of nanoslits or nanopores? Is it enough for only one dimension to be smaller than the Debye length to break neutrality? To gain a better physical intuition to guide our expectations, let us first revisit the meaning of the "screening length."

## 2.3 Screening Length for Ions Confined to Lower Dimensions

A central ion in an aqueous solution is surrounded by a screening cloud meaning that ions in its vicinity tend to be of opposite charge. In three dimensions, we can find an analytical expression for the shape of the screening cloud, achieved by solving the linearized Poisson-Boltzmann equation. The density profile of screening ions decays exponentially with a characteristic length, the "Debye length" ( $\lambda_D$ ). When ions are restricted to different dimensionality, still interacting with a  $1/r$  pair-wise potential, there is no similarly tractable equation to determine the shape and size of the screening cloud. We will show in the following sections, that an equivalent screening length exists and plays an important role in the physics of lower dimension electrolytes, but it formally requires a cumbersome derivation. Before we delve into a

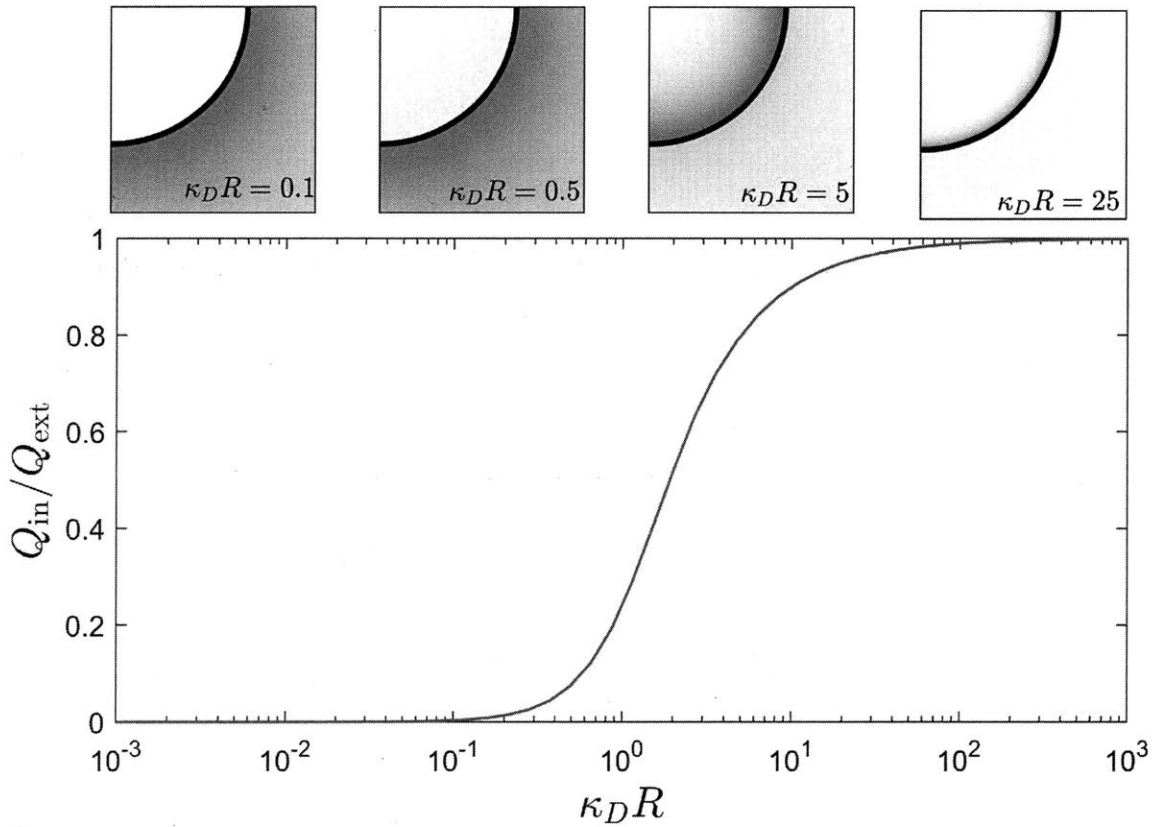


Figure 2-2: Electroneutrality breakdown for a spherical nanopore in equilibrium with an external reservoir. The surface charge is not fully screened by the confined electrolyte, as electric fields extend into the solid matrix (assumed here to have the same dielectric constant as the pore). Bottom: the accumulated charge inside the sphere, relative to the total surface charge, as a function of the ratio of the radius to the Debye length. Top: an illustration of the electric field intensity for different Debye lengths. As the Debye length decreases, the electric fields are screened from the outer region and are concentrated in a narrow region near the surface of the sphere.

more rigorous formalism, we first present a simple scaling argument for the screening length that holds in any dimension.

The screening length, in essence, is the distance at which entropic and electrostatic forces balance each other. The electrostatic force pulls the screening cloud closer to the central ion, while entropy favors uniform charge distributions and pushes the screening cloud away. If we consider a screening cloud of radius  $\lambda_s$  with  $N_s$  ions around a negatively charged univalent ion, the probability of each ion to have charge  $+e$  equals  $p_i^+ = 1/2 + 1/2N_s$ . Maximal entropy is achieved if there is an equal probability for an ion to be positive or negative. By forcing the ions to screen the central charge, the probability of positively charged ions slightly increases, and the entropy is reduced. Note that the ions outside the screening cloud have equal probabilities to have positive/negative charge. The entropy associated with this screening cloud equals (assuming  $N_s \rightarrow \infty$ , which corresponds to the dilute limit):

$$\begin{aligned}
S &= -k_B \sum_{i=1}^N [p_i^+ \log p_i^+ + p_i^- \log p_i^-] \\
&= -N_s k_B \left[ \left( \frac{N_s + 1}{2N_s} \right) \log \left( \frac{N_s + 1}{2N_s} \right) \right. \\
&\quad \left. + \left( \frac{N_s - 1}{2N_s} \right) \log \left( \frac{N_s - 1}{2N_s} \right) \right] + (N - N_s) k_B \log 2 \\
&\approx k_B \left( N \log 2 - \frac{1}{2N_s} \right), \tag{2.5}
\end{aligned}$$

where  $N$  is the total number of ions in the system, both inside and outside the screening cloud. The first term is constant (does not depend on  $N_s$ ) and can be ignored. Note that this is only the entropy associated with the possibility of each ion to be positive or negative, and positional entropy is neglected. Relating the entropy to the  $d$ -dimensional sphere volume[182],  $V = A_d \lambda_s^d / d$ , where  $A_d$  is the surface area of a unit sphere, and average ionic pair concentration ( $2c = N_s / V$ ), we find that the entropy of ions inside the sphere is reduced by:

$$\Delta S = -\frac{dk_B}{4A_d c \lambda_s^d}. \tag{2.6}$$

The electrostatic energy of a uniformly distributed screening cloud equals:

$$\begin{aligned}
 U &= -\frac{e^2 A_d}{4\pi\epsilon V} \int_a^{\lambda_s} r^{d-2} dr \\
 &= -\frac{e^2}{4\pi\epsilon\lambda_s} \times \begin{cases} \frac{d}{d-1}, & d > 1. \\ \log \frac{\lambda_s}{a}, & d = 1, \end{cases} \quad (2.7)
 \end{aligned}$$

where  $a$  is the ion size, assumed to be much smaller than  $\lambda_s$ . Here, we make the critical assumption of a 3d Coulomb potential decaying as  $1/r$ , which effectively spills out of the confining geometry, and neglect for now any dielectric response of the surrounding matrix, which modifies the result but does not alter the basic scaling arguments (as shown below).

Minimizing the free energy ( $F = U - T\Delta S$ ) with respect to  $\lambda_s$ , and ignoring the numerical prefactors, yields the following scaling behavior for the screening length:

$$\lambda_s \propto \begin{cases} (cl_B)^{\frac{1}{1-d}}, & d > 1 \\ a \exp(\frac{1}{8cl_B}), & d = 1, \end{cases} \quad (2.8)$$

where  $l_B = e^2/4\pi k_B T \epsilon$  is the Bjerrum length. In three dimensions, we recover the standard Debye screening:  $\lambda_s \propto \lambda_D = (8\pi cl_B)^{-1/2}$ . In a nanoslit geometry of two dimensions, the screening length is proportional to  $(cl_B)^{-1}$ . Forcing ions to reside on a two-dimensional plane reduces electrostatic interactions, and slightly increases the size of the screening clouds. A much more dramatic effect is observed for one-dimensional confinement in a long, thin nanopore, where the screening length is *exponentially* large, as shown in Fig. 2-3.

If we consider our one-dimensional system to be a cylinder with radius  $R$ , length  $L$ , and a 3d concentration (per volume) of  $c_0$ , the corresponding 1d concentration (per length) in the axial direction is  $c^{1d} = \pi R^2 c_0$ . In terms of these bulk properties, we find that the dimensionless factor,  $c^{1d} l_B = \pi R^2 c_0 l_B$ , is related to the ratio of Debye length to pore radius, which enters the exponential scaling of the screening length in one dimension:  $\lambda_s \propto a \exp[(\lambda_D/R)^2]$ . For narrow pores in dilute electrolytes, the

Debye length can easily be greater than the pore radius, which is the traditional limit of “thick double layers” ( $\lambda_D \gg R$ ), but in contrast to classical continuum models, we predict that this results in an extremely large screening length, easily exceeding all geometrical scales in the problem. In particular, when the screening length exceeds the total length of the channel ( $\lambda_s \gg L$ ), the central ion is no longer screened, and electroneutrality breaks down.

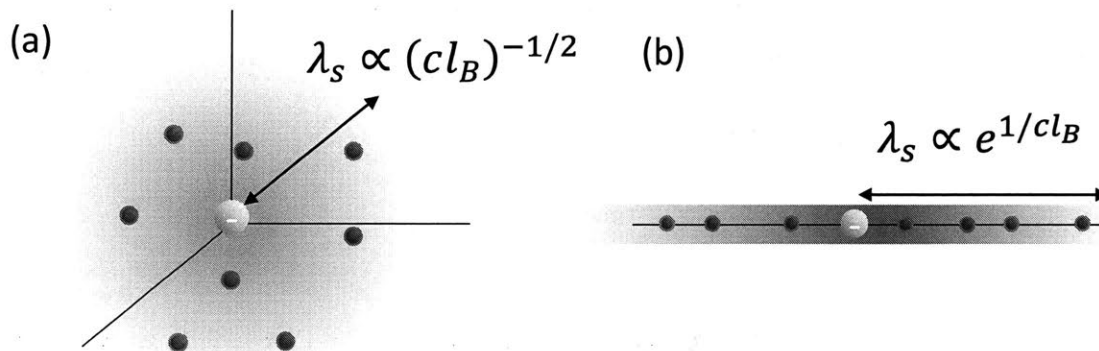


Figure 2-3: Illustration of the standard Debye screening in 3d(a), and the extended screening length of 1d(b), according to Eq. 2.8.

## 2.4 Uniform Embedded Pore model

The scaling analysis of the previous section suggests that if we numerically solve Eq. 2.1 in a long and narrow cylinder, we expect that overlapping double layers will be accompanied by a net charge of the pore. With this intuition in mind, let us now introduce a quantitative model of a uniformly charged pore embedded in a constant dielectric medium. This “Uniform Embedded Pore” (UEP) model is closely related to the widely used “Uniform Potential” (UP) model [214, 226, 59, 241, 41, 131, 201], also known as Teorell-Meyers-Sievers theory [58, 237, 184], which takes advantage of the narrow pore geometry to approximate a constant charge distribution in the radial direction. This approximation is further adapted in the “Leaky membrane model”, which describes the concentration polarization in porous media, based on similar microscopic assumptions [176, 253, 70]. While we make the same assumption about the charge distribution within the pore, we recognize that the surrounding dielectric

matrix cannot be neglected. At first, to keep matters simple, we only consider the case where the dielectric constants inside and outside of the pore are equal.

### 2.4.1 Derivation

The free energy functional of  $M$  ionic species immersed in a dielectric continuum with permittivity  $\varepsilon$ , assuming ideal mixing entropy, with thermal de Broglie wavelength  $\lambda_T$ , reads:

$$\begin{aligned}
F[\{c_i(\mathbf{r})\}] &= \frac{1}{2} \int_V d^3\mathbf{r} \int_V d^3\mathbf{r}' \frac{\rho(\mathbf{r})\rho(\mathbf{r}')}{4\pi\varepsilon|\mathbf{r}-\mathbf{r}'|} \\
&+ k_B T \int_V d^3\mathbf{r} \sum_{i=1}^M c_i(\mathbf{r}) [\log(\lambda_T^3 c_i(\mathbf{r})) - 1] \\
\rho(\mathbf{r}) &= \sum_{i=1}^M e z_i c_i(\mathbf{r}) + \rho_{\text{ext}},
\end{aligned} \tag{2.9}$$

where  $c_i(\mathbf{r})$  and  $z_i$  are the concentration and valency of the  $i$ -th ionic species, respectively, and  $\rho_{\text{ext}}$  is an external charge distribution. For a uniform ionic density we write the free energy as a function of the mean ionic concentrations:

$$\begin{aligned}
F[\{c_i\}] &= \frac{e^2}{2} \sum_{i=1}^M \sum_{j=1}^M z_i z_j c_i c_j \int_V d^3\mathbf{r} \int_V d^3\mathbf{r}' \frac{1}{4\pi\varepsilon|\mathbf{r}-\mathbf{r}'|} \\
&+ \int_V d^3\mathbf{r} \int_V d^3\mathbf{r}' \frac{\rho_{\text{ext}}(\mathbf{r})\rho_{\text{ext}}(\mathbf{r}')}{4\pi\varepsilon|\mathbf{r}-\mathbf{r}'|} \\
&+ \sum_{i=1}^M e z_i c_i \int_V d^3\mathbf{r} \int_V d^3\mathbf{r}' \frac{\rho_{\text{ext}}(\mathbf{r})}{8\pi\varepsilon|\mathbf{r}-\mathbf{r}'|} \\
&+ V k_B T \sum_{i=1}^M c_i [\log(\lambda_T^3 c_i) - 1]
\end{aligned} \tag{2.10}$$

The ‘‘mean-interaction’’ integrals in the above equation describe the electrostatic energy associated with uniformly distributed charge inside a volume,  $V$ . They depend only on the external charge and geometry, so it is convenient to define the following

integrals:

$$\begin{aligned}\gamma &= \frac{l_B}{eV} \int_V d^3\mathbf{r} \int_V d^3\mathbf{r}' \frac{1}{|\mathbf{r} - \mathbf{r}'|}, \\ \rho_{\text{ext}}^0 &= \frac{l_B}{e\gamma V} \int_V d^3\mathbf{r} \int_V d^3\mathbf{r}' \frac{\rho_{\text{ext}}(\mathbf{r})}{|\mathbf{r} - \mathbf{r}'|}.\end{aligned}\quad (2.11)$$

The free energy density is now simplified:

$$\begin{aligned}\frac{\beta F[\{c_i\}]}{V} &= \sum_{i=1}^M \left[ \gamma z_i c_i \left( \sum_{j=1}^M \frac{e z_j c_j}{2} + \rho_{\text{ext}}^0 \right) \right. \\ &\quad \left. + c_i (\log(\lambda_T^3 c_i) - 1) \right],\end{aligned}\quad (2.12)$$

where we neglect constant contributions to the free energy. The chemical potential is the derivative of the free energy density with respect to concentration:

$$\beta \mu_i = \gamma z_i \left( \sum_{j=1}^M e z_j c_j + \rho_{\text{ext}}^0 \right) + \log(\lambda_T^3 c_i). \quad (2.13)$$

The first term in the LHS of Eq. 2.13 describes the excess free energy due to electrostatic interactions, while the second term is the ideal gas entropy. If our system is in chemical equilibrium with a bulk reservoir, the chemical potential will only have the second term ( $\beta \mu_i^0 = \log(\lambda_T^3 c_i^0)$ ), with the bulk values of ionic concentrations. Equating the chemical potential in Eq. 2.13 to the bulk value, we find the following equation for the average ionic density,  $c_i$ :

$$\begin{aligned}\log(\lambda_T^3 c_i^0) &= \gamma z_i \left( \sum_{j=1}^M e z_j c_j + \rho_{\text{ext}}^0 \right) + \log(\lambda_T^3 c_i) \\ c_i &= c_i^0 \exp \left[ \gamma z_i \left( \sum_{j=1}^M e z_j c_j + \rho_{\text{ext}}^0 \right) \right].\end{aligned}\quad (2.14)$$

The average charge density,  $\rho^0 = \sum e z_i c_i$ , therefore, satisfies the following equa-

tion:

$$\rho^0 = \sum_{i=1}^M e z_i c_i^0 \exp[-z_i \gamma (\rho_{\text{ext}}^0 + \rho^0)], \quad (2.15)$$

We can incorporate non-idealities to the system by adding an excess chemical potential to Eq. 2.13. If this were the case, the  $c_i^0$  would be replaced by the ionic activities, rather than the concentrations.

The equation for the mean charge in the UEP model, Eq. 2.14, is written in terms of the average charge density,  $\rho^0$ , which makes it easier to solve. To see its relation with the set of PB/Laplace equations discussed in section II, we write Eq. 2.14 in terms of the electrostatic potential. Note that the term in the exponent is the electrostatic potential, averaged over the volume of the electrolyte, and multiplied by  $z_i e \beta$ . Furthermore, the Poisson equation relates charge density and electrostatic potential,  $\rho^0 = -\varepsilon \nabla^2 \phi$ , and thus Eq. 2.14 becomes a partial differential equation:

$$\varepsilon \nabla^2 \phi(\mathbf{r}) = - \sum_{i=1}^M e z_i c_i^0 \exp[-z_i e \beta \overline{\phi(\mathbf{r})}]. \quad (2.16)$$

Hence, the uniform embedded pore model is an approximation of the standard PB equation, where we replace the electrostatic potential with its volume average. The complete set of equations for the potential in the UEP model includes in addition the Laplace equation in the outer dielectric medium, and the boundary conditions of Eq. 2.2. This set of equations is mathematically equivalent to Eq. 2.14, as long as the permittivity is everywhere the same.

Under electroneutrality the charge density,  $\rho^0$ , exactly cancels out the external charge distribution,  $\rho_{\text{ext}}^0$ . A criterion for electroneutrality to be satisfied, for weakly charged systems, is obtained by linearizing equation 2.14:

$$\rho^0 = - \frac{\rho_{\text{ext}}^0}{1 + (e \gamma \sum_{i=1}^M z_i^2 c_i^0)^{-1}}. \quad (2.17)$$

Hence, the condition for electroneutrality is  $e \gamma \sum_{i=1}^M z_i^2 c_i^0 \gg 1$ . Using the definition

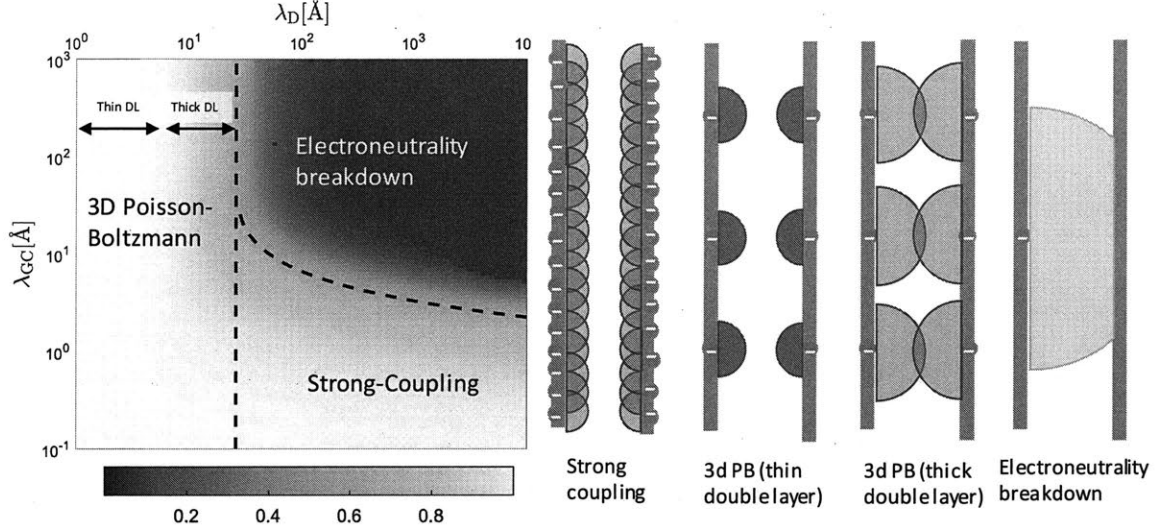


Figure 2-4: Left: Phase diagram for electroneutrality, as a function of the Gouy-Chapman length ( $\lambda_{GC}$ ) which is related to the surface charge, and Debye screening length ( $\lambda_D$ ), which is related to the bulk ionic concentration. The color intensity indicates the ratio of total accumulated charge inside a nanochannel to the surface charge and is obtained by solving Eq. 2.22. In electroneutral systems, this ratio is 1. The dashed mark the transition to electroneutrality Eq. (2.25-2.26). Right: illustration of the 4 regimes of the phase diagram. The blue circles mark the Debye screening length.

of  $\gamma$  (Eq. 2.11), we can write this condition in terms of the bulk Debye length-  
 $\lambda_D^{-2} = 4\pi l_B (\sum_{i=1}^M z_i^2 c_i^0)$ :

$$\int_V \frac{d^3\mathbf{r}}{V} \int_V \frac{d^3\mathbf{r}'}{\lambda_D^2 |\mathbf{r} - \mathbf{r}'|} \gg 1 \quad (2.18)$$

In typical 2 and 3 dimensional systems, this condition is satisfied if the characteristic size of the system is larger than Debye length, but in 1d we find a very different result.

## 2.4.2 Cylindrical Nanopore Geometry: a Phase Diagram

Our scaling argument (Eq. 2.8) suggests that electroneutrality breaks down for cylindrical nanopores if the Debye length is greater than the pore radius. We can now see that this is a property of the cylindrical mean-interaction integral. Let us consider a cylinder with radius  $R$ , length  $L$ , and a surface charge density  $q_s$  ( $\rho_{\text{ext}} = q_s \delta(r - R)$ ). The mean-interaction integrals,  $\gamma$ , and  $\rho_{\text{ext}}$ , can be approximated to a good precision

by considering a test charge located at the center of the pore:

$$\begin{aligned}
\gamma^{\text{apprx}} &= \frac{l_B}{eV} \int_V d^3\mathbf{r} \int_V d^3\mathbf{r}' \frac{1}{|\mathbf{r}|} \\
&= \frac{l_B}{e} \int_0^R \int_{-L/2}^{L/2} \frac{2\pi r dr dz}{\sqrt{r^2 + z^2}} = \frac{2\pi R^2 l_B}{e} \log\left(\frac{L}{2R}\right), \\
\rho_{\text{ext}}^{0,\text{apprx}} &= \frac{l_B}{e\gamma^{\text{apprx}}V} \int_V \frac{d^3\mathbf{r}}{|\mathbf{r}|} \int_V d^3\mathbf{r}' q_s \delta(r' - R). \\
&= \frac{2\pi RLq_s}{V} = \frac{2q_s}{R}.
\end{aligned} \tag{2.19}$$

Interestingly, this approximation deviates by only a few percents from an accurate numerical evaluation of the mean-interaction integrals. Based on this approximation, the electroneutrality condition ( $e\gamma^{\text{apprx}} \sum z_i^2 c_i^0 \gg 1$ ) in nanopores can be expressed in terms of the natural system length scales, in agreement with the scaling argument:

$$L \gg (2R) \exp\left(\frac{2\lambda_D^2}{R^2}\right) \tag{2.20}$$

To extend the electroneutrality condition beyond weakly charged systems, the full solution of Eq. 2.14 is required. For a monovalent binary electrolyte, Eq. 2.14 reads:

$$\begin{aligned}
\rho^0 &= ec_i^0 \exp[-\gamma(\rho_{\text{ext}}^0 + \rho^0)] - ec_i^0 \exp[\gamma(\rho_{\text{ext}}^0 + \rho^0)] \\
&= -2ec_i^0 \sinh[\gamma(\rho_{\text{ext}}^0 + \rho^0)]. \\
&\approx -2ec_i^0 \sinh[\gamma^{\text{apprx}}(\rho_{\text{ext}}^{0,\text{apprx}} + \rho^0)].
\end{aligned} \tag{2.21}$$

We note that  $\gamma^{\text{apprx}}$  has dimensions of inverse charge density, so it is instructive to study the dimensionless charge density,  $\tilde{\rho} = \gamma^{\text{apprx}}\rho^0$ . According to Eq. 2.19, a dimensionless charge density with a value of 1 describes a system where the distance between ions is proportional to the Bjerrum length. Hence, we expect strong ion-ion interaction when the dimensionless charge density is large, while for weak charge densities ( $\tilde{\rho} \ll 1$ ), we expect weak electrostatic interactions, that would result in the breakdown of electroneutrality.

In terms of the dimensionless charge density we obtain the following algebraic

equation:

$$\tilde{\rho} = -\xi \sinh(\tilde{\rho}_{\text{ext}} + \tilde{\rho}), \quad (2.22)$$

where the two parameters,  $\xi$  and  $\tilde{\rho}_{\text{ext}}$ , are related to two important length-scales of the system, the Debye-length and the Gouy-Chapman length:

$$\begin{aligned} \tilde{\rho}_{\text{ext}} &= \gamma^{\text{apprx}} \rho_{\text{ext}}^{0,\text{apprx}} = \frac{2R}{\lambda_{\text{GC}}} \log\left(\frac{L}{2R}\right) \\ \xi &= 2ec_0\gamma^{\text{apprx}} = \frac{1}{2} \left(\frac{R}{\lambda_D}\right)^2 \log\left(\frac{L}{2R}\right). \end{aligned} \quad (2.23)$$

The Gouy-Chapman length ( $\lambda_{\text{GC}} = e/2\pi q_s l_B$ ) characterizes the distance from a charged surface at which its electrostatic and thermal energies are equal. If this distance is much smaller than the pore radius, the system is effectively three-dimensional, and electroneutrality holds. As pore charge decreases,  $\lambda_{\text{GC}}$  becomes comparable with the pore radius and the one-dimensional geometry is recovered. Our parameter space is therefore described by three length-scales: the Debye screening length, Gouy-Chapman length, and the pore diameter. The breakdown of electroneutrality into a disordered phase is further augmented by the aspect ratio of the system, which effectively re-scales the pore diameter.

The solution to Eq. 2.22 can be written as  $\tilde{\rho} = -\tilde{\rho}_{\text{ext}} + f_\xi^{-1}(\tilde{\rho}_{\text{ext}})$ , where  $f_\xi(x) = x + \xi \sinh(x)$ . Approximated solutions can be found for highly and weakly charged pores:

$$\tilde{\rho} = f_\xi^{-1}(\tilde{\rho}_{\text{ext}}) - \tilde{\rho}_{\text{ext}} = \begin{cases} -\frac{\tilde{\rho}_{\text{ext}}}{1+\xi^{-1}}, & \tilde{\rho}_{\text{ext}} \ll 1. \\ \log\left(\frac{\tilde{\rho}_{\text{ext}}}{\xi}\right) - \tilde{\rho}_{\text{ext}}. & \tilde{\rho}_{\text{ext}} \gg 1. \end{cases} \quad (2.24)$$

This solution is illustrated in Fig. 2-4 as a function of  $\lambda_{\text{GC}}$  and  $\lambda_D$ , for a pore with dimensions  $R = 1\text{nm}$  and  $L = 100\text{nm}$ . We identify four different regimes, as shown in the four panels of Fig. 2-4. At low surface charge (large  $\lambda_{\text{GC}}$ ) and short screening

lengths (thin double layer), the system can be described by the standard DH approximation, and the electroneutrality assumption is valid. This theory also covers the beginning thick double layer regime, where the double layers begin to overlap. For high surface charges the linearized Poisson-Boltzmann equation is no longer valid. In this strong coupling regime the full non-linear equation is required, but interestingly, it also ensures the ions will completely screen any surface charge. Our solution, however, predicts a fourth regime, of low surface charge and small concentration. Under these conditions, electroneutrality is broken, and external fields must be accounted for.

Two theoretical curves mark the boundaries of the electroneutral phase. The vertical line is derived from the weak charge approximation, as the Debye length at half screening:

$$\lambda_D = R\sqrt{2\log\frac{L}{2R}}. \quad (2.25)$$

The second curve mark the transition to electroneutrality due to high surface charge, and is obtained by requiring half screening in the strong coupling limit of Eq. 2.24:

$$\lambda_D = \sqrt{\lambda_{GC}R} \left(\frac{L}{2R}\right)^{R/2\lambda_{GC}}, \quad (2.26)$$

which asymptotes to a horizontal line at  $\lambda_{GC} \approx R$  as the concentration decreases. Note that the transition to electroneutrality is slow, and spans roughly an order of magnitude change in the parameters. Electroneutrality breakdown can thus play a major role in the physics of nanopores.

The total ionic concentration inside the nanopore, depicted in Fig. 2-5, is related to the pore charge by Donnan equilibrium:

$$c_{\text{tot}} = \sqrt{(2c_0)^2 + (\rho^0/e)^2}. \quad (2.27)$$

In electroneutral systems the concentration reaches a plateau in the dilute limit, where the only ions inside the channel balance the surface charge. Accounting for

electroneutrality breakdown, however, significantly alters the behavior in the dilute limit.

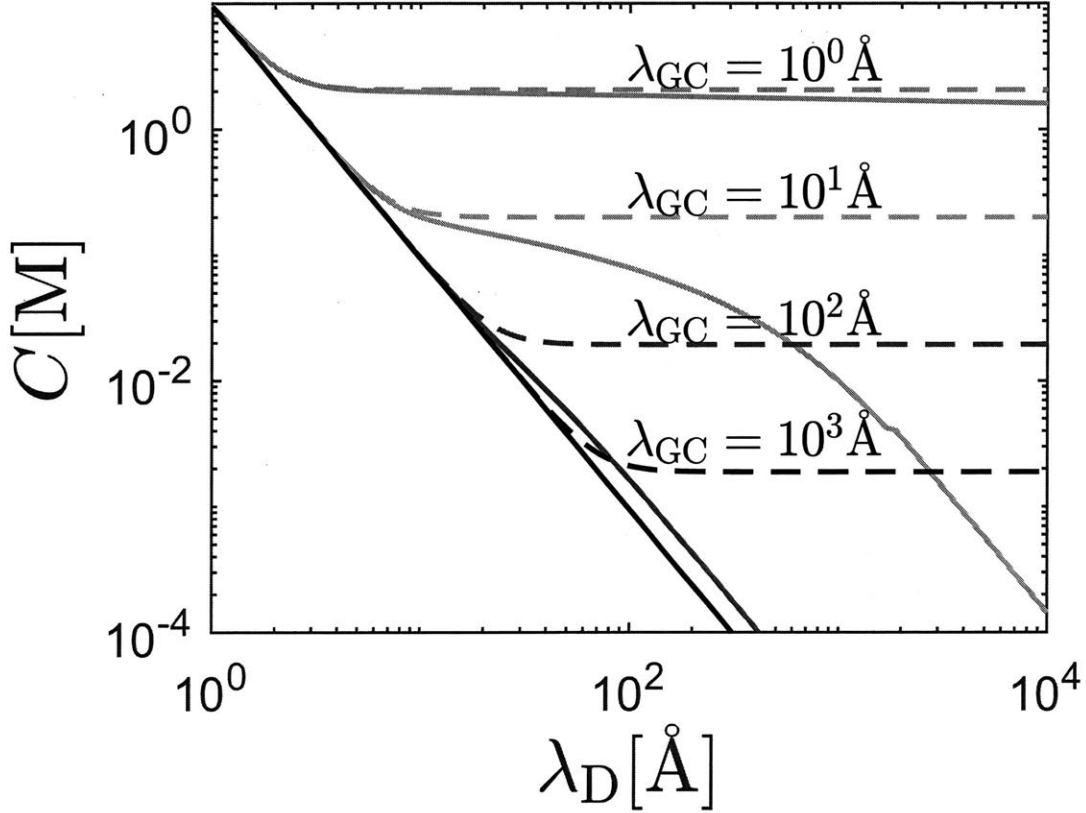


Figure 2-5: The total ionic concentration in a nanotube, as a function of concentration for different surface charges. Dashed lines show concentration calculated for electroneutral pores.

### 2.4.3 Sub-nanometer Nanopores: Dehydration and Images Forces

Ion specific effects have important consequences on the behavior of nanopores, especially in the sub-nanometer scale. In extremely narrow pores ions have to remove their hydration shell, which creates a large energy barrier for entering the pore [73, 210]. Denoting this energetic cost for the  $i$ th specie by  $E_i$ , we generalize the self-consistent equation for the mean charge distribution:

$$\rho^0 = \sum_{i=1}^N e z_i c_i^0 \exp [-\beta E_i - z_i \gamma (\rho^0 + \rho_{\text{ext}}^0)]. \quad (2.28)$$

In the monovalent case the pore-charge equation takes a similar form to Eq. (2.22), with re-scaled coupling parameter  $\xi$  and external charge  $\tilde{\rho}_{\text{ext}}$ :

$$\begin{aligned}\tilde{\rho}_{\text{ext}} &= \frac{2R}{\lambda_{\text{GC}}} \log\left(\frac{L}{2R}\right) + \frac{E_+ - E_-}{2k_{\text{B}}T} \\ \xi &= 2\left(\frac{R}{\lambda_D}\right)^2 \log\left(\frac{L}{2R}\right) \exp\left(-\frac{E_+ + E_-}{2k_{\text{B}}T}\right).\end{aligned}\quad (2.29)$$

Hence, the phase diagram (Fig. 2-4) remains similar, but skewed: the x-axis is rescaled by the average Boltzmann weight, while the y-axis is shifted by dimensionless energy difference. Any asymmetry in the dehydration energy will result in an excess charge within the pore since the dehydration energy plays a similar role to that of the surface charge.

Even though we incorporate in our model an energy barrier, it is important to emphasize again that we are considering a model with a constant permittivity everywhere. The differences in self-energies are only one aspect of a dielectric mismatch, that can change ion-ion and ion-wall interactions as well[129, 256, 257, 159, 38].

## 2.5 Mean-field Theory on a One-dimensional Lattice

In the next section we compare the UEP model with experimental data, and show it can be used to interpret conductance curves. Before doing so, we would first like to show quantitatively how electroneutrality breakdown is a fundamental property of 1d confinement, by considering a system of ions restricted to reside along a line. This will also allow us to explore ion-ion correlations along the pore axis, and observe a transition from order to disorder.

We study a lattice-gas model, and not a continuum model, for two reasons. First, it will enable us to discuss packing constraints at the high concentration limit. A more fundamental reason was hinted in section III: there is no equivalent continuum PB model in 1d. The scaling argument showed that the screening length depends on the minimal distance between ions ( $a$ ), and this will remain valid in the analysis here as well. As a result, we cannot find a corresponding differential equation that describes

the system in the continuum limit. Note that in contrast to many previous 1d models of electrolytes ([72, 158, 62]), the electrostatic interaction is three dimensional ( $1/r$ ): we study point-like ions along a line, and not parallel charged sheets.

For mathematical convenience, we consider the free energy functional of a 1d periodic lattice model (a ring), with lattice spacing equal to the ionic size,  $a$  (see Fig. 2-6). The  $i^{\text{th}}$  site can be occupied by a positive ion, negative ion or a vacancy, with probabilities  $p_i^+$ ,  $p_i^-$  and  $1 - p_i^- - p_i^+$ , respectively. The electrostatic energy,  $U$ , is given by:

$$U = \frac{1}{8\pi} \sum_{i \neq j} \frac{e^2(p_i^+ - p_i^-)(p_j^+ - p_j^-)}{a\varepsilon|i - j|} + \sum_i e(p_i^+ - p_i^-)\phi_i^{\text{ext}}, \quad (2.30)$$

where  $\phi_i^{\text{ext}}$  is an external electrostatic potential. We denote the dimensionless average charge vector  $q_i = (p_i^+ - p_i^-)$  and the dimensionless interaction matrix  $\tilde{\Phi}_{ij} = |i - j|^{-1}$ , so the electrostatic energy reads:

$$U = \frac{e^2}{8\pi a\varepsilon} (\mathbf{q}^T \tilde{\Phi} \mathbf{q}) + e\mathbf{q}^T \phi^{\text{ext}}. \quad (2.31)$$

To calculate the free energy, we add the entropy of mixing:

$$S = -k_B \sum_i [p_i^+ \log p_i^+ + p_i^- \log p_i^- + (1 - p_i^+ - p_i^-) \log(1 - p_i^+ - p_i^-)]. \quad (2.32)$$

If connected to a particle reservoir, the chemical potential is set externally and is calculated by the functional derivative of the free energy density  $f = (U - TS)/a$  with respect to concentration ( $c_i^\pm = p_i^\pm/a$ ):

$$\mu_\pm = k_B T \log \left( \frac{\mathbf{p}_\pm}{\mathbf{1} - \mathbf{p}_+ - \mathbf{p}_-} \right) \pm \frac{e^2 \tilde{\Phi} \mathbf{q}}{4\pi a\varepsilon} \pm e\phi^{\text{ext}}. \quad (2.33)$$

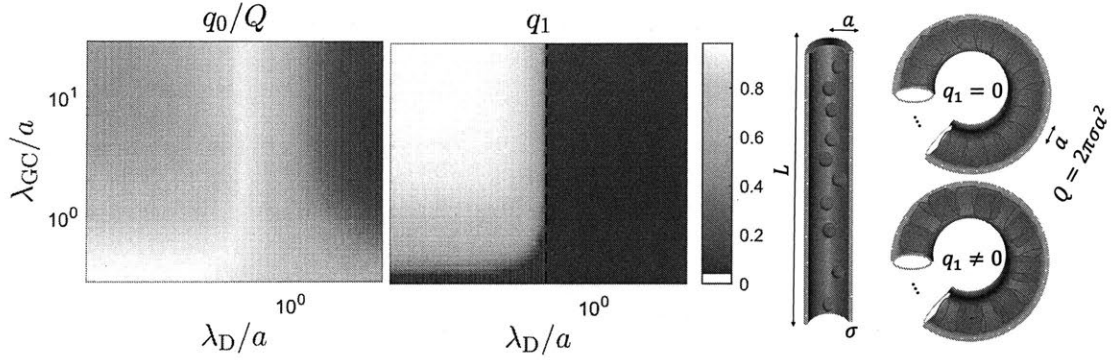


Figure 2-6: Solution of the 1D-ring equation with uniform surface charge (Eq. 2.37). The solution,  $q_i = q_0 + q_1(-1)^i$ , has an average part ( $q_0$ , left figure) that screens the external charge ( $Q$ ) and an oscillatory part ( $q_1$ , right figure). Solutions are presented as a function of the bulk Debye length ( $\lambda_D$ ) and the Gouy-Chapman length ( $\lambda_{GC}$ ). The dashed vertical line is the critical Debye length, calculated by Eq. 2.39.

Rearranging the terms, we obtain the 1d analog of the Bikerman model ([26, 40, 144, 130, 19]):

$$\mathbf{q} = -\frac{2\Lambda \sinh \left[ \frac{l_B}{a} \tilde{\Phi} \mathbf{q} + e\beta\phi^{\text{ext}} \right]}{1 + 2\Lambda \cosh \left[ \frac{l_B}{a} \tilde{\Phi} \mathbf{q} + e\beta\phi^{\text{ext}} \right]}, \quad (2.34)$$

where the fugacity  $\Lambda = e^{\beta\mu}$  is proportional to the bulk reservoir ion activity.

The general form of the 1d ring equation is not very illuminating, and specific examples are required to show how ion-ion correlations play an essential role in this model. We study two systems: a charged homogeneous nanopore and the charge distribution around a central ion. In the dilute limit, we recover the behavior described in the previous section. As ionic concentration increases, the model naturally predicts a transition to an ordered structure, including the short-range over-screening phenomenon in intermediate concentrations.

### 2.5.1 A Uniformly Charged 1-d Nanopore

Let us assume we have a homogeneous charge density in our system:  $q_i = q$ ,  $\phi_i^{\text{ext}} = \phi^{\text{ext}}$ . For periodic boundary conditions, a uniform charge distribution is an eigenvector of the interaction matrix  $\tilde{\Phi}$ , where the eigenvalue is twice the harmonic number  $H_{L/a}$ .

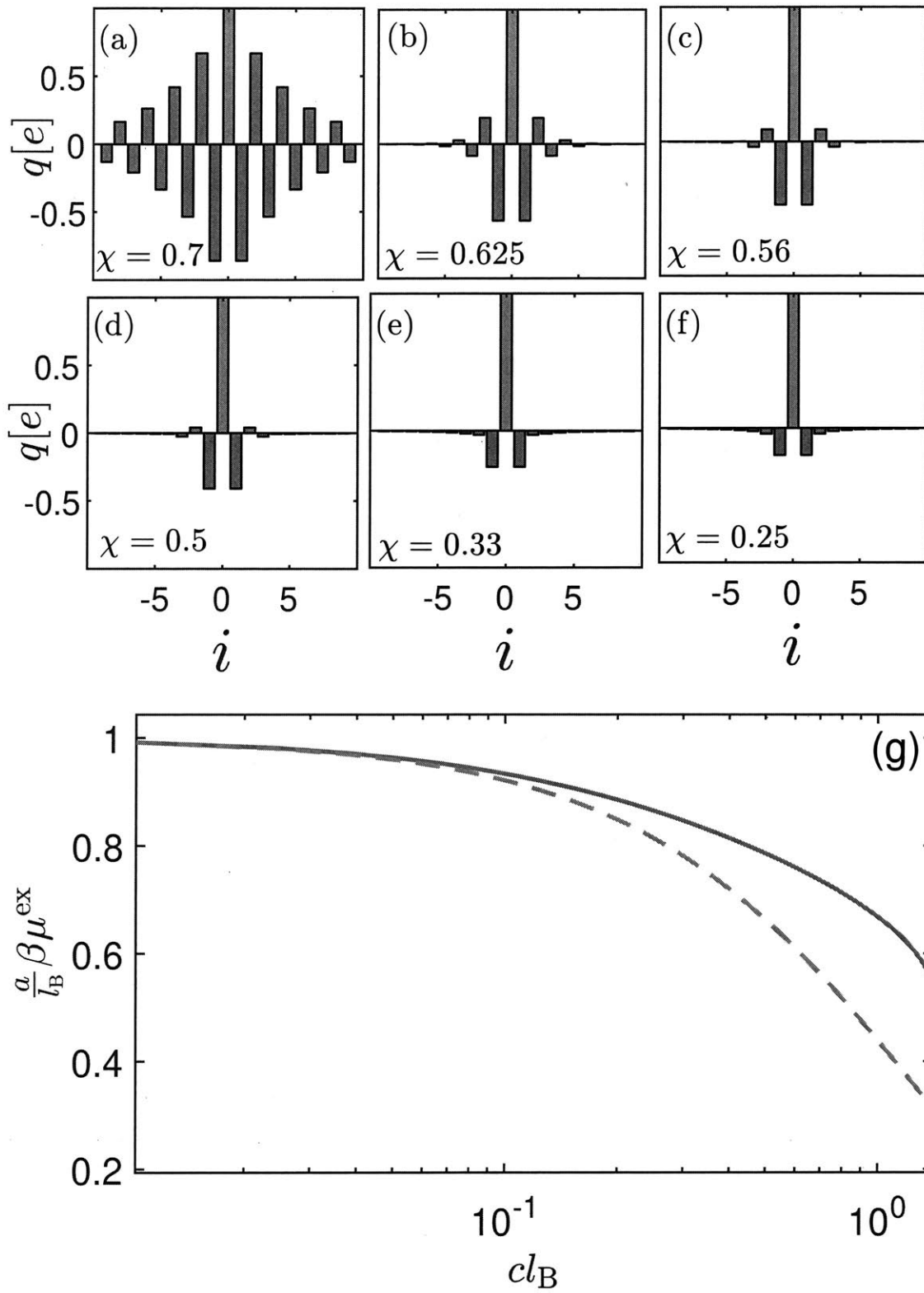


Figure 2-7: Charge distribution around a central ion and the resulting activity coefficient, for different concentrations. (a-f) Charge distribution around a central ion for six different coupling strengths ( $\chi$ ). For weak coupling, the central ion is screened only by oppositely charged ions (e-f). As the coupling increases, over screening and oscillations are observed. (g) Ionic activity in a nanopore, based on the exact 1D solution for the mean field equation (Eq. 2.45, solid blue line) and the dilute limit approximation (Eq. 2.46, dashed red line).

For a long chain ( $L \gg a$ ) the harmonic number can be expanded:

$$H_{L/a} \approx \log\left(\frac{L}{a}\right) + \gamma_{\text{Euler}} + \frac{a}{2L} + \dots, \quad (2.35)$$

If the external potential is due to a uniform charge distribution on the pore walls ( $Q$  per site), Eq. 2.34 becomes the following algebraic equation:

$$q = -\frac{2\Lambda \sinh\left[2\frac{l_B}{a} H_{\frac{L}{a}}(q+Q)\right]}{1 + 2\Lambda \cosh\left[2\frac{l_B}{a} H_{\frac{L}{a}}(q+Q)\right]}, \quad (2.36)$$

In the dilute limit, this equation has a similar form to Eq. 2.22. As the external charge increases, a maximal charge density of one charge per lattice site prevents an unphysical accumulation of charges inside the pore.

Limiting the 1d-ring equation to only uniform distributions explicitly neglects any ion-ion correlations. When ion-ion interactions are strong enough, the system will form a crystal structure. In contrast to the 3-dimensional case, where the PB equation cannot predict ordered structures, our 1d model can be easily extended to include the expected phase transition. To account for patterns of alternating signs, we generalize our argument and replace the constant charge density with the form:  $q_i = q_0 + q_1(-1)^i$ . Both uniform charge density and an alternating pattern are eigenvectors of the interaction matrix  $\tilde{\Phi}$ , where the eigenvalue of  $(-1)^i$  equals  $-2 \log 2$ . With this functional form we obtain a set of coupled non-linear algebraic equations, for the average charge at even/odd locations:

$$\begin{aligned} q_0 - q_1 &= -\frac{2\Lambda \sinh\left[-2q_1 \frac{l_B}{a} \log(2) + 2\frac{l_B}{a} H_{\frac{L}{a}}(q_0 + Q)\right]}{1 + 2\Lambda \cosh\left[2q_1 \frac{l_B}{a} \log(2) + 2\frac{l_B}{a} H_{\frac{L}{a}}(q_0 + Q)\right]} \\ q_0 + q_1 &= -\frac{2\Lambda \sinh\left[2q_1 \frac{l_B}{a} \log(2) + 2\frac{l_B}{a} H_{\frac{L}{a}}(q_0 + Q)\right]}{1 + 2\Lambda \cosh\left[-2q_1 \frac{l_B}{a} \log(2) + 2\frac{l_B}{a} H_{\frac{L}{a}}(q_0 + Q)\right]}, \end{aligned} \quad (2.37)$$

Exploring the space of solutions of Eq. 2.37 is shown as a phase diagram in Fig. 2-6,

for  $a = 5\text{\AA}$  and  $L = 100\text{\AA}$ . As long as the ion-ion correlations are weak, we recover the same behavior found in the continuum model, including electroneutrality breakdown in the dilute limit. However, we find another breakdown of electroneutrality in the high concentration limit. This is the oscillatory regime ( $q_1 > 0$ ). Since  $q_1 + q_0 < 1$ , an increase of oscillating term,  $q_1$ , has to come at the expense of the average term,  $q_0$ , and electroneutrality is broken. With an increase of external charge, oscillations are suppressed and electroneutrality is again favored. As shown in Fig. 2-6, the order-disorder phase boundary only weakly depends on the surface charge and can be evaluated analytically based on the  $Q = 0$  limit. In this limit the average charge is  $q_0 = 0$ , and the number of solutions is determined by a single algebraic equation:

$$q_1 = \frac{2\Lambda \sinh\left(2q_1 \frac{l_B}{a} \log 2\right)}{1 + 2\Lambda \cosh\left(2q_1 \frac{l_B}{a} \log 2\right)} \quad (2.38)$$

The RHS of Eq. (2.38) is monotonically increasing, starting from 0, and has a monotonically decreasing slope. Hence, a second solution is available only if the slope at  $q_1 = 0$  is greater than 1, which leads to a critical fugacity of:

$$\Lambda_{\text{cr}} = \frac{a}{4l_B \log 2 - 2a}. \quad (2.39)$$

The results in Fig. 2-6 are displayed in terms of the standard 3d system parameters. With a pore radius  $a$ , the surface charge density equals  $q_s = Q/(2\pi a^2)$ . The bulk ionic concentration is related to the fugacity  $c^{3D} = \Lambda/\pi a^3$ . The Gouy-Chapman length and the Debye length are defined as usual.

## 2.5.2 Charge Distribution around a Central Ion

Bulk oscillations are maintained only for concentrations beyond a critical concentration, with persisting long-range order. Slightly below the critical density, we expect temporary short ranged decaying oscillations, that will eventually be replaced by monotonic decaying fluctuations in the dilute limit. We show how this behavior

emerges with a standard Debye-Hückel approach, by solving for the charge distribution around a central ion.

We take advantage of the periodic boundary conditions, and constrain the  $i = 0$  site to have a charge  $Qe$  by adding a term  $\alpha e^2/a\varepsilon(q_0 - Q)$  to the free energy functional (Eq. 2.31), where  $\alpha e^2/a\varepsilon$  is a Lagrange multiplier. The resulting mean-field equation reads:

$$\mathbf{q} = -\frac{2\Lambda \sinh \left[ \frac{l_B}{a} \left( \tilde{\Phi} \mathbf{q} + \alpha \delta_{i,0} \right) \right]}{1 + 2\Lambda \cosh \left[ \frac{l_B}{a} \left( \tilde{\Phi} \mathbf{q} + \alpha \delta_{i,0} \right) \right]}, \quad (2.40)$$

which we solve in the linear Debye-Hückel regime:

$$q_i = -\alpha \left( \tilde{\Phi} + \chi^{-1} \right)_{i,j}^{-1} \delta_{j,0}, \quad (2.41)$$

where the coupling parameter  $\chi = \frac{2\Lambda l_B}{a}$  is defined as the ratio of ionic spacing ( $a/2\Lambda$ ) and the Bjerrum length. By the translation symmetry of the matrix  $\tilde{\Phi}_{ij} = \tilde{\Phi}_{|i-j|}$ , we find a closed-form expression in the discrete Fourier space:

$$q_i = \frac{\alpha}{4\pi} \int_{2\pi} d\omega \frac{\cos(\omega i)}{2 \log \left| 2 \sin \frac{\omega}{2} \right| - \chi^{-1}}, \quad (2.42)$$

where the normalization constant  $\alpha$  is set such that  $q_0 = Q$ . Note that the solution is only valid in the disordered phase, where  $\chi^{-1} > 2 \log 2$ , which coincides with the critical fugacity (Eq. 2.39) in uniformly charged nanopores if size effects are neglected ( $a \ll l_B$ ). Fig. 2-7 shows charge density profiles for different concentration, illustrating how Eq. 2.42 is able to capture both the dilute Coulomb gas limit and the onset of long-range ordering, and predict the transition from screening, to over screening and oscillations.

So far we assumed an infinitely long chain, that allowed us to get a closed-form solution in Fourier space (Eq. 2.42). As a consequence, the electroneutrality is guar-

anteed, and the total charge along the pore accumulates to 0:

$$\sum_{i=0}^{\infty} q_i = \alpha \lim_{\omega \rightarrow 0} \frac{1}{2 \log |2 \sin \frac{\omega}{2}| - \chi^{-1}} \rightarrow 0. \quad (2.43)$$

However, the decay rate is *very* slow, and the screening cloud extends many lattice sites. If we look at  $\tilde{q}(\omega)$ , the Fourier transform of  $q_i$ , we find a steep increase near  $\omega = 0$ , on its way to its maximal value at  $\omega = \pi$ . We evaluate its width by finding the frequency at which  $\tilde{q}(\omega)$  reaches half of its maximal height:

$$\frac{1}{2 \log |\Delta\omega| - \chi^{-1}} = \frac{1/2}{2 \log 2 - \chi^{-1}} \rightarrow \Delta\omega = 4e^{-\frac{\alpha}{4\lambda l_B}}. \quad (2.44)$$

Invoking the uncertainty principle, we conclude that the width of the screening cloud scales as  $e^{\frac{\alpha}{4\lambda l_B}}$ , in agreement with our scaling analysis (Eq. 2.8) and the electroneutrality condition (Eq. 2.18).

Finally, we use our explicit solution of the screening cloud to evaluate the activity coefficient. For this purpose, the electroneutrality breakdown plays only a minor role. Ignoring the finite length of the system, the Debye-Hückel activity coefficient can be written as an integral expression:

$$\beta\mu^{\text{ex}} = \frac{l_B}{a} \sum_i \frac{q_i}{i} = \frac{\alpha l_B}{2\pi a} \int_{2\pi} d\omega \frac{\log |2 \sin \frac{\omega}{2}|}{2 \log |2 \sin \frac{\omega}{2}| - \chi^{-1}}, \quad (2.45)$$

where  $\mu^{\text{ex}}$  is the excess chemical potential. In dilute systems we can expand the activity coefficient to lowest order in the coupling parameter  $\chi$ , and get:

$$\beta\mu^{\text{ex}} \approx -\frac{2\pi^2 l_B^2}{3a^2} \Lambda. \quad (2.46)$$

The activity coefficient in confinement is much smaller than the bulk value. As ions cross over to the nanopore, they effectively shed off their ionic screening cloud. For

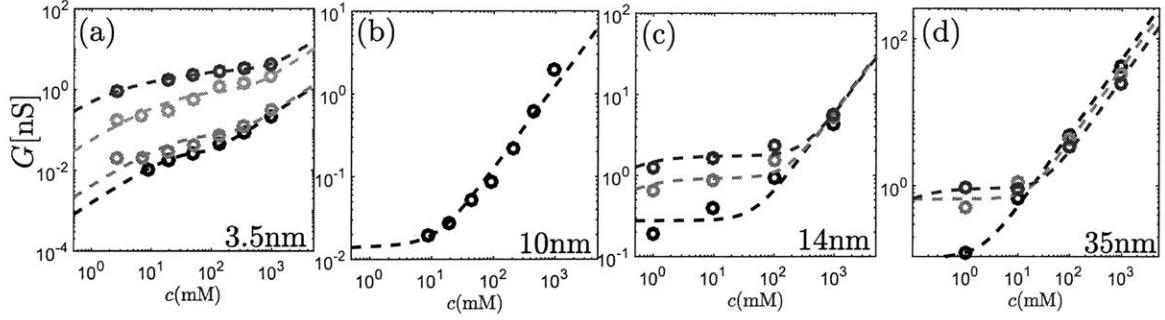


Figure 2-8: Conductance of a KCl solution as a function of concentration, inside CNT with varying surface charge and radii, fitted according to our model (dashed lines). The experimental data (circles) was adapted from [219], where the surface charge was controlled by changing the pH . (a) - A 3.5nm wide pore, fitted barrier energy of  $4.6k_B T$  and 4 different surface charges, from bottom to top:  $-3\text{mC/m}^2$  (black),  $-1.6\text{mC/m}^2$  (red),  $3.4\text{mC/m}^2$  (green),  $5.2\text{mC/m}^2$  (blue). (b) - A 10nm wide pore, with only one surface charge:  $12\text{mC/m}^2$ . (c) - A 14nm wide pore, with 3 different surface charge, fitted to:  $63\text{mC/m}^2$  (black),  $213\text{mC/m}^2$  (red) and  $417\text{mC/m}^2$  (blue). (d)- A 34nm wide pore, with fitted surface charge of:  $-7\text{mC/m}^2$  (black),  $55\text{mC/m}^2$  (red) and  $110\text{mC/m}^2$  (blue).

a nanopore of radius  $a$ , with bulk ionic concentration ( $c = \Lambda/\pi a^3$ ), the 1d activity is only a fraction of the bulk one:

$$\frac{\mu^{1D}}{\mu^{3D}} = \frac{\pi^2 a}{24 \lambda_D}, \quad (2.47)$$

where we used the standard Debye-Hückel activity coefficient,  $\beta\mu^{3D} = l_B/2\lambda_D$ .

As shown in Fig. 2-7, this approximation is only valid in the dilute limit. As concentration increases, screening and over-screening dominates the electrostatic interactions, and reduce the activity coefficient further.

## 2.6 Comparison with Experiments

### 2.6.1 Single Digit Nanopores

Our model predicts a non-trivial charge accumulation within the nanopore, due to the breakdown of electroneutrality, which has a direct implication on the measured conductivity of the pore. Assuming equal mobilities for all ions ( $\mu_D$ ), the conductance

of the pore is given by:

$$G = e^2 \mu_D \frac{\pi R^2}{L} c, \quad (2.48)$$

where the concentration,  $c$ , is related to the accumulated charge by Eq. 2.27. We compare our results with conductance measurements in carbon nanotubes (CNT), taken from Ref. [219]. It is important to note that the conductance behavior can be explained by different models. The CNT data was originally assumed to have a concentration-dependent surface charge and was later fitted by predicting the adsorption of hydroxyl ions to CNT pore walls ([25]). Our goal is not to underestimate the importance of a charge regulation mechanism, that can lead to concentration-dependent surface charge by affecting the adsorption rate ([68]), but to suggest a plausible alternative with a constant surface charge. We show that the 1d geometry by itself can lead to the variety of conductance curves observed in experiments.

Fig. 2-8 shows the conductance curves for CNTs with varying pore size and surface charge, as a function of KCl concentration. The experimental data were fitted according to Eq. 2.29, with three fitting parameters- the ionic mobility, surface charge, and energy barrier.

For the larger pore sizes, shown in Fig. 2-8(b-d), the energy barrier for entering the pore ( $E_{\pm}$ ) was neglected, and the fitted ionic mobilities were on the order of the bulk mobility of KCl, and varied from  $5 - 10 \times 10^{-8} \text{m}^2/\text{Vs}$ , compared to the bulk value of  $7.62 \times 10^{-8} \text{m}^2/\text{Vs}$  (see Fig. 2-10, bulk value of ionic mobility was taken from [165]). This effectively only leaves one fitting parameter to determine the shape of the curves- the surface charge. As surface charge increases, electroneutrality is maintained especially for the larger pore radii. The curve approaches a constant in the dilute limit (see top curves in figures 2-8c and 2-8d). However, for smaller surface charges, the apparent decrease in conductance in the dilute limit is due to electroneutrality breakdown.

In the narrow nanopore (Fig. 2-8a) the behavior is more complicated. First, a small energy barrier of  $\approx 2k_B T$  is needed to obtain the correct trend. This small

energy barrier is expected due to a lower dielectric constant inside the nanopores, related to the confinement of water. More importantly, the fitted mobility, in this case, is significantly higher: 12 times higher than bulk value for the lower two surface charges, and more than a 100 times greater for the high surface charge (Fig. 2-10). The large mobility in the high surface charge limit can be due to ion-ion correlations, where the positive charges push each other to move faster. It can also be related to enhanced water flow, due to an increased slip length [115, 248].

## 2.6.2 Sub-nanometer Channels

We conclude by applying our model to sub-nanometer channels, which is the relevant limit for ion channels in nature. The most prominent example of a biological nanochannel is the Gramicidin-A channel. With a pore diameter of about  $4\text{\AA}$ , it is truly a one-dimensional system. It is often described using Michaelis-Menten type conductance: ions which travel through a channel that connects reservoirs A and B are transitioning between three possible states ("A", "B" and "in channel"). This framework is successful since it naturally ignores any charge neutrality constraints. It predicts a linear dependence in dilute solutions and a saturation at high concentrations, limited by the maximal occupancy of the pore. Despite its good agreement with experimental data, it can only describe systems with a handful of ions. Continuum models, on the other hand, which are much better suited to handle numerous ions, cannot predict the dilute limit linear behavior as long as electroneutrality is assumed.

We consider two experimental datasets: a conductance measurement Gramicidin-A channel (taken from [83]), and more recent conductance measurement in a CNT porin experiment (taken from [239]). We fit the data according to Eq. 2.48 as before, with one important modification. As water molecules are excluded from these channels, the dielectric constant is now much smaller and was chosen to be  $\epsilon = 5$ .

As shown in Fig. 2-9, our model is able to capture both neutral (linear conductance) and charged (Michaelis-Menten conductance) sub-nanometer nanopore behavior. The plateau at high concentrations is not predicted, as our model fails in the concentrated regime. For higher concentrations, a more detailed picture of the (cou-

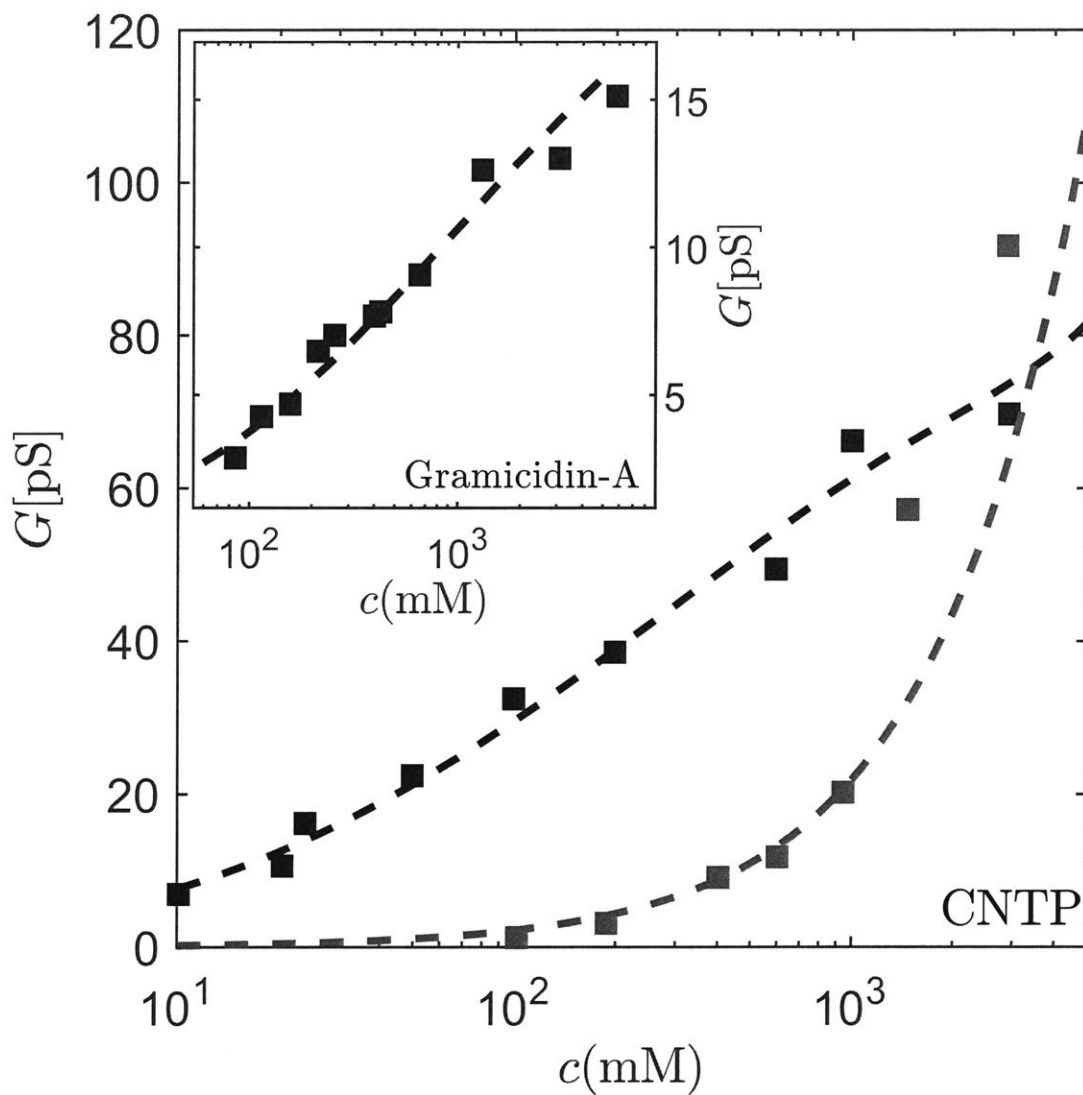


Figure 2-9: Conductance of sub-nanometer pores as a function of ionic concentration. Main figure: Conductance of a 3.5Å wide CNT porin as a function of KCl concentration (filled squares), adapted from [239] and fitted according to our model (dashed lines). The bottom curve (blue) has pH 3.5, which corresponds to zero charge, while the upper (black) curve has pH 7.5, and is fitted to a surface charge of  $6\text{mC}/\text{m}^2$ . Inset: conductance in Gramicidin-A channel as a function of NaCl concentration (filled squares, adapted from [83]) and its fit (dashed lines). The fitted surface charge is  $13\text{mC}/\text{m}^2$ .

pled) fluxes has to be accounted for and is beyond the scope of this thesis. As shown by the lattice model (see Fig. 2-6), ion-ion correlations can lead to a decrease in the total charge with increased concentration and eventually to an overall reduction in conductance.

The predicted energy barriers for both experiments were similar ( $5k_B T$ ). This energy is much smaller than the Born solvation energy in the vacuum, which might imply that dehydration is not complete, and is compensated by the interactions of ions with the pore walls. It is also smaller compared with energy barriers estimated by Michalis-Mentan type theories, which are of the order of  $10k_B T$  [113]. We note, however, that in order to keep the model simple, we assumed a constant energy difference between the pore and its surrounding. Entrance effects were smeared throughout the system, so a smaller energy barrier is expected. A more careful derivation is required to accurately separate the pore mouth contribution to transport.

Another interesting result is that the ionic mobility in GA is much lower compared to bulk water, while the CNT porins have higher mobility. The biological channel has fitted mobility of  $5.7 \times 10^{-9} \text{m}^2/\text{Vs}$  which is an order of magnitude less than the bulk ionic mobility (see Fig. 2-10). The CNTP fitted mobility is closer to bulk KCl and equals  $11 \times 10^{-9} \text{m}^2/\text{Vs}$  and  $50 \times 10^{-9} \text{m}^2/\text{Vs}$  for the neutral and charged pores, respectively. The reduced mobility compared to isolated ions in a solvent (water) can be understood from the strong attraction of ions and the opposite fixed wall charge and hence larger friction for relative motion. Our expression for conductance is derived based on a normal Nernst-Einstein relation with uncoupled fluxes of each ion. This is only valid for "pseudo binary" transport where each specie only interacts with an abundant solvent. Generally, the Stefan-Maxwell picture has a diffusion tensor with coupled fluxes between each pair of species [64, 15], and can be extended to a "dusty gas model," if wall molecules are treated as a fixed specie [76, 86].

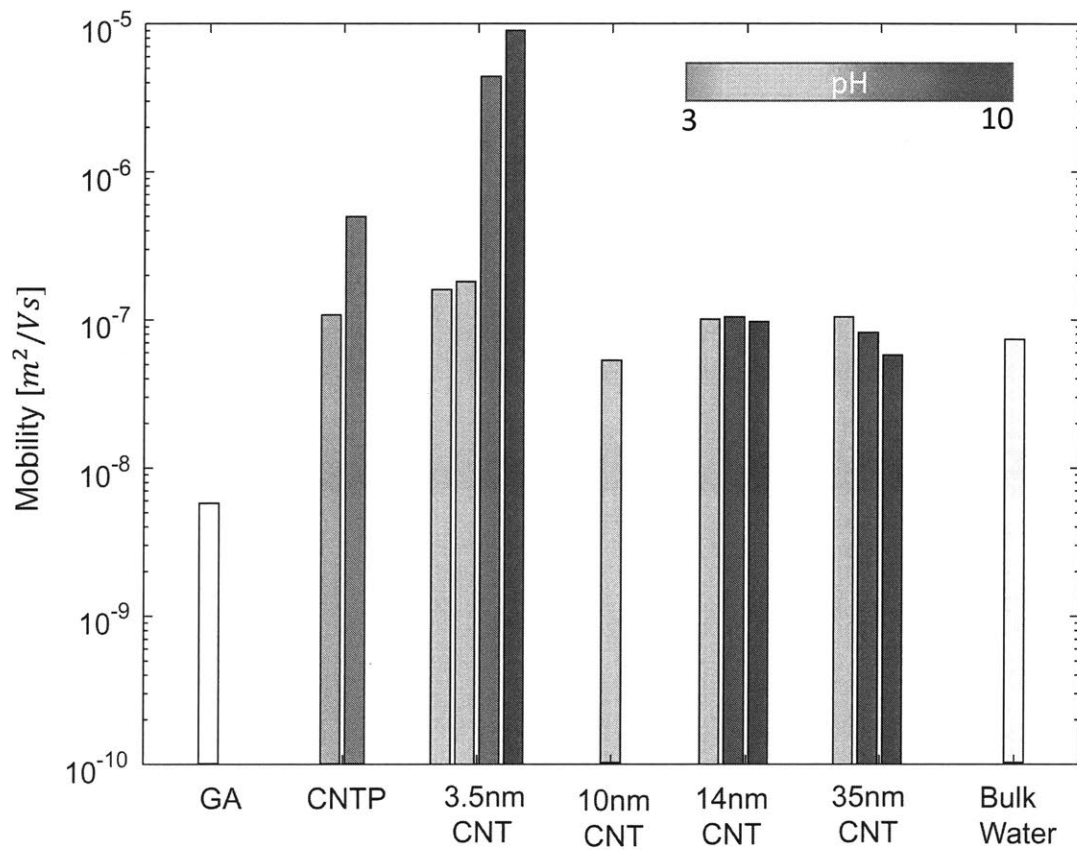


Figure 2-10: Fitted mobilities. The mobilities of 6 datasets, Gramicidin-A, CNT Porin, and 4 different CNT experiments, were fitted according to Eq. 2.48. Experimental data and fits are shown in Figs. 7-8. Each pH was fitted separately, and within each experiment the bins are ordered from low pH to high. The bulk value for KCl mobility (last column) was taken from [165]

## 2.7 Conclusions

We have analyzed ions in a 1d electrolyte interacting with 3d electrostatic interactions, which is the appropriate limit for single-digit nanopores. In 3d systems the fluctuations around electroneutrality are limited only to the microscopic length-scale. The strong Coloumbic cost of large-scale deviations is much greater than the thermal energy. In contrast, when ions are forced to reside along a line, even macroscopically-long charged chains can spontaneously form.

We first showed directly how the competition between electrostatic forces and entropy determines the screening length. In three dimensions we recover the classical Debye screening length, but in 1d we find an exponentially large screening length. We then developed two mean-field models and showed that when the screening length exceeds the length of the system, electroneutrality is broken. We predicted a phase diagram for the accumulated charge inside the pore, that depends on two length-scales: the Debye screening length and the Gouy-Chapman length. If both length-scales are larger than the pore diameter, the ions do not know about the 3d nature of the system, and electroneutrality is broken.

In our efforts to provide analytical results with a clear physical meaning, we neglected several important aspects of the problem. Most notably, our models fail to account for the polarization charge induced by a discontinuity of the dielectric constant. A large mismatch in the dielectric constant can alter ion-ion interactions inside the pore[159, 38], and can lead, for example, to a 1d Coulomb interactions in short nanopores[256]. Molecular dynamics studies have shown that the interactions with images forces are especially relevant for selectivity in ion channels [34, 33, 35]. Selectivity is also sensitive to the size of the ions, and a proper theory of confined electrolytes must include finite size effects.

Within the uniform embedded pore model, we derived approximated but accurate closed-form expressions for the expected charge and ionic concentration inside a charged pore, and the resulting ionic conductance. With two fitting parameters, the surface charge and ionic mobility, we were able to fit a wide range of conductance

curves in narrow nanopores. We interpret the unusual scaling behavior observed as a consequence of the breakdown of electroneutrality.

While transport measurements are an extremely useful tool for studying nanopores, inferring the ionic concentrations is a difficult task. Ion-ion, ion-water and water-pore interactions all play a role in the complicated transport phenomena. A more complete description that explicitly accounts for water flow is required to correctly predict the conductance. Moreover, the mobility of the ions may vary under confinement and composition[74, 67], and the linear relation with concentration is only appropriate in infinite dilution.

Another important aspect of ionic transport, especially relevant to short nanopores, are entrance effects and access resistance. The transition from a microchannel to a nano-channel adds additional resistance to the system, and the access resistance decreases with increasing concentration, which is an alternative explanation for the scaling observed in the conductance, as argued in recent papers[101, 100]. The entrance effects are of even greater importance if charges are added to the pore mouth, for example, to increase selectivity[57, 50, 99].

With current available data, we cannot rule out alternative explanations to describe the scaling and shape of the conductance curves. However, as concentration decreases, our predictions deviate substantially from other models. For example, we predict a linear conductivity in the very dilute limit, and not a plateau. Experiments with a wider range of dilute concentrations are therefore needed to correctly identify the key mechanism.

Added complexities are surely required to adequately describe the transport of ions through nanopores. In the next chapter we relax some of our simplifying assumptions and build a more general theory of transport. Yet, as extremely long and narrow nanopores become technologically accessible, determining their net charge is a crucial first step. In our quest to understand the physics of single-digit nanopores, we highlight a simple but consequential observation on the nature of geometrical confinement: it breaks charge neutrality.



# Chapter 3

## Transport in nanopores

In the previous chapter, we concluded that the 1d nature of narrow channels has profound implications on the transport properties of nanopores, especially in the "Single Digit" regime. In particular, we found that due to exponentially long screening length, the widely held assumption that charged nanopores are overall neutral is broken. We derived an approximated algebraic equation for the overall charge in the channel and used it in a linear model of conductance to illustrate how a peculiar scaling behavior emerges under these conditions.

To simplify our model and obtain closed-form expressions, we neglected the charge density profile inside the nanopore and assumed that charges are uniformly distributed in a "Uniform Embedded Pore" (UEP) model. In this chapter, we go beyond the UEP model and account for non-uniform charge density. This allows us to obtain a much more accurate description of the conductivity, to couple it with the electro-osmotic flow, and even consider a coupling between the fluxes of the anions and cations.

### 3.1 Equilibrium Density Profile: The Consequence of Electroneutrality Breakdown

Let us first start by finding an exact solution for the density profile of ions inside a channel. While this is going to be slightly cumbersome, it will allow us to estimate

the validity of different approximated schemes. An ionic channel, connected in both ends to a reservoir with a binary monovalent ionic solution with concentration  $c_0$ , and embedded in a dielectric matrix is depicted in Fig. 3-1. Denoting the dielectric constant inside the channel  $\varepsilon_{\text{in}}$  and the permittivity of the outer matrix  $\varepsilon_{\text{out}}$ , the electrostatic potential ( $\phi$ ) is described by a set of Laplace and Poisson-Boltzmann equations (see discussion in the previous chapter):

$$\varepsilon_{\text{in}} \nabla^2 \phi(\mathbf{r}) = \begin{cases} 2ec_0 \sinh(e\beta\phi) & r < R, 0 < z < L, \\ 0 & \text{else,} \end{cases} \quad (3.1)$$

where  $R$  is the radius of the channel,  $L$  its length and  $\beta = 1/k_{\text{B}}T$  is the inverse temperature. Assuming a fixed charge density  $q_s$  on the channel walls, the boundary conditions are:

$$[\varepsilon_{\text{out}} \partial_r \phi_{\text{out}}(R, z) - \varepsilon_{\text{in}} \partial_r \phi_{\text{in}}(R, z)] = -q_s (0 < z < L) \quad (3.2)$$

Remarkably, despite numerous theoretical investigations of ionic channels, there is currently no analysis of this simple and fundamental problem, to the best of our knowledge. In many cases, this problem is oversimplified by disregarding the outer dielectric matrix[25, 201, 102, 77, 212]. As shown in the previous chapter, this assumption is only valid for either large charge densities or wide channels.

This set of PDEs can only be solved numerically, for example using software such as COMSOL. Fig. 3-1(e-f) shows an example of such numerical simulation for a nanopore configuration and the resulting electric field in a plane crossing the cylinder<sup>1</sup>. Note that there is a significant 'leakage' of the electric field into the dielectric matrix, demonstrating the invalidity of the local electroneutrality assumption.

---

<sup>1</sup>This simulation was performed by Pedro J. de Souza and was adopted with permission

### 3.1.1 An Exact Solution for Weakly Charged Cylinders

While generally, we are only able to find numerical solutions to the charge distribution of ionic channels, we show here the solution for a weakly charged cylinder, in the form of an infinite sum. Two key simplifications allow us to achieve an analytical result. First, we are interested in the limit of weakly charged pores, allowing us to use the Debye-Huckel approximation. Second, following [16], we also imposed that the potential vanishes at the ends of the cylinder. The second assumption would limit this solution to the small aspect ratio limit where end-effects are negligible.

The set of Debye-Huckel and Laplace equations, derived by linearizing Eq. 3.1, are:

$$\begin{cases} \nabla^2 \phi_{\text{in}}(\mathbf{r}) = \lambda_D^{-2} \phi_{\text{in}}(\mathbf{r}) & r < R \\ \nabla^2 \phi_{\text{out}}(\mathbf{r}) = 0 & r > R, \end{cases} \quad (3.3)$$

where  $\lambda_D = \sqrt{2c_0 e^2 / \varepsilon_{\text{in}} k_B T}$ . The full set of boundary conditions in this geometry read:

$$\begin{aligned} [\phi_{\text{out}}(R, z) - \phi_{\text{in}}(R, z)] &= 0 \\ [\varepsilon_{\text{out}} \partial_r \phi_{\text{out}}(R, z) - \varepsilon_{\text{in}} \partial_r \phi_{\text{in}}(R, z)] &= -q_s (0 < z < L) \\ \phi_{\text{out}}(\mathbf{r})|_{r \rightarrow \infty} &= 0 \\ \phi_{\text{in}}(R, z = 0) = \phi_{\text{out}}(R, z = 0) &= 0 \\ \phi_{\text{in}}(R, z = L) = \phi_{\text{out}}(R, z = L) &= 0. \end{aligned} \quad (3.4)$$

Taking advantage of the azimuthal symmetry, we can write the inner and outer solutions as an infinite sum:

$$\begin{aligned} \phi_{\text{in}}(r, z) &= \sum_{n=1}^{\infty} A_n \sin(\omega_n z) I_0(\sqrt{\omega_n^2 + \kappa_D^2} r) \\ \phi_{\text{out}}(r, z) &= \sum_{n=1}^{\infty} B_n \sin(\omega_n z) K_0(\omega_n r), \end{aligned} \quad (3.5)$$

where  $\kappa_D = 1/\lambda_D$  is the inverse Debye length,  $I_0(x)$  and  $K_0(x)$  are the 0<sup>th</sup> order modified Bessel function of first and second kind, respectively, and  $\omega_n = \pi n/L$ . Note that we wrote the solution in a manner that satisfies the last three boundary conditions. To find  $A_n$  and  $B_n$ , we plug in the expansion to the first two boundary conditions, where the second boundary condition is expanded in a similar way:

$$[\varepsilon_{\text{out}}\partial_r\phi_{\text{out}}(R, z) - \varepsilon_{\text{in}}\partial_r\phi_{\text{in}}(R, z)] = -q_s \sum_{n\text{ odd}} \frac{4 \sin(\omega_n z)}{\omega_n L}. \quad (3.6)$$

Clearly, for even  $n$  we have  $A_n = B_n = 0$ . For odd  $n$ , we obtain the following equations for the expansion coefficients:

$$\begin{aligned} A_n I_0(\sqrt{\omega_n^2 + \kappa_D^2} R) &= B_n K_0(\omega_n R), \\ A_n \varepsilon_{\text{in}} \sqrt{\omega_n^2 + \kappa_D^2} I_1(\sqrt{\omega_n^2 + \kappa_D^2} R) &= -B_n \varepsilon_{\text{out}} \omega_n K_1(\omega_n R) + \frac{4q_s}{\omega_n L}. \end{aligned} \quad (3.7)$$

Finally, we get:

$$\begin{aligned} \phi_{\text{in}}(r, z) &= \frac{2q_s}{L} \sum_{n\text{ odd}} \frac{1}{\omega_n \varepsilon_{\text{out}} \sqrt{\omega_n^2 + \kappa_D^2} K_0(\omega_n R) I_1(\sqrt{\omega_n^2 + \kappa_D^2} R) + \varepsilon_{\text{out}} \omega_n I_0(\sqrt{\omega_n^2 + \kappa_D^2} R) K_1(\omega_n R)} \frac{K_0(\omega_n R) \sin(\omega_n z) I_0(\sqrt{\omega_n^2 + \kappa_D^2} r)}{\omega_n \varepsilon_{\text{out}} \sqrt{\omega_n^2 + \kappa_D^2} K_0(\omega_n R) I_1(\sqrt{\omega_n^2 + \kappa_D^2} R) + \varepsilon_{\text{out}} \omega_n I_0(\sqrt{\omega_n^2 + \kappa_D^2} R) K_1(\omega_n R)}, \\ \phi_{\text{out}}(r, z) &= \frac{2q_s}{L} \sum_{n\text{ odd}} \frac{1}{\omega_n \varepsilon_{\text{out}} \sqrt{\omega_n^2 + \kappa_D^2} K_0(\omega_n R) I_1(\sqrt{\omega_n^2 + \kappa_D^2} R) + \varepsilon_{\text{out}} \omega_n I_0(\sqrt{\omega_n^2 + \kappa_D^2} R) K_1(\omega_n R)} \frac{K_0(\omega_n r) \sin(\omega_n z) I_0(\sqrt{\omega_n^2 + \kappa_D^2} R)}{\omega_n \varepsilon_{\text{out}} \sqrt{\omega_n^2 + \kappa_D^2} K_0(\omega_n R) I_1(\sqrt{\omega_n^2 + \kappa_D^2} R) + \varepsilon_{\text{out}} \omega_n I_0(\sqrt{\omega_n^2 + \kappa_D^2} R) K_1(\omega_n R)}. \end{aligned} \quad (3.8)$$

As shown in Fig. 3-1(b-d) there is a remarkable match between the numerical COMSOL solutions and the analytical solution, which improves as the length of the channel increases. Yet, even in very short channels our solution only slightly deviates from the full numerical analysis.

## 3.2 The "Electric Leakage" Boundary Condition

From a computational standpoint, the exact solution is much more tractable compared with the numerical investigation of a 3D problem. Moreover, the exact solution accuracy increases with increased aspect ratio, since end effects become negligible for very long and narrow pores. This regime is most challenging for a numerical solver, and analytical results are of value.

Yet, from a theoretical viewpoint, an infinite sum does not illuminate the physics of the system. In this section, we explore new boundary conditions, that are much more accurate compared with the local electroneutrality assumption, but it is just as simple. For pedagogical reasons, let us start our discussion not with a channel (a cylinder) but instead we return to the "toy model" of a spherical cavity presented in the previous chapter.

### 3.2.1 The "Electric Leakage" Boundary Condition in a Spherical Cavity

When ions are confined to a small region in space, separated by a charged surface from an external dielectric matrix, the outer region can play an important role. Within the mean-field approximation, one should account for both regions by solving a combination of the Poisson-Boltzmann (PB) equation inside the confined electrolyte, and the Laplace equation in the dielectric medium.

In some highly symmetric cases, however, we can simplify matters significantly by replacing the Laplace equation with a boundary condition for the PB equation. In a spherical cavity, the radial symmetry dictates that the outer electric electrostatic potential has a simple form:  $\phi = Q_{\text{total}}/4\pi\epsilon r$ , where  $Q_{\text{total}}$  is the total charge enclosed in a sphere of radius  $r$ . The radial component of the electric field in the outer region is hence:

$$E_r = -\partial_r\phi(r) = \frac{Q_{\text{total}}}{4\pi\epsilon r^2} = \frac{\phi}{r}. \quad (3.9)$$

Note that Eq. 3.9 only requires radial symmetry, and describes both the inner and

outer regions of the sphere. Using the continuity of the potential at the surface, we can relate the electrostatic potential and electric field inside as well. If we consider an electrolyte confined to a sphere of radius  $R$ , with a dielectric constant  $\varepsilon_{\text{in}}$ , separated by a wall with surface charge  $q_s$  from a dielectric matrix with permittivity  $\varepsilon_{\text{out}}$  we find the following boundary condition to hold:

$$\begin{aligned}
[\varepsilon_{\text{out}}\partial_r\phi_{\text{out}}(R, z) - \varepsilon_{\text{in}}\partial_r\phi_{\text{in}}(R, z)] &= \\
\left[-\varepsilon_{\text{out}}\frac{\phi_{\text{out}}}{R}(R, z) - \varepsilon_{\text{in}}\partial_r\phi_{\text{in}}(R, z)\right] &= \\
\left[-\varepsilon_{\text{out}}\frac{\phi_{\text{in}}}{R}(R, z) - \varepsilon_{\text{in}}\partial_r\phi_{\text{in}}(R, z)\right] &= -q_s,
\end{aligned}
\tag{3.10}$$

where we used the continuity of the electrostatic potential to get a Robin-type boundary condition that does not require us to solve separately the outer region.

### 3.2.2 The "Electric Leakage" Boundary Condition in a Nanopore

A similar idea can be applied for a nanopore cylindrical geometry. In this case, we use the azimuthal symmetry and convert the solution of the Laplace equation in the dielectric matrix to a boundary condition inside the electrolyte. This "trick", however, only works in the limit of small aspect ratios, which is the relevant limit for long and narrow nanopores. As we know (see the previous chapter), a truly infinite channel guarantees electroneutrality and vanishing electric fields outside. It is, therefore, useful to find the lowest order correction in the aspect ratio. Since the outer region satisfies the Laplace equation, and as long as we have azimuthal symmetry, the electrostatic potential at the surface can be written as the following sum:

$$\phi_{\text{out}}(R, z) = \sum_{n=1}^{\infty} B_n \sin\left(n\pi\frac{z}{L}\right) K_0\left(n\pi\frac{R}{L}\right),
\tag{3.11}$$

Note that we are not limited to the linearized DH region as in in Appex. A. In the limit  $L \gg R$ , the modified Bessel function is approximated to lowest order:

$$\begin{aligned} \phi_{\text{out}}(R, z) &= - \sum_{n=1}^{\infty} B_n \sin\left(n\pi \frac{z}{L}\right) \left( \log\left(\frac{n\pi R}{2L}\right) + \gamma_{\text{Euler}} \right) \\ &+ O\left(\left(\frac{R}{L}\right)^2 \log\left(\frac{R}{L}\right)\right), \end{aligned} \quad (3.12)$$

where  $\gamma_{\text{Euler}} \approx 0.577$  is Euler's constant. We note that to lowest order in  $\log(L/R)$  we find:

$$\log\left(\frac{n\pi R}{2L}\right) = \log\left(\frac{\pi R}{2L}\right) + \log(n) \approx \log\left(\frac{\pi R}{2L}\right). \quad (3.13)$$

which leads to the following approximation for the electrostatic potential:

$$\phi_{\text{out}}(R) \approx M_{L/R} \sum_{n=1}^{\infty} B_n \sin(\omega_n z), \quad (3.14)$$

where  $M_{L/R}$  is defined as:

$$M_{L/R} = \log\left(\frac{2L}{\pi R}\right) - \gamma_{\text{Euler}}. \quad (3.15)$$

Our next step is to relate the derivative of the potential to the potential itself, which will allow us to mask the solution as a boundary condition. Taking the first derivative of the electrostatic potential we obtain:

$$\partial_r \phi_{\text{out}}(R, z) = - \sum_{n=1}^{\infty} B_n \omega_n K_1(\omega_n R) \sin(\omega_n z). \quad (3.16)$$

Luckily, we find that to lowest order ( $K_1(x) \approx 1/x$ ) it is indeed proportional to the electrostatic potential:

$$\partial_r \phi_{\text{out}}(R, z) \approx - \sum_{n=1}^{\infty} B_n \frac{\sin(\omega_n z)}{R} = - \frac{\phi_{\text{out}}(R, z)}{M_{L/R} R}. \quad (3.17)$$

Finally, assuming a surface charge on the pore walls ( $q_s$ ), we get a new boundary condition for nanopores:

$$\partial_r \phi_{in}(R) = \frac{q_s}{\epsilon_{in}} - \frac{\epsilon_{out}}{\epsilon_{in}} \frac{\phi_{in}(R)}{RM_{L/R}}. \quad (3.18)$$

In Fig. 3-1 we compare the solution of the Poisson-Boltzmann equation with this new boundary condition to the full analytical solution (Eq. 3.8), as well as the approximated UEP model presented in the previous chapter (Eq. 2.17) and a numerical COMSOL simulation. Note our comparison is for weakly charged pores, but the "electric leakage" boundary condition applies more generally. Fixing the radius of the pore to 5nm, we change the length of the pore from 20nm to 100nm. Interestingly, our boundary conditions work well even for an aspect ratio as large as 1/4. We further note that all approximated schemes work well in the dilute region. Moreover, the UEP model actually *underestimates* the amount of neutrality breakdown.

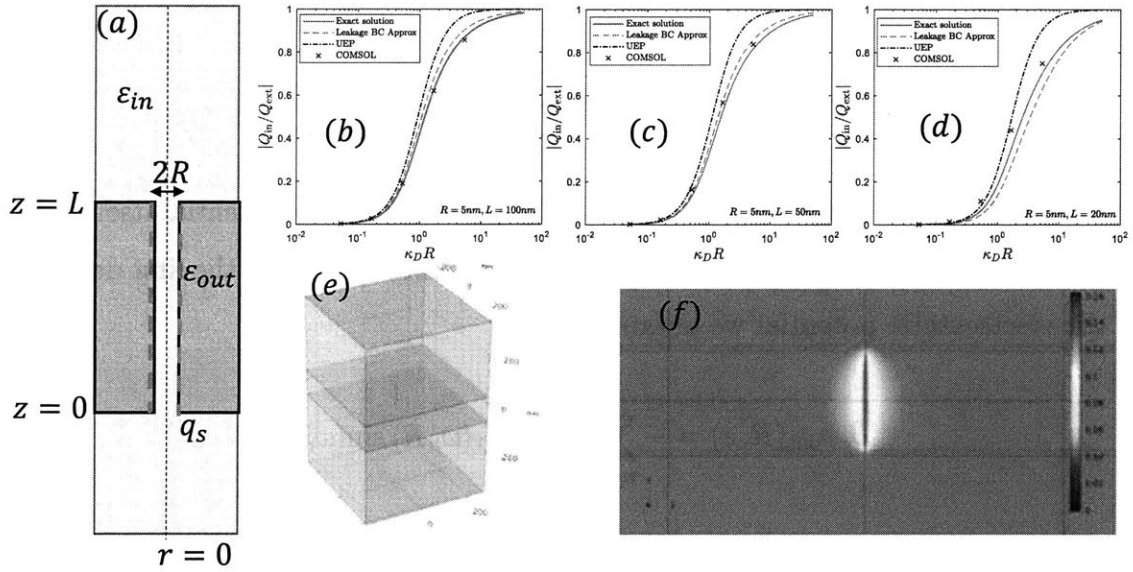


Figure 3-1: Electroneutrality breakdown in nanopores: simulations, exact analytical results and approximated schemes. (a) illustration of the nanopore configuration, a narrow channel connected to two reservoirs, and surrounded by a dielectric matrix with different permittivity. (b-d) Electroneutrality breakdown (ratio of ionic charge to surface charge) calculated for a pore with  $R = 5\text{nm}$ , and  $L = 100\text{nm}$  (b),  $L = 50\text{nm}$  (c) and  $L = 20\text{nm}$  (d). Results are based on the UEP model (2.14), dot-dash black line), solution of the PB equation with "electric leakage" boundary conditions (3.18, dashed red line), exact solution (3.8, solid blue line) and COMSOL simulation (black X). (f) An illustration of COMSOL simulation box. (e) A cross section of the electric field found by the numerical simulation in the nanopore.

## Charge Regulation and Energy Barriers

We conclude this section by modifying the boundary conditions to include two additional mechanisms that can potentially govern the number of ions in the channel: charge regulation and energy barrier.

As shown in the previous chapter, asymmetry in the affinity of ions to the channel is indistinguishable from surface charge. It worth stressing that this is a direct implication of electroneutrality breakdown, and has significant consequences for the selectivity of the channel. Let us now incorporate this effect into the "electric leakage" boundary condition. We introduce a uniform energy penalty for ions to be inside the pore, denoted by  $E_{\pm}$ , leading to the following Poisson-Boltzmann equation:

$$\varepsilon_{\text{in}} \nabla^2 \phi(\mathbf{r}) = ec_0 \exp(-\beta E_+ + e\beta\phi(\mathbf{r})) - ec_0 \exp(-\beta E_- - e\beta\phi(\mathbf{r})). \quad (3.19)$$

Defining an effective ionic concentration  $c^* = c_0 \exp[-\beta(E_+ + E_-)/2]$ , and denoting the energy difference as  $\Delta = E_+ - E_-$ , we can rewrite Eq. 3.19:

$$\begin{aligned} \varepsilon_{\text{in}} \nabla^2 \phi(\mathbf{r}) &= 2c^* \exp(\beta E_-/2 - \beta E_+/2 + e\beta\phi(\mathbf{r})) - ec^* \exp(\beta E_+/2 - \beta E_-/2 - e\beta\phi(\mathbf{r})) \\ &= 2ec^* \sinh \left[ \beta \left( e\phi(\mathbf{r}) - \frac{\Delta}{2} \right) \right]. \end{aligned} \quad (3.20)$$

Finally, by shifting the reference potential by  $\phi^* = \phi - \Delta/2e$  we obtain the standard PB equation:

$$\varepsilon_{\text{in}} \nabla^2 \phi^*(\mathbf{r}) = 2ec^* \sinh(\phi^*(\mathbf{r})). \quad (3.21)$$

The important difference, other than the re-scaled concentration, is that  $\phi^*$  on the surface differs from the actual electrostatic potential. If electroneutrality is imposed, this difference is insignificant, as the boundary conditions are only on the derivative of the potential. However, in the more general case, we find the following, most general, boundary condition:

$$\partial_r \phi_{\text{in}}(R) = \frac{q_s}{\varepsilon_{\text{in}}} - \frac{\varepsilon_{\text{out}}}{\varepsilon_{\text{in}}} \frac{(\phi_{\text{in}}(R) + \Delta/2e)}{RM_{L/R}}. \quad (3.22)$$

Let us now extend the boundary condition to describe a surface of ionizable charges rather than a fixed charge. For ionizable charges, the electrostatic potential at the surface changed the chemical potential and the binding probability of ions to the wall. This process is best described with a site-binding model, assuming the surface has  $N$  possible ionizable sites, which leads to a Langmuir 1-pK adsorption isotherm [25, 219, 240, 13]:

$$q_s = -eN \frac{1}{1 + 10^{pK - pH_\infty} \exp(-e\beta\phi(R))}, \quad (3.23)$$

where  $pH_\infty$  is the pH of the bulk reservoir, and  $pK$  describe the affinity of ions to the surface. Replacing  $q_s$  in Eq. 3.22 yields the most general boundary conditions for the Poisson-Boltzmann equation in nanopores:

$$\partial_r \phi_{\text{in}}(R) = \frac{1}{\varepsilon_{\text{in}}} \frac{-eN}{1 + 10^{pK^* - pH_\infty} \exp(-\phi(R))} - \frac{\varepsilon_{\text{out}} (\phi_{\text{in}}(R) + \Delta/2e)}{\varepsilon_{\text{in}} R M_{L/R}}. \quad (3.24)$$

where  $K^* = K^* + \beta\Delta \log_{10}(e)/2$  is a re-scaled association parameter.

### 3.2.3 Revisiting the Poisson-Boltzmann Equation

Equipped with the new boundary conditions, we can easily find numerical solutions to describe the charge density profile in nanopores. In this section, we explore three limiting cases where exact analytical solutions are available: the linear Debye-Huckel (DH) approximation, one-component plasma, and uniform embedded pore.

#### The Debye-Huckel Approximation

In Section 2 we derived an exact analytical solution for the case of weak surface charges, in the form of an infinite series. Let us now calculate the electrostatic potential under the same conditions by solving the DH equation (Eq. 3.3) using the "electric leakage" boundary conditions. Note that the "electric leakage" boundary conditions do not depend on  $z$ , and our solution is only in the radial direction.

The most general solution for the DH with radial symmetry reads, that does not

diverge at  $r = 0$  reads:

$$\phi(r) = AI_0(\kappa_D r), \quad (3.25)$$

where  $A$  is a parameter to be found,  $I_0$  is the zeroth-order modified Bessel function of the first kind. Setting the boundary condition of Eq. 3.18 we find:

$$A\kappa_D I_1(\kappa_D R) = \frac{q_s}{\varepsilon_{\text{in}}} - A \frac{\varepsilon_{\text{out}}}{\varepsilon_{\text{in}}} \frac{I_0(\kappa_D R)}{RM_{L/R}}. \quad (3.26)$$

Solving for  $A$ , we find that the electrostatic potential equals:

$$\phi(r) = \frac{q_s R}{\varepsilon_{\text{in}}} \frac{I_0(\kappa_D r)}{\kappa_D R I_1(\kappa_D R) + \varepsilon_r \frac{I_0(\kappa_D R)}{M_{L/R}}}, \quad (3.27)$$

where  $\varepsilon_r = \varepsilon_{\text{out}}/\varepsilon_{\text{in}}$  is the relative permittivity between inner and outer regions. The total charge inside the nanopore equals:

$$Q_{\text{in}} = -Q_{\text{ext}} \frac{1}{1 + \frac{\varepsilon_{\text{out}}}{\varepsilon_{\text{in}}} M_{L/R}^{-1} \frac{I_0(\kappa_D R)}{(\kappa_D R) I_1(\kappa_D R)}} \quad (3.28)$$

## One-component Plasma

A second interesting example to look at is the one-component plasma (OCP). Note we are considering OCP in the grand-canonical ensemble, where the number of ions is not known. Without allowing for electroneutrality to break, the number of counter-ions is just fixed by the surface charge. In the grand-canonical framework, the OCP limit is also the limit of large electrostatic fields ( $|e\beta\phi| \gg 1$ ) of the PB equation (Eq. 3.1):

$$\frac{1}{r} \frac{\partial}{\partial r} [r \partial_r e\beta\phi(r)] = \frac{\lambda_D^{-2}}{2} e^{e\beta\phi(r)}. \quad (3.29)$$

We are interested in finding the total charge that accumulates in the pore. Generally, this charge can be smaller, greater or equal to the surface charge in its magnitude. To find the charge, we only need to know the electric field on the surface. We start by multiplying the two sides of Eq. 3.29 by  $r^2 \partial_r e\beta\phi(r)$ , integrate from 0 to  $R$  and

using integration by parts:

$$\begin{aligned} \int_0^R dr [r\partial_r e\beta\phi(r)] \frac{\partial}{\partial r} [r\partial_r \phi(r)] &= \frac{\kappa_D^2}{2} \int_0^R e^{\beta\phi(r)} e\beta\phi'(r) r^2 dr. \\ \frac{1}{2} [R\partial_r e\beta\phi(R)]^2 &= \frac{(\kappa_D R)^2}{2} e^{\beta\phi(R)} - \kappa_D^2 \int_0^R e^{\beta\phi(r)} r dr, \end{aligned} \quad (3.30)$$

Inserting Eq. 3.29 to the second integral, we find the following relation between the potential and its derivative at the surface of the pore:

$$\begin{aligned} \frac{1}{2} [\partial_r e\beta\phi(R)]^2 &= \frac{(\kappa_D R)^2}{2} e^{\beta\phi(R)} - \kappa_D^2 \int_0^R \frac{\partial}{\partial r} [r\partial_r e\beta\phi(r)] dr \\ &= \frac{(\kappa_D R)^2}{2} e^{\beta\phi(R)} - 2 [R\partial_r e\beta\phi(R)] \end{aligned} \quad (3.31)$$

Together with the boundary condition (Eq. 3.18), we have set of two equations for the electrostatic potential and its derivative at the surface. The electrostatic potential at the surface is proportional to the total accumulated charge. The solution, in terms of  $Q_{\text{in}}$  reads:

$$\frac{Q_{\text{in}}}{Q_{\text{ext}}} = - \frac{W \left[ M_{L/R} \frac{(\kappa_D^{\text{out}} R)^2}{2} \exp \left( \frac{4\pi q_s l_B R}{e} \frac{\varepsilon_{\text{in}}}{\varepsilon_{\text{out}}} M_{L/R} \right) \right]}{\frac{4\pi q_s l_B R}{e} \frac{\varepsilon_{\text{in}}}{\varepsilon_{\text{out}}} M_{L/R}}. \quad (3.32)$$

where  $W$  is the Lambert  $W$ -function.

## Re-deriving the Uniform Embedded Pore model

In the previous chapter we derived the UEP model by explicitly considering the free energy of uniform pores, rather than starting from the usual PB equation. We now conclude this section by showing the UEP model can be directly derived from the PB equation with the "electric leakage" boundary conditions. We first replace the potential in the RHS of the PB equation with its volume average, as was shown in Eq. 2.16:

$$\nabla^2 e\beta\phi(\mathbf{r}) = \lambda_D^{-2} \sinh(\overline{e\beta\phi(\mathbf{r})}). \quad (3.33)$$

Note that the RHS in Eq. 3.33 is a constant, so the solution can be found by integrating the equation twice:

$$\phi(r) = \phi(0) + \frac{ec_0r^2}{2\varepsilon_{\text{in}}} \sinh(e\beta\overline{\phi(r)}) \quad (3.34)$$

Taking the volume average on both sides, we find an algebraic equation for  $\overline{\phi(r)}$ :

$$\overline{\phi(r)} = \phi(0) + \frac{3}{5} \frac{ec_0r^2}{2\varepsilon_{\text{in}}} \sinh(e\beta\overline{\phi(r)}) \quad (3.35)$$

To find  $\phi(0)$ , we use the boundary condition of Eq. 3.18. The potential and electric field at the surface read:

$$\begin{aligned} \phi(R) &= \phi(0) + \frac{ec_0R^2}{2\varepsilon_{\text{in}}} \sinh(e\beta\overline{\phi(r)}) \\ \partial_r\phi(R) &= \frac{ec_0R}{\varepsilon_{\text{in}}} \sinh(e\beta\overline{\phi(r)}). \end{aligned} \quad (3.36)$$

Together with the boundary conditions, we have a set of 4 equations with 4 unknowns ( $\phi(0)$ ,  $\phi(R)$ ,  $\partial_r\phi(R)$  and  $\overline{\phi(r)}$ ). The solution given by the following self-consistent equation for the average potential:

$$e\beta\overline{\phi} + \frac{\varepsilon_{\text{out}}}{\varepsilon_{\text{in}}} M_{L/R}(\kappa_D R)^2 \sinh(e\beta\overline{\phi}) = \frac{R}{2\pi\lambda_{\text{GC}}}. \quad (3.37)$$

where  $\lambda_{\text{GC}} = e/2\pi q_s l_B$  is the Gouy-Chapman length. This algebraic equation is equivalent to Eq. 2.22, that was written in terms of  $\overline{\rho} = 2ec_0 \sinh(e\beta\overline{\phi})$ .

### 3.3 Transport in Nanopores: Stefan-Maxwell Coupled Fluxes

Equipped with a new boundary condition that accurately describes equilibrium charge densities in pores, we can now revisit the transport of ions when a force (mechanical, chemical or electrical) is applied. We follow the classical derivation of the Poisson-Nernst-Planck equations[201], but include one additional component: coupling between the fluxes of the different species[27, 206, 15]. Similarly to the new boundary

conditions presented in the previous section, this will result in a small change to the formalism and a big impact on the predicted conductivity of narrow channels.

Qualitatively, incorporating the friction between the ionic species will serve as a possible mechanism of the saturation of current with increased ionic concentration. This is a well-known observation from biological ionic channels[83], but have been observed in synthetic channels as well[239]. At very small concentrations, only one ionic specie occupies the channel and can move freely. As concentration increases, the channel becomes less selective, and the two streams are moving in the opposite direction, limiting the overall flow.

### 3.3.1 Fickian vs Stephan-Maxwell Diffusion

In the previous chapter, we naively predicted that conductance is linear in concentration. This bulk conductance expression is based on Fick's law of diffusion, which is only suitable for dilute systems. When ions are confined to an extremely narrow channel, the fluxes of the positive and negative charges are necessarily coupled, and the appropriate framework is the Stefan-Maxwell's equations[166]:

$$\begin{aligned} c_+ \nabla \mu_+ &= \frac{k_B T}{c_+ + c_- + c_w} \left[ \frac{c_w c_+}{\mathcal{D}_{w+}} (\mathbf{v}_w - \mathbf{v}_+) + \frac{c_- c_+}{\mathcal{D}_{\pm}} (\mathbf{v}_- - \mathbf{v}_+) \right] \\ c_- \nabla \mu_- &= \frac{k_B T}{c_+ + c_- + c_w} \left[ \frac{c_w c_-}{\mathcal{D}_{w-}} (\mathbf{v}_w - \mathbf{v}_-) + \frac{c_- c_+}{\mathcal{D}_{\pm}} (\mathbf{v}_+ - \mathbf{v}_-) \right], \end{aligned} \quad (3.38)$$

where the  $\mathcal{D}_{w\pm}$  and  $\mathcal{D}_{\pm}$  are the water-ions and ion-ion diffusion coefficients,  $\mu_{\pm}$  are the chemical potential of the ions,  $c_{\pm}$  are the local ionic concentrations,  $\mathbf{v}_{\pm}$  are the ionic velocities and  $\mathbf{v}_w$  is the water velocity. Applying an electric field ( $\nabla \mu_{\pm} = \pm e \nabla \psi$ ), we solve the SM equations and obtain the following ionic current. Note that we use  $\psi$  to denote the small perturbation to the equilibrium electrostatic potential  $\phi$ . We assume here that this perturbation does not change the local density profile of the ions, which is determined by solving the Poisson-Boltzmann equation, as discussed in

the previous section. The ionic fluxes,  $\mathbf{j}_\pm = \pm ec_\pm \mathbf{v}_\pm$  read [15]:

$$\begin{aligned} \mathbf{j}_+ &= ec_+ \mathbf{v}_w - \frac{c_T c_+ \mathcal{D}_{w+} \mathcal{D}_{w-} (c_+ - c_-) + c_w \mathcal{D}_{w+} \mathcal{D}_\pm c_+}{c_w (c_- \mathcal{D}_{w+} + c_+ \mathcal{D}_{w-} + c_w \mathcal{D}_\pm)} \frac{e \nabla \phi}{k_B T}, \\ \mathbf{j}_- &= -ec_- \mathbf{v}_w + \frac{c_T c_- \mathcal{D}_{w+} \mathcal{D}_{w-} (c_+ - c_-) - c_w \mathcal{D}_{w-} \mathcal{D}_\pm c_-}{c_w (c_- \mathcal{D}_{w+} + c_+ \mathcal{D}_{w-} + c_w \mathcal{D}_\pm)} \frac{e \nabla \phi}{k_B T}. \end{aligned} \quad (3.39)$$

where  $c_T = c_w + c_+ c_-$  is the total concentration. The total ionic current then equals:

$$j_{\text{ch}}(\mathbf{r}) = \rho \mathbf{v}_w + \frac{c_T (\mathcal{D}_{w+c_+} + \mathcal{D}_{w-c_-}) + \frac{\mathcal{D}_- \mathcal{D}_+}{\mathcal{D}_\pm} (c_+ - c_-)^2}{c_w (1 + (\mathcal{D}_{w-c_+} + \mathcal{D}_{w+c_-})/\mathcal{D}_\pm)} \frac{\nabla \phi}{\phi_B}. \quad (3.40)$$

Let us now use the fact that the ionic concentration is Boltzmann distributed,  $c_\pm = c_0 \exp(-e\beta\phi)$ , to simplify the expression above. Note that any asymmetry in the diffusion coefficient is similar to a change in the local potential:

$$\begin{aligned} \mathcal{D}_{w+c_+} + \mathcal{D}_{w-c_-} &= c_0 [\mathcal{D}_{w+} \exp(e\beta\phi) + \mathcal{D}_{w-} \exp(-e\beta\phi)] \\ &= 2\sqrt{\mathcal{D}_{w+} \mathcal{D}_{w-}} c_0 \cosh \left[ e\beta\phi + \log \frac{\mathcal{D}_{w+}}{\mathcal{D}_{w-}} \right] \\ &= 2c_0 D_0 \cosh(e\beta\phi^*) \end{aligned} \quad (3.41)$$

where the  $D_0 = \sqrt{\mathcal{D}_{w+} \mathcal{D}_{w-}}$  is the average diffusion coefficient, and  $\phi^* = \phi + \phi_B \log \frac{\mathcal{D}_{w+}}{\mathcal{D}_{w-}}$  is the effective electrostatic potential. Similarly, we define  $\phi^{**} = \phi - \phi_B \log \frac{\mathcal{D}_{w+}}{\mathcal{D}_{w-}}$  to describe the effective potential in the denominator of Eq. 3.40. Finally, we get:

$$j_{\text{ch}}(\mathbf{r}) = \rho \mathbf{v}_w - 2D_0 c_0 \frac{c_T \cosh e\beta\phi^* + 2\chi \sinh^2 e\beta\phi}{c_w (1 + \chi \cosh e\beta\phi^{**})} \frac{\nabla \phi}{\phi_B} \quad (3.42)$$

where the coupling parameter  $\chi$  is defined as:

$$\chi = \frac{D_0}{\mathcal{D}_\pm}. \quad (3.43)$$

Note that as  $\chi \rightarrow 0$  we recover the usual Fickian diffusion which leads to a standard conductivity that is linear with concentration. In the opposite limit, the conductivity scales with the charge (squared) and is suppressed when we have an equal amount of positive and negative charges.

### 3.3.2 Electro-osmotic Flow: The Slip Length Approximation

To find the conductivity in the general case, we have to include the water flow as well. The ionic current, as shown in equations 3.42, depends on the velocity of the water. The velocity, in its turn, depends on the charge distribution. Since we are only considering transport in uniform pressure and concentration, we did not present the full linear electrokinetic theory. Nevertheless, we should keep in mind that we are only focusing on a particular setting of the full problem. Following Ref. [201], we use non-compressible Navier-Stokes equations to describe the laminar water flow:

$$\mu \nabla^2 u(x, r) - \rho(x, r) \nabla \psi(x, r) = 0 \quad (3.44)$$

$$\nabla \cdot u(x, r) = 0. \quad (3.45)$$

Note that the pressure gradient term was omitted. Two simple approximations for the boundary conditions of the water flow are either no-slip (see Ref. [201]) or a fixed slip-length ([175, 49]). It has been reported that nanochannels exhibit enhanced slip length[248, 174], so we will choose here the later boundary condition, defined as:

$$\partial_r v_w(x, r)|_{r=R} = \frac{1}{b} u|_{r=R}, \quad (3.46)$$

where  $b$  is the slip length. A second boundary condition is that  $\partial_r(x, r = 0) = 0$ . For a uniform flow in the axial direction, Eq. 3.44 reads:

$$\frac{1}{r} \frac{\partial}{\partial r} \left( r \frac{\partial v_x^w(r)}{\partial r} \right) = -\frac{2ec_0}{\mu} \sinh[e\beta\phi(r)] \frac{\partial \psi}{\partial x} \quad (3.47)$$

The PB equation satisfies the radial component of the potential,  $\phi(r)$ , so the NS equations are simplified:

$$\frac{1}{r} \frac{\partial}{\partial r} \left( r \frac{\partial u_x(r)}{\partial r} \right) = -\frac{\varepsilon}{\mu} \frac{1}{r} \frac{\partial}{\partial r} \left( r \frac{\partial \phi(r)}{\partial r} \right) \frac{\partial \psi}{\partial x}. \quad (3.48)$$

Integrating once from 0 to  $r$  yields:

$$\left( r \frac{\partial u_x(r)}{\partial r} \right) = \frac{\varepsilon}{\mu} \left( r \frac{\partial \phi(r)}{\partial r} \right) \frac{\partial \psi}{\partial x}. \quad (3.49)$$

Integrating once more from  $r$  to  $R$  reads:

$$v_x^w(r) - v_x^w(R) = \frac{\varepsilon}{\mu} (\phi(r) - \phi_w) \frac{\partial \psi}{\partial x}. \quad (3.50)$$

Applying a slip-length boundary condition we find that the velocity field inside the channel is proportional to the external electric field:

$$v_x^w(r) = \frac{\varepsilon}{\mu} [\phi(r) + (b\partial_r\phi_w - \phi_w)] \frac{\partial \psi}{\partial x}. \quad (3.51)$$

Hence, the total ionic current equals:

$$j_x(r) = \left[ \frac{2ec_0\varepsilon}{\mu} \sinh e\beta\phi [\phi(r) + (b\partial_r\phi_w - \phi_w)] + \frac{c_T c_0 D_0}{c_w \phi_B} \frac{\cosh e\beta\phi^* + 2\chi \sinh^2 e\beta\phi}{1 + \chi \cosh e\beta\phi^{**}} \right] \partial_x \psi(x). \quad (3.52)$$

Hence, we obtain Ohm's law with the following conductance:

$$G = 4\pi \int_0^R r dr \left[ \frac{2ec_0\varepsilon}{\mu} \sinh e\beta\phi [\phi(r) + (b\partial_r\phi_w - \phi_w)] + \frac{c_T c_0 D_0}{c_w \phi_B} \frac{\cosh e\beta\phi^* + 2\chi \sinh^2 e\beta\phi}{1 + \chi \cosh e\beta\phi^{**}} \right]. \quad (3.53)$$

We note that a similar expression appears in the literature for the limit of  $\chi \rightarrow 0$  or  $b \rightarrow 0$ .

## 3.4 Results

In the classical theory of ionic channels, a simple relation is observed between ionic concentration and conductance. At low concentrations, the only charge carriers in the channel are the screening ions, independent of reservoir ionic strength. As concentration increases, the additional screening charges are negligible, leading to a linear profile of conductance. The transition occurs at concentrations for which the Debye

length and the ionic radius are comparable. This transition can be modeled using the PB theory, but to a good approximation, it is sufficient to consider two types of transport: bulk and surface.

The classical picture breaks down in long and narrow cylindrical pores. Solving the general electrokinetic problem shows a very different qualitative picture, with non-trivial scaling dependence in both low and high concentrations. In recent years there has been a focus on two important mechanisms impacting the shape of the conductance curves: charge regulations [219, 25, 201] and increased slip length [49, 175]. In this work, we present two additional physical phenomena that can play an important role: electroneutrality breakdown and coupled fluxes.

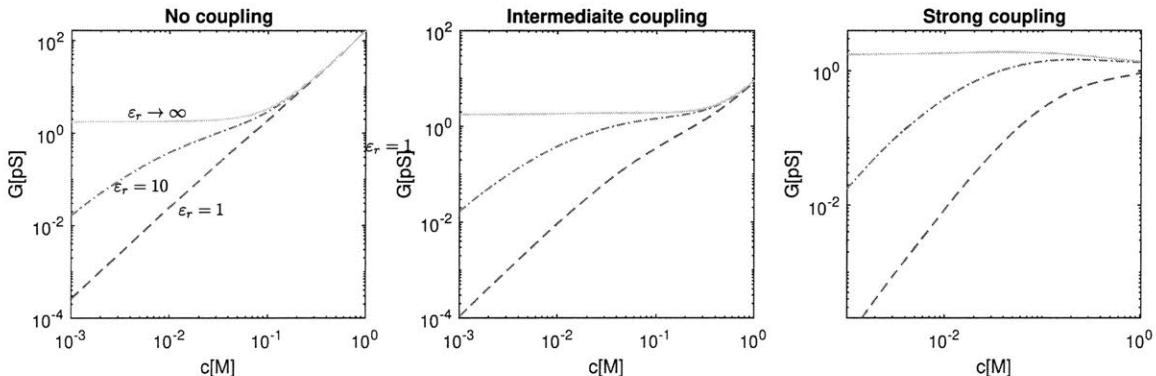


Figure 3-2: Effect of neutrality breakdown and coupled fluxes on nanopore conductance. Conductance was calculated by Eq. 3.53 with no-slip condition, and by solving the PB equation with boundary conditions from Eq. 3.18. (a) No coupling limit ( $\chi = 0$ ). (b) Intermediate coupling ( $\chi = 10$ ). (c) Strong coupling ( $\chi = 1000$ ).

In the previous sections, we showed how these mechanisms can be simplified to fit with the usual electrokinetic theory framework. We, therefore, proceed in the same way: we first solve the PB equation with the general boundary condition (Eq. 3.24) and then calculate the conductance using Eq. 3.53. The results are illustrated in Fig. 3-2, for different relative dielectric constant and coupling constants. Without coupled fluxes ( $\chi = 0$ ) and with strong dielectric mismatch ( $\epsilon_{\text{out}} \gg \epsilon_{\text{in}}$ ), we recover the classical behavior of saturation at the dilute limit. For more typical values of dielectric mismatch, we get a significant decrease in the expected conductance. As we increase the coupling parameter, the concentrated regime begins to show saturation. For simplicity, we are at a constant surface charge regime (high pH), with zero slip-

length ( $b = 0$ ).

## 3.5 Discussion

The peculiar scaling relations observed in conductivity curves in extreme confinement sparked the interest of the modeling community in recent years[219, 175, 25]. Applying classical Poisson-Nernst-Planck equations, coupled with Navier-Stokes and a charge-regulation boundary condition, provides one possible explanation of this phenomena. Yet, there is currently no direct evidence that such mechanism exists in carbon nanotubes. In the previous chapter, we have shown that a simple algebraic equation, based on the concept of electroneutrality breakdown, suffices to explain the conductance curves.

We devoted this chapter to reformulate electroneutrality breakdown in the framework of linear electrokinetic theory. The approximated boundary conditions we found (Eq. 3.24) allows us to consider more complicated and realistic models and weigh the effect of different physical phenomena. This chapter complements the more fundamental analysis we introduced earlier on the origins of electroneutrality breakdown, and its emergence as a unique feature of 1d physics.

The combination of the full conductance formula (Eq. 3.53) with the new boundary condition is the main result of this chapter. We note, however, that we introduced many parameters: energy barriers, the flux coupling constant and the slip length are usually not known. Moreover, our boundary condition is very sensitive to the dielectric constant of both the inner and outer regions, which are not always known. The currently available data cannot be used to determine the dominating effect for the conductance of single-digit nanopores and more carefully crafted experiments are required.



# Chapter 4

## Spin-Glass Charge Ordering in Ionic Liquids

Except for minor edits, the contents of this chapter have been published in [164].

### 4.1 Introduction

In recent years, room temperature ionic liquids (RTIL) have emerged as promising electrolytes for synthetic chemistry and electrochemical energy storage[82, 132, 218, 88, 221]. In the absence of solvent molecules, strong electrostatic interactions limit the applicability of classical mean-field approximations, such as the ubiquitous Poisson-Boltzmann (PB) theory [61] for dilute solutions. Extensions are available for steric effects [20, 40, 26, 130, 144], short ranged ion-ion forces [63, 242, 95, 95, 4, 90], ion-solvent interactions [3, 94] and Gaussian perturbations beyond mean-field [190], but no theory can fully describe the solvent-free limit of RTIL.

At electrified interfaces, ionic liquids share similarities with dilute electrolytes, and some aspects can be described by modified continuum models. Direct surface force measurements reveal a diffuse electric double layer (EDL) structure, akin to that of a dilute aqueous solution[92], although the extent of this analogy is debated[153]. Nevertheless, there have been some successful applications of mean-field continuum models to RTIL[144, 79, 82]. Additionally, strong electrostatic correlations, which induce

charge ordering and oscillations[81], can be captured surprisingly well by higher-order PB type equations [211, 109, 21, 167, 91, 29, 65].

Strong charge correlations imply a non-local dielectric response, similar to that of polar solvents[139, 112]. Bazant, Storey, and Kornyshev (BSK) extended the PB free energy functional to include both correlations and crowding effects and introduced the concept of a dielectric permittivity operator to approximate the non-local ionic polarization[21]. The BSK framework was subsequently used to describe a wide variety of structural [155, 254, 186, 169] and dynamical [151, 9, 126, 125, 232] properties of ionic liquids and concentrated electrolytes. Continuum models continue to extend their predictive power to capture aspects of both long-range under-screening and over-screening[200, 225, 152, 95, 90], yet they remain incomplete in their description of complex many-body correlation effects. Other phenomena, such as charge-driven 3D structures of the double layer[122, 121, 209, 145], are not well explained with a mean-field approach, and coarse-grained charge profiles generally obscure correlated nano-structures[238, 45, 14].

In this chapter, we use molecular dynamics (MD) simulations to reveal an essential and overlooked mechanism that determines the charge profile in ionic liquids: geometrical frustration. Given the network of neighboring ionic positions in a symmetric binary mixture, we show that the charge distribution corresponds to the ground state of an effective spin-glass Hamiltonian [71]. We propose a minimization scheme based on a modified Goemans-Williamson (GW) algorithm[93] and perform spin-glass reconstructions of MD simulations of four materials: 1-Ethyl-3-methylimidazolium bis(trifluoromethylsulfonyl)imide (EMIM-TFSI), a commonly studied aprotic RTIL[195, 149, 180, 220], protic RTIL trimethylammonium-triflate (TMA-OTF), molten sodium chloride and so-called "water-in-salt" electrolytes (WiSE), recently introduced for Li-ion batteries [235, 234, 181]. Finally, we consider turbulence in bacterial suspensions [69] and illustrate how spin-glass ordering emerges in any strongly interacting anti-ferromagnetic disordered system.

## 4.2 Theory

The partition function of ionic liquids (neglecting non-idealities) can be written as a sum over all spatial configurations ( $\{\mathbf{r}_i\}$ ) and valencies ( $z_i$ ):

$$\begin{aligned} Z &= \int \prod_{i=1}^N d\mathbf{r}_i \left[ \sum_{\{z_i\}} \exp \left( -l_B \sum_{i \neq j} \frac{z_i z_j}{|\mathbf{r}_i - \mathbf{r}_j|} \right) \right] \\ &= \int \prod d\mathbf{r}_i Z_r[\{\mathbf{r}_i\}], \end{aligned} \quad (4.1)$$

where  $l_B = \beta e^2 / \epsilon$  is the Bjerrum length,  $e$  the elementary charge,  $\beta = (k_B T)^{-1}$  the inverse temperature, and  $\epsilon$  the dielectric constant of the medium.  $Z_r$  is a reduced partition function that depends on the ionic positions. We emphasize that Eq. 4.1 is purposely simplified, excluding any non-electrostatic physics, such as asymmetric molecular shapes/sizes/interactions, which are vital in inducing positional disorder in the fluid[199, 198]. We may exclude such effects, because once the positions are given, as in this framework, non-electrostatic physics play only a minor role in charge ordering.

The reduced partition function is similar to a spin-glass, with the following Hamiltonian:

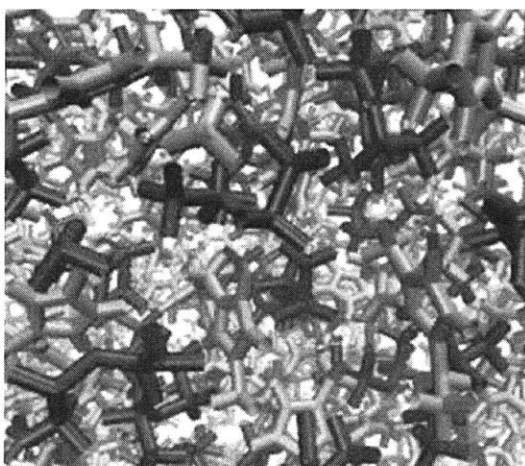
$$H = \frac{1}{2} \sum_{i \neq j} J_{ij} z_i z_j, \quad \text{where} \quad J_{ij} = \frac{l_B}{|\mathbf{r}_i - \mathbf{r}_j|}. \quad (4.2)$$

In the dilute limit ( $l_B \rightarrow 0$ ) the Debye-Huckel mean-field approximation becomes valid, at rather small salt concentrations ( $< 100\text{mM}$ ) for aqueous solutions ( $l_B \approx 7\text{\AA}$ ). In the opposite limit ( $l_B \rightarrow \infty$ ) relevant for ionic liquids, when the Bjerrum length is large compared to the ionic spacing, temperature induced charge fluctuations around the ground state are negligible, and the charge distribution is better approximated by minimizing the Coulomb energy.

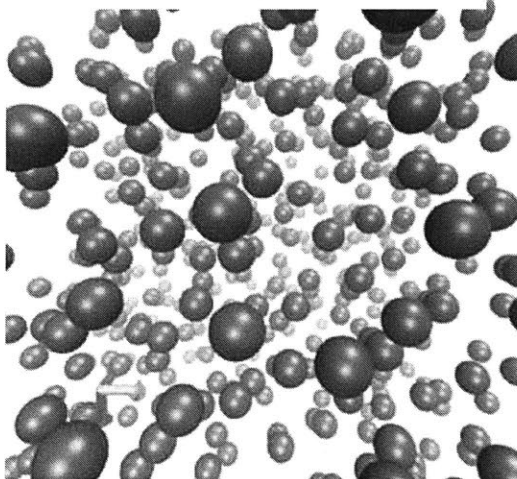
Minimizing a spin-glass Hamiltonian is a well-known NP-complete problem [89] that cannot be solved exactly. The difficulty lies in the "Ising-like" constraint on the charges:  $z_i = \pm 1$ , which can be expressed efficiently via a matrix,  $Z_{ij} = z_i z_j$ . By

## Spin glass reconstruction of ionic liquids

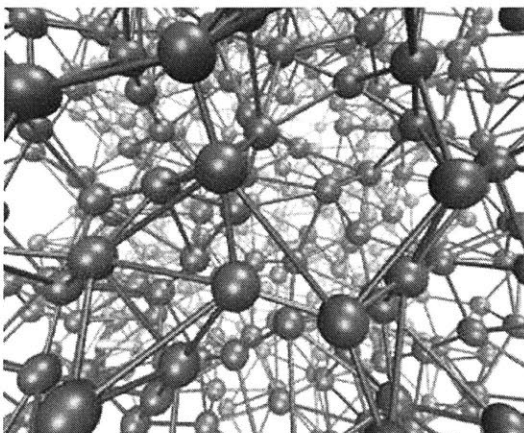
1. Perform MD simulation



2. Extract ion positions



3. Build connectivity network



4. Reconstruct ions identities

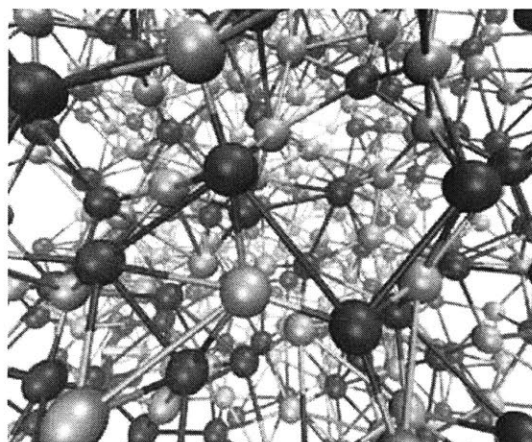


Figure 4-1: Illustration of the reconstruction procedure. 1 - the input is a full MD simulation of the ionic liquids. 2- The first step is to take a single snapshot, calculate the position of each molecule (as an average over its atomic positions), and delete the molecule identity. 3- Based on molecular positions, we construct a connectivity network, by connecting each molecule to its nearest neighbors. 4- Minimizing the spin-glass Hamiltonian for the network yields identities for the molecules, marked by orange and blue in the figure. The minimization is carried for each snapshot separately.

construction, the rank of  $Z$  equals 1, and its diagonal is  $Z_{ii} = 1$ . The Hamiltonian, in terms of  $Z$ , is simply  $\text{Tr}(ZJ)$ . Relaxing the constraint on the rank of  $Z$ , and letting it take a full rank, greatly simplifies the problem, and allows for a polynomial time solution. This is the celebrated Goemans-Williamson (GW) max-cut algorithm [93]. In the context of spin-glasses, the GW algorithm can be interpreted as letting the spins rotate in an  $N$ -dimensional space, where  $N$  is the total number of spins in the system [51].

The GW algorithm steps are as follows: 1) Minimize  $\text{Tr}(ZJ)$  subject to  $Z_{ii} = 1$ ; 2) find the Cholesky decomposition of  $Z$  ( $Z = SS^T$ ); and 3) choose a plane in the  $N$  dimensional space, and assign the  $i^{\text{th}}$  Ising spin a sign (charge) according to the side of the plane where the  $N$  dimensional spin  $S_{ik}$  lies. To solve the minimization problem, we use CVX, a package for specifying and solving convex programs [98, 97].

The GW algorithm can be applied to any pair-wise interaction, and interestingly, we find that fully connected systems yield poor results. Instead, a dramatic improvement is achieved by considering an effective Hamiltonian with only short-range interactions, such as the following (empirical) interaction between an ion and its  $n$ th nearest neighbor:

$$J_n^{\text{eff}} = \begin{cases} e^{-n} & n=1 \dots 5 \\ 0 & n > 5. \end{cases} \quad (4.3)$$

Due to screening, ion-ion interactions are thus limited to only a handful of nearest neighbor pairs. We further update the results of the GW algorithm according to a "local electro-neutrality" condition, until convergence:

$$z_i = -\text{sign} \left( \sum_{j \neq i} \frac{z_j l_B}{|\mathbf{r}_i - \mathbf{r}_j|} \right). \quad (4.4)$$

Finally, the algorithm is accelerated by selecting the bisecting plane perpendicular to the first principal component of  $S$ .

## 4.3 Results

Let us now apply the modified GW algorithm to test our main hypothesis—i.e., the charge distribution is determined by the ground state of a spin-glass Hamiltonian, given the positional configuration. A useful starting point is to examine systems in complete disorder, by simulating hard-sphere liquids with different packing fractions (see appendix A for a detailed description of the simulations.). Fig. 4-2(b) shows the charge distribution around a central ion in the ground state. We notice an interesting trade-off between the distance of closest approach and over-screening. When ions are free to approach each other, it is almost always favorable for the nearest neighbor to be of opposite charge, regardless of other ions in the environment. Neighbors further away are much less correlated. As ionic radii increase, ions tend to be more evenly spaced and screening is shared by several neighbors; a longer ranged oscillatory structure emerges.

### 4.3.1 Ionic Liquids

Ionic liquids display a much longer correlation length. Data from scattering experiments, as well as MD simulations, reveal complicated nano-structures [238, 14, 90, 91] with oscillations that span many neighbors. We simulate an EMIM-TFSI ionic liquid to study these structures (see Appx. A information for simulation details). As illustrated in Fig. 4-1, the Hamiltonian is constructed from ionic positions extracted from MD simulation snapshots. The minimization scheme is carried separately for each snapshot, and the results shown are averaged over all snapshots. Despite the complexity of the full atomistic MD simulations, the spin-glass model actually captures all the necessary physics: ionic valency almost exactly minimizes the Coulomb interactions. No other non-electrostatic ingredient is needed to recover the charge-density long ranged correlations.

Figure. 4-2(c-d) compares results from MD simulations to the spin-glass reconstruction process. In bulk simulations, we recover the exact charge of almost 98% of the ions. Consequently, the predicted charge distribution is almost indistinguishable

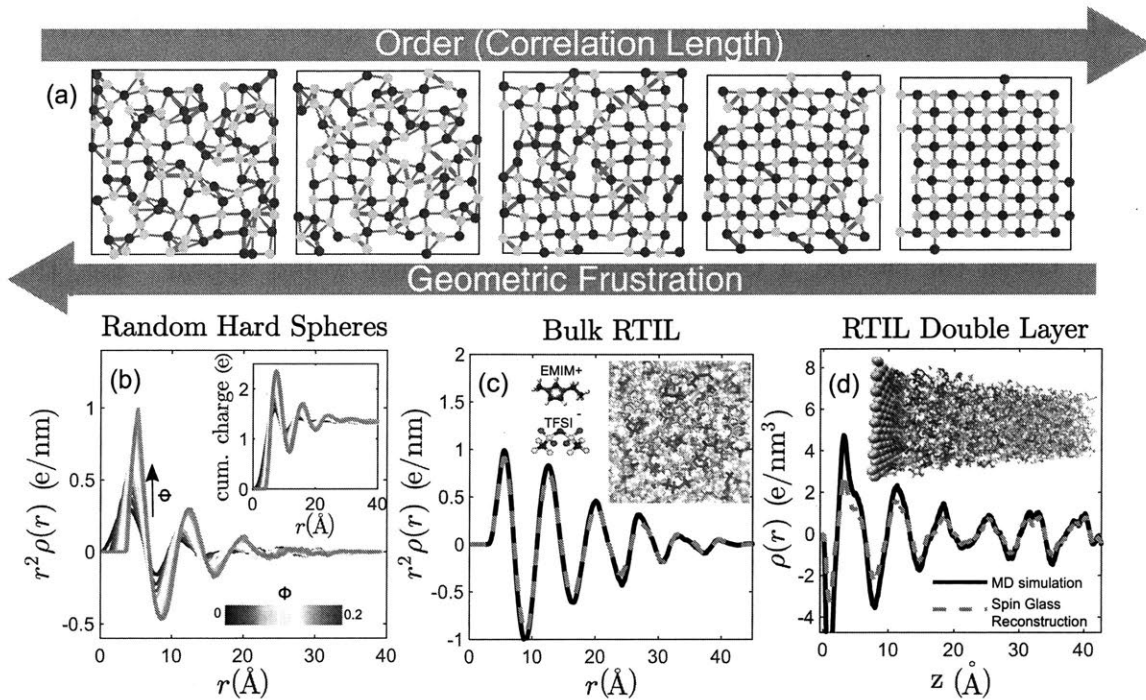


Figure 4-2: Order vs. Frustration in Ionic Liquids. **Top-** examples of 2D Ising model, with different degree of order. Red lines mark connections between parallel spins. The more ordered the system (right), more connections are satisfied. **Bottom-** examples of 3D spin-glass with Coulomb interaction. (b)- Charge distribution around a central ion in a Random hard sphere model, for different packing fractions ( $\Phi$ ), ranging from 0 to 0.2 in steps of 0.02. (inset: cumulative charge distribution. Over-screening is defined as the maximum of this curve). (c) - Charge distribution around a central TFSI ion in EMIM-TFSI, based on MD simulation (black line) and the spin-glass reconstruction (dashed red) (inset: a snapshot from the MD simulation). (d) - EMIM-TFSI charge density near a weakly charged surface ( $0.01\text{C}/\text{m}^2$ ), based on MD simulation (black line) and spin-glass reconstruction (dashed red) (inset: a snapshot from the MD simulation).

from the simulated one (Fig. 4-2c). This exceptional match hints towards a unique ground state, and a high degree of order in the ionic positions. The reconstructed double-layer structure (Fig. 4-2d) fits reasonably well the simulated EDL, despite completely neglecting the interaction with the electrode. For weak surface charges, this interaction is only a secondary effect, but will have to be considered as electrode charge increases. A weakly charge electrode also exhibits a dramatic over-screening. The first layer can have a charge that is up to 15 (!) times greater than the electrode charge. For comparison, BSK predicts an over-screening of only a few percent, which is more realistic for larger surface charges.

The spin-glass ground state aims to create long-ranged structures of alternating signs. Given the chance, a true long-range charge order would appear. Yet, this requires a high degree of order in the ionic positions. Even slight deviations from a perfect crystal structure lead to geometric frustrations: the pattern of alternating signs has to be broken in some direction (See Fig. 4-2(a) for illustration). The positional disorder can be traced back to the particular size and shape of the ions[199, 198]. Simple ions favor positional ordering and form ionic solids at room temperature, or long-ranged ordered liquids beyond the melting point, which are well captured by the spin-glass model (see below). This coupling of density and charge ordering have been extensively studied in the context of solid-liquid phase transition[106, 17, 196]. Conversely, in complete disorder correlations are limited to few neighbors only (Fig. 4-2(b)). In Ionic-liquids, and especially near charged surfaces, partial disorder facilitates the large correlation lengths (Fig. 4-2(c-d)).

The order (or disorder) in ionic positions can take different forms: from short-ranged ion clusters to hydrogen-bond (H-bond) networks and micelle-like morphologies [110]. In some protic (H-bonding) ionic liquids, for example, complex nanostructures may be formed by the interplay of Coulomb forces and strong H-bond interactions[110]. However, this type of behavior is not just unique to protic RTIL's. For example, aprotic  $[C_n\text{mim}][\text{PF}_6]$  ionic liquids tend to break into polar and nonpolar nano-regions[47]. In both cases, non-electrostatic forces play an important role in determining the type of bulk nanostructures. We cannot rule out that these mecha-

nisms affect charge ordering as well, but to demonstrate the generality of our method, we performed an additional simulation of trimethylammonium-triflate or TMA-OTF. TMA-OTf is an example of a protic ionic liquid, where H-bonds play a major role. Protic and aprotic ionic liquids are the two main classifications of ionic liquids, and EMIM-TFSI is an example of the latter. The reconstruction results are shown in Fig. 4-5: despite the formation of H-bonds, once the positions are known the charge ordering exactly followed the spin-glass minimization.

### 4.3.2 Water-in-Salt Electrolyte

Let us now examine MD simulations of LiTFSI ‘Water-in-Salt’ Electrolyte (WiSE) at varying concentrations of salt. WiSE’s have emerged as promising candidates to replace organic electrolytes in Lithium-ion Batteries [235, 234, 181]. They exhibit much shorter correlation lengths, even when the solvent concentration is small (Fig. 4-3). For moderate to high salt concentrations ( $> 5\text{mol/Kg}$ ), where ionic spacing is small compared to the Bjerrum length, our spin-glass framework is applicable.

Due to in large part to ion size asymmetry, the spin-glass reconstruction only semi-quantitatively matches the simulations. The high molality limit ( $21m$ ) is best reproduced by the minimization process, with about 80% of ionic charges recovered. Similarly to RTIL, the hidden positional order stands behind this unique and easily accessible ground state. With increasing water content ( $21m \rightarrow 7m$ ), the order gradually disappears, and we are only able to capture the general structure of the screening cloud. Upon decreasing ionic concentration further ( $7m$  and especially  $2m$ ), thermal fluctuations become predominant and the spin-glass model breaks down. Yet, traditional mean-field models are unsuitable for that regime as well, and ion-specific effects determine the correlation function.

When ionic positions are disordered, the charge distribution matches the random hard-sphere model (dashed blue lines in Fig. 4-3). Similarities are even more pronounced when only considering ordering relative to neighbor-number. The spin-glass reconstruction scheme captures the general charge ordering structure, but not the fine details. The precise location of the nearest neighbor, for example, is determined by

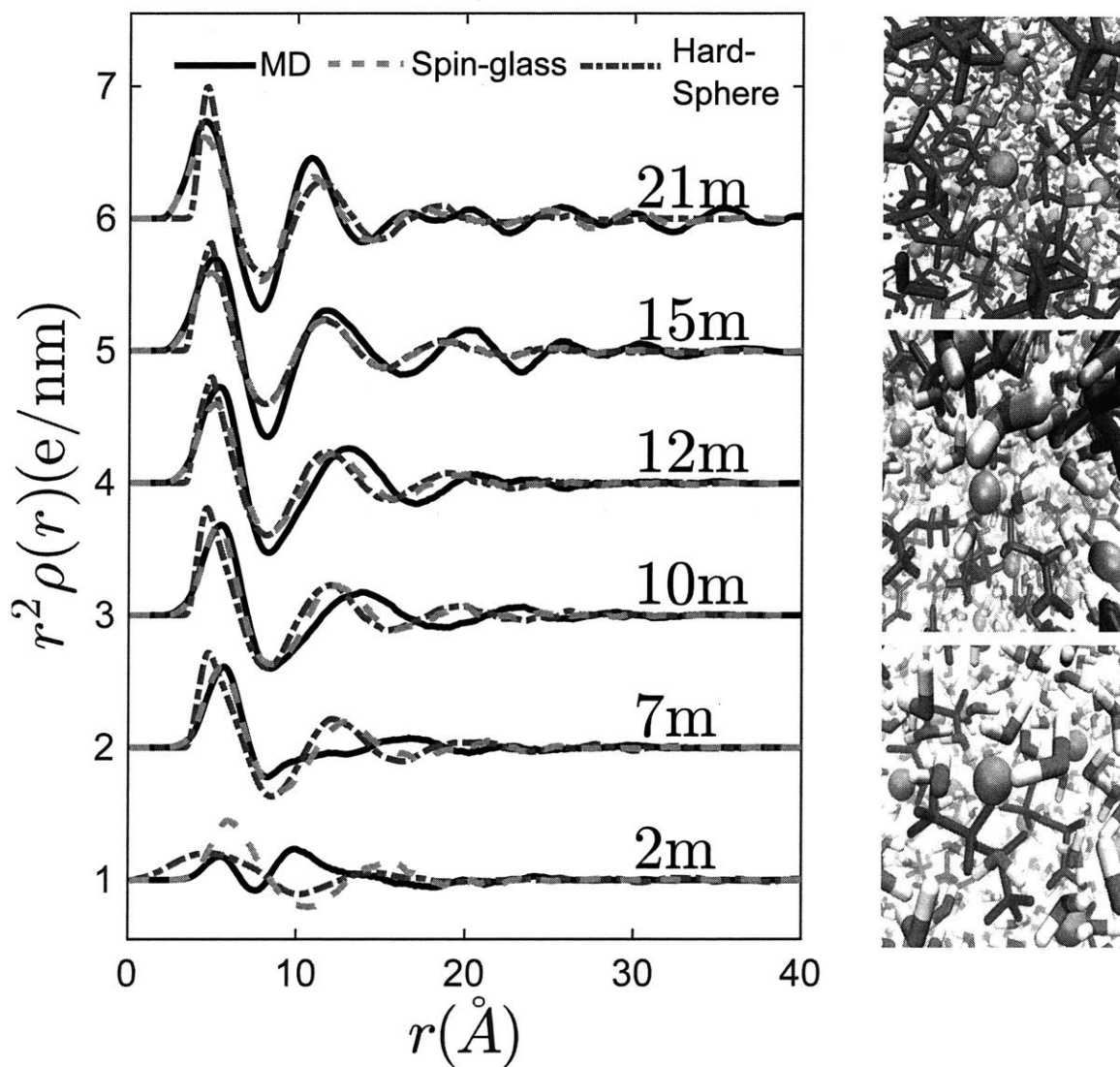


Figure 4-3: LiTFSI in Water- from concentrated electrolyte to WiSE: Charge distribution around a central TFSI ion is shown for different molality (1 mol/kg solvent = 1m), from 2m to 21m. Each graph is plotted with an offset of 1e/nm. Results from MD simulation (solid black line) are compared with random hard-sphere toy model (dashed-dot blue) and the spin-glass reconstruction (dashed red). Snapshots are shown from the LiTFSI MD simulation for 2m(bottom), 7m(middle) and 21m (top). The hard sphere diameter equals 4.12 $\text{\AA}$ .

van der Waals interactions rather than electrostatics. Hence, the charge distribution around a central ion is expected to depend on the simulated system. Conversely, the average charge as a function of the neighbor number, which depends on the topology of the network, has a more universal behavior. Fig. 4-4 shows the first 10 neighbors for both random-hard sphere model and aqueous LiTFSI simulation, for similar water content as in Fig. 4-3. A reasonable match is observed, especially in moderate concentrations (7 – 15m) where disorder is strongest.

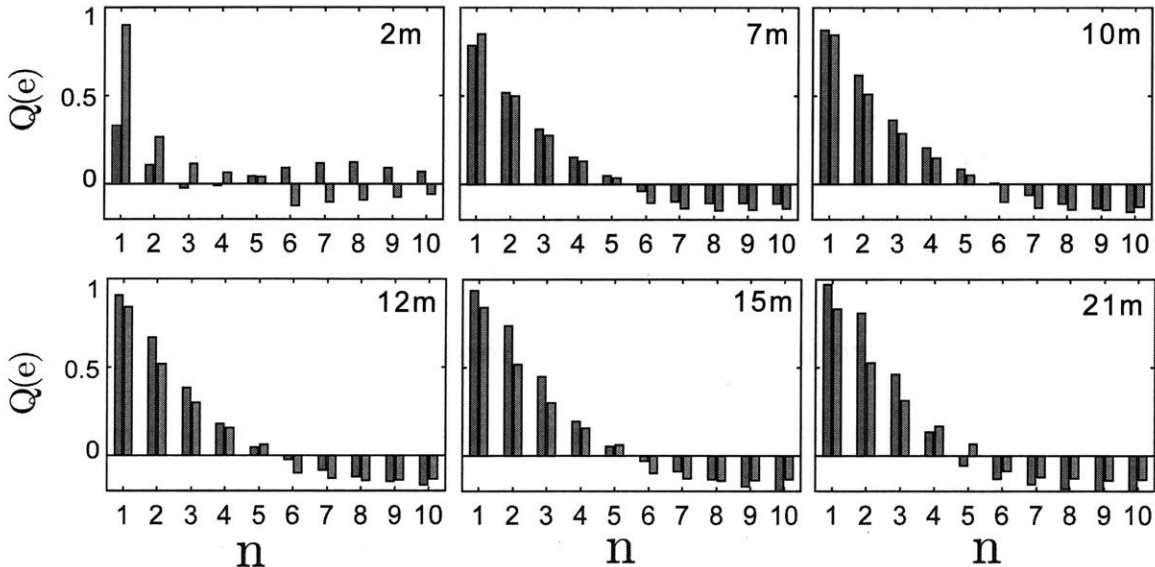


Figure 4-4: Screening cloud around a central TFSI ion is shown for different molality (1 mol/kg solvent = 1m), from 2m to 21m. Results from MD simulation (right blue bars) are compared with random hard-sphere toy model (left red bars). The hard sphere diameter equals 4.12Å.

The reason for this high degree of disorder, compared with the RTIL, is twofold. First, there is a large positional entropy associated with small lithium ions, which is costly to suppress. Second, the solvent molecules weaken the electrostatic interactions. Maintaining a positional order is therefore unfavorable, and the WiSE resembles a hard-sphere liquid.

### 4.3.3 Molten Salts

The origin of disorder in high-temperature molten salts is the increased temperature. Due to their structure, simple salts form ionic-solids at room temperature and keep a high degree of order even after their melting point. Molten salts have been exten-

sively studied by restrictive primitive models (charged hard-spheres), and their charge distribution is well described by integral equations methods[106]. We performed an MD simulation for a NaCl-like molten salt at a temperature of 1500K. The simulation was performed using the same protocol as for the EMIM-TFSI, TMA-OTF, and LiTFSI electrolytes. Our reconstruction scheme exactly reproduced the charge distribution around a central ion (Fig. 4). This excellent match is even better than the one found for ionic liquids or water-in-salts and exemplifies how positional ordering of the molten salts generates an easily accessible ground-state for the corresponding spin-glass Hamiltonian.

The success of our reconstruction scheme in capturing charge ordering for the variety of ionic systems displayed above demonstrates the potential of our method to apply to other ionic liquid systems, as well.

#### 4.3.4 Turbulence in Bacterial Suspensions

Our analysis is not restricted to ionic liquids or Coloumbic system. Disordered systems with strong anti-ferromagnetic interactions are expected to show similar behavior. We demonstrate the generality of the spin-glass reconstruction scheme, by considering turbulence in bacterial suspensions. A bacterial colony of *Bacillus subtilis* self-organizes into collective movement, and forms vortices under confinement[69]. To minimize drag forces and reduce friction adjacent vortices prefer to rotate in opposite directions. The details of this interaction follow complicated hydrodynamic equations, but as long as the anti-ferromagnetic interaction is strong, "spin" ordering is expected to dominate the emerging structure. We study the system with an effective spin-glass Hamiltonian, where the vortex directionality plays the role of spin, and the positions of the vortices cores are extracted from simulations. We use simulation data of swimming bacteria, adapted from [69]. 23 core positional were extracted manually from a snapshot image the simulated flow field (Fig. 4-6-a).

We arbitrarily choose the same form of local interactions as the effective RTIL Hamiltonian (Eq. 4) but restrict connectivity only to vortices that are in physical contact via Delaunay triangulation. The minimization process was carried out using

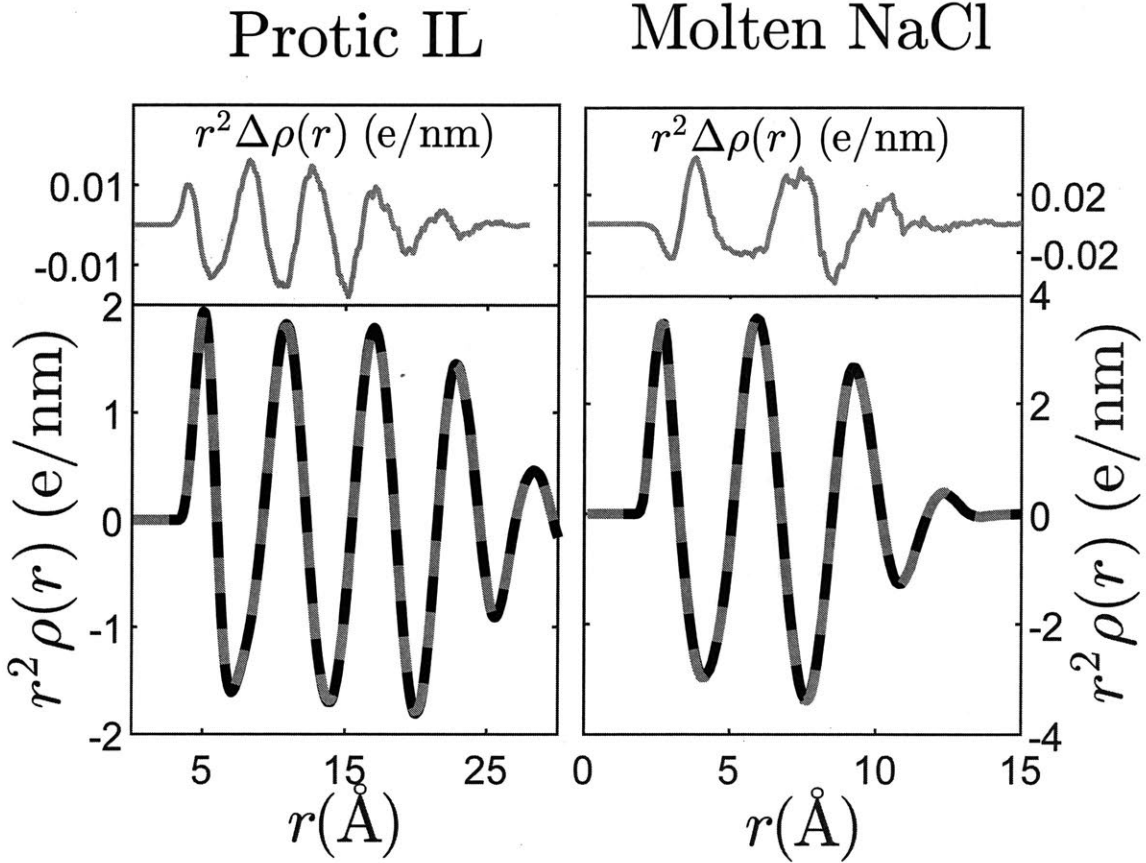


Figure 4-5: Charge distribution around a central ion in a NaCl-type molten salt and TMA-OTF. Right- comparison of spin-glass reconstruction (dashed red line) vs MD simulation results (solid black line) for a molten salt. Left - testing the reconstruction scheme on a protic ionic liquid, TMA-OTF (dashed red line) with MD simulation results (solid black line). The difference in both cases is less than 1%, as shown in the top figures. The small difference is due to the fact that an overwhelming majority of ions were identified correctly.

the modified GW algorithm, omitting the last stage of requiring electro-neutrality. Out of the 23 vortices, the directionality of 19 of them was reconstructed correctly (Fig. 4-6-b). To illustrate the reconstructed vorticity (Fig. 4-6-c), we superimpose a Lamb-Oseen (Gaussian) vortex at each core location, with angular velocity  $\Omega(r) \propto [1 - \exp[-(r/r_m)^2]]/r^2$ , and a radius of  $r_m = 25\mu\text{m}$ . The nice qualitative match illustrates the universality of our approach. The emerging structures in disordered anti-ferromagnetic systems are governed by the geometry and are insensitive to details of their physical origin.

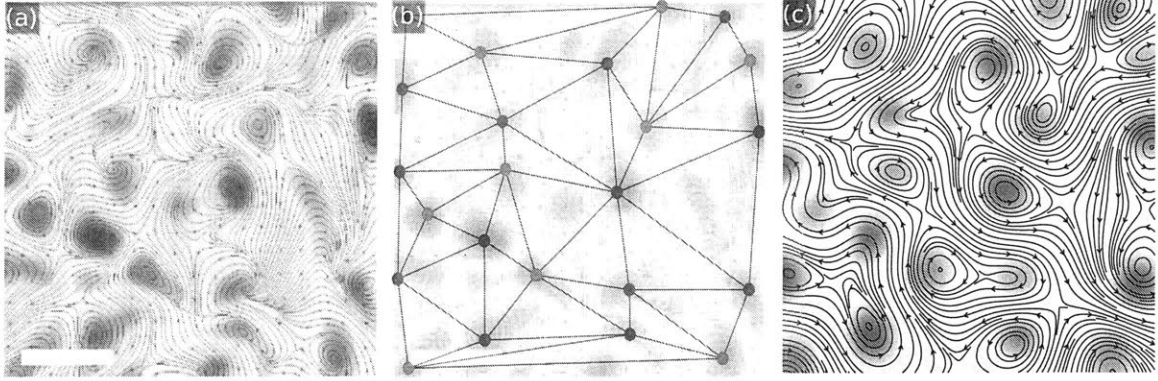


Figure 4-6: Applying spin-glass reconstruction for swimming bacteria. (a)- snapshot of simulated flow field (adapted from [69] with permission) . (b)- A vortex network constructed by extracting the vortices centers as nodes. The sign of each node, clockwise (red) or counter-clockwise (blue) rotation, was derived from minimizing spin-glass Hamiltonian and matches 19 out of the 23 nodes of the simulation. (c)- Illustration of the reconstructed flow field, based on a superposition of independent Lamb-Åseen vortices

## 4.4 Discussion

The spin-glass model is a strong-coupling theory. It simplifies the complex interactions in ionic liquids and Water-in-Salt electrolytes to a minimization of a Hamiltonian with only local interactions (though corrections for electroneutrality are required).

The correlation length is governed by geometric frustrations and increases with positional order. Such structures would emerge in any binary liquid with strong "anti-ferromagnetic" interactions and are not limited to Coulomb forces. Other examples include 2d vortex patterns that arise in super-fluids or bacterial turbulence[2, 249] . This is markedly different from the typical Debye-Huckel behavior, where electrostatic attraction competes with entropic "repulsion".

Interestingly, the positional order may not be apparent at first sight, and does not significantly affect the density-density pair correlation function. Nevertheless, as we show via the minimization process, long-range charge ordering is a manifestation of the hidden positional ordering. The ionic positions, as disordered as they may seem, carry all the information about the ionic identities. It is not surprising that charge and density ordering are coupled: ionic positions are determined by the charges and vice versa. However, our analysis offers a new way to understand the charge distribution

in the bulk, and reveals its intimate link to the positional configurations.

For solvent-free ionic liquids, the ground-state of the spin-glass Hamiltonian is easily accessible, and correlations are long-ranged. This might be the onset of a true long-range order in ionic-crystals. Room temperature ionic-crystals have much stronger interactions due to their small size, but we speculate that a similar regime of hidden positional order must exist, and play a role in the thermodynamics of melting. As solvent content increases, the energy landscape becomes more rugged, yet the system is still described well by its ground-state, and non-idealities are safely neglected. Eventually, in the moderately concentrated electrolyte regime ( $< 7\text{m}$ ), thermal fluctuations, as well as ion and solvent specific effects are dominating, and the spin-glass approach is no longer valid.

While further exploration is needed to determine the generality of our approach, we have shown it to work well for 4 classes of Coloumbic liquids: priotic ILs, a-priotic ILs, molten salts and Water-in-Salt electrolytes. In each case the positional ordering was different, but the charge ordering was shown to be uniquely determined via spin-glass minimization. We note, however, that we only focus on the nanometer length-scale, which is suitable for atomistic simulations. Longer range phenomena, such as extremely long-ranged charge correlations, are beyond the scope of this work. Interestingly, we were not able to observe under-screening [200], despite its emergence in the relevant length-scales.

Another important limitation of our model is that it is inherently symmetric in size and shape. In many cases, it is the asymmetry of the ions that favors disordered structures and make them good ionic liquids in the first place. Remarkably, even in extremely asymmetric cases like LiTFSI, the spin-glass Hamiltonian qualitatively captures correctly the charge distribution. This is in part due to a universal behavior of complete disordered, which does not depend on the details of the materials.

Though we do not offer here a general theory of ionic liquids and concentrated electrolytes, we believe our observations highlight the important physics. The close interplay between the positional configurations and charge ordering, which plays an important role in long-range ordering near phase transitions, is observed to be sig-

nificant even in partial or complete disorder. Geometric frustrations and positional ordering determine the correlations lengths, and might be considered as some of the underlying microscopic driving forces to include for accurate continuum models.

## 4.A MD Simulation Details

In this study, we performed all-atom classical MD simulations using LAMMPS [204]. We performed a set of simulations for two different systems: one set for a neat ionic liquid (IL), EMIM-TFSI and another for the Water-in-Salt Electrolyte (WiSE), LiTFSI (at varying concentrations). EMIM-TFSI was simulated in both full periodic geometries in order to study bulk-like properties, as well as nano-slit (slab) geometries in order to study the electrical double layer. For the nano-slit geometry, we prescribe a constant surface charge density of  $\pm 0.1 C/m^2$  at two electrodes that sandwich the ionic liquid. LiTFSI electrolyte was simulated in fully-periodic geometries each set of simulations at molal concentrations of 2m, 7m, 10m, 12m, 15m, and 21m.

*Simulation Details:* For EMIM-TFSI in the periodic geometries, we performed simulations containing 300 ion pairs. For the aqueous LiTFSI systems we performed simulations containing 1000 water molecules and enough ion pairs to make 2m, 7m, 10m, 12m, 15m, and 21m solutions. The simulations were performed at fixed temperature (300 K) and pressure (1 bar), with Nose-Hoover thermostat and barostat until the density of the fluid relaxed to a constant, which required 12 ns, with 1 fs time steps. Next, we switched to constant volume simulation box still with a fixed temperature of 300 K, again using the Nose-Hoover thermostat, and equilibrate for an additional 6 ns. Finally, production runs were performed for an additional 6 ns. The initial configurations for all simulations were generated using the open-source software, PACKMOL [179]. MD simulations were visualized using the open-source software, VMD [119].

In the nano-slit geometry, we simulated the system at constant volume and temperature, filling a  $33 \times 33 \times 200 \text{ \AA}^3$  simulation box, with two  $33 \times 33 \times 33 \text{ \AA}^3$  electrodes, composed of Lennard-Jones Spheres made to resemble gold in an FCC lattice. The

electrodes sandwich the electrolyte fluid, which is filled in the box at densities determined from the periodic simulations. The box contained 528 ion pairs and 4096 gold atoms. Surface charges were applied by placing partial charges on the first atomic layer (128 atoms) of gold, according to the specified surface charge density of  $\pm 0.01 C/m^2$ . Equilibration runs of about 12 ns were performed initially with no applied potential/charge, with 1 fs time steps. Then the surface charge was stepped up from zero, allowing for 12 ns of equilibration and 6 ns of production at the  $\pm 0.01 C/m^2$  electrode surface charge.

*Force Field Details:* For all ionic species, we employed the CL&P force field, which was developed for ionic liquids, with same functional form as the OPLSAA force field[46]. For water, we employed the spc/e force field[23]. Interatomic interactions are determined using Lorentz-Berthelot mixing rules. Finally, for nano-slit simulations, we require force fields for the gold electrode. We did not explicitly model the dynamics of the electrode, omitting the need for a gold-gold force field. The gold was made to interact with the fluid mainly via Coulomb interactions, as the surface layer of gold atoms are charged according to the prescribed surface charge density. We also include Lennard-Jones interactions, which were made to be the same no matter what atom is interacting with gold (LJ well depth:  $\epsilon = 0.001\text{eV}$ , LJ radius:  $\sigma = 3\text{\AA}$ ). We made the Lennard-Jones parameters constant for all species so that conclusions from the simulations that are not specific to the choice of the electrode material. Long range electrostatic interactions were computed using the Particle-Particle Particle-Mesh (PPPM) solver (with a cut-off length of  $12\text{\AA}$ ), which maps particle charge to a 3D mesh for the periodic simulations and a 2D mesh in the transverse direction for the nano-slit simulation[114].

To demonstrate the generality of our approach to disordered fluids, we performed an MD simulations for an NaCl-like molten salt at a temperature of  $1500K$ , and trimethylammonium-OTf at room temperature. The simulations were performed using the same protocol as for the EMIM-TFSI RTIL and LiTFSI Water-in-Salt electrolyte. The force field parameters for trimethylammonium-OTf, were obtained from the CL&P force field, just as for the EMIM-TFSI system [46]. The force field param-

eters for the NaCl-like molten salt are given below in table 4.1.

	Charge (e)	$\sigma$ ,	$\varepsilon$ , kJ/mol
Na <sup>+</sup>	+1	3.33	0.0116
Cl <sup>-</sup>	-1	3.65	0.8300

Table 4.1: Force Field Parameters used for model molten salt (representative of NaCl).

## Chapter 5

# Activity Coefficients: Correlations and finite size effect in a BSK model

The activity coefficients of concentrated aqueous solutions play an important role in different biological and electrochemical systems[191], and indeed, many models to describe the ionic activity have been proposed over the years. In the original Debye and Huckel paper from 1923[61], the activity coefficient was calculated based on a linearized version of the Poisson-Boltzmann (PB) equation. This resulted in the well-known Debye-Huckel (DH) equation:

$$\ln \gamma = -\frac{A|z_+z_-|\sqrt{I}}{1 + Ba\sqrt{I}}, \quad (5.1)$$

where  $\gamma$  is the activity coefficient,  $z_{\pm}$  are the valencies of the ions,  $I = \sum_{i=\pm} c_i z_i^2$  is the ionic strength,  $c_{\pm}$  are the ionic concentrations,  $a$  is an effective ionic radius, and  $A$  and  $B$  are constant values. The DH equation works well for very dilute electrolytes, but fails to even qualitatively capture the activity behavior at higher concentrations. In a following work[118], Huckel added an important term for the activity: the change in self energy due to variations in the dielectric constant. Experiments measuring the static dielectric constant of ionic solutions were not available at the time, so the proposed model treated the dielectric constant as a fitting parameter. Assuming the dielectric constant of water,  $\epsilon_w$ , is decreased proportionally to the ionic concentration

$c$  ( $\varepsilon \approx \varepsilon_w - \delta c$ ), the correction to the Debye-Huckel equation is a simple linear term in concentration. Remarkably, fitting this model to existing activity data actually estimated the dielectric decrement pretty close to measured values, an observation first noted by Hasted et al[108] in their paper on the dielectric properties of ionic solutions.

A linear correction for the Debye-Huckel equation also emerges when considering short-range repulsive forces, via a virial expansion. The virial expansion offers a systematic way to include even higher order terms in concentration. First suggested by Guggenheim[104], and further developed by Pitzer[203], accounting for the second and third virial coefficients leads to a very powerful description of the activity. The Pitzer formula, which is essentially the regular Debye-Huckel with corrections to second order in the concentration, is in excellent experimental agreement for hundreds of compounds[133]:

$$\begin{aligned} \ln \gamma = & -A|z_+z_-| \left[ \frac{-\sqrt{I}}{1 + ba\sqrt{I}} + \frac{2}{b} \ln(1 + b\sqrt{I}) \right] \\ & + 4m \left( \frac{s_+s_-}{s_+ + s_-} \right) (B_{MX} + \frac{I}{2}B'_{MX}) + 6m^2 \frac{s_+s_-}{s_+ + s_-} s_+z_+ C_{MX}, \end{aligned} \quad (5.2)$$

where  $m$  is the molality,  $B_{MX}$ ,  $B'_{MX}$  and  $C_{MX}$  are parameters related to the second and third virial coefficient. To achieve its high accuracy, the Pitzer model hence requires several fitting parameters: the virial coefficients are not derived from first principles, and the ionic radii are an empirical parameters as well. Closely related models were subsequently derived by Bromley[42], Meissner[148] and Chen[54].

While the Pitzer formula is very useful, it only gives a vague interpretation for the physics of aqueous solutions. Other microscopical models have been developed in the past half a century. Many of them are of the integral equations type, and are based on different closures for the Ornstein-Zernik equation. The Hyper-Netted Chain approximation (HNC) and the Mean Spherical Approximations (MSA) are examples for a microscopic derivations of the activity coefficient[222, 44, 224]. Assuming a hard-sphere repulsion in addition to the coulombic attraction, the integral equation theories

give an approximated way to calculate the pair correlation function between any two ions. Usually numerical methods are required to solve the integral equations. The activity is expressed in terms of the correlation function, without a simple closed-form formula. Another drawback of the integral equation model is that they too require some fitting parameters.

Can we get rid of all the fitting parameters, and have a consistent theory that is described only in terms of physically sound variables? A purely microscopical description might not be the best starting point for such an attempt. Important microscopic details, such as the interplay of ions and dipoles, are difficult to account for and are usually omitted. This limits the predictive power of such theories, and is compensated by extra fitting parameters. On the other hand, a purely phenomenological description, such as the virial expansion, naturally generates more free parameters than we can handle. A middle ground can be found in modified Poisson-Boltzmann theories that have been proposed in recent years.

Replacing the Coulomb pair-potential with a more general pair-wise interaction, allows us to overcome some of the limitation of the Poisson-Boltzmann equation, without losing the simplicity and physical intuition of the theory. In 2006, Santangelo[211] added to the long-range Coulomb interaction a short distance term, to account for the ion-ion interactions in one-component plasma. Bazant et al[18] noted on the importance of such correlation term to Ionic solutions. Eventually, Bazant, Storey and Kornyshev (BSK) introduced a modified PB equation[21] with a 4<sup>th</sup> order correlation term on a lattice model. The BSK framework was subsequently implemented to describe a variety of physical phenomena in both ionic liquids and concentrated electrolytes systems. Examples include electro-kinetics and transport[231, 151], the electrical double layer structure and capacitance [21, 254], and electrophoresis[232]. Moreover, Molecular Dynamic simulations too showed good agreement with the BSK predictions [125].

Recently, Liu and Eisenberg derived the activity coefficient by numerically solving the BSK equation. Taking the correlation length to be the ionic size, they view the higher order terms as a form of non-local dielectric property of the solvent. A different

approach was taken by Schlumpberger et al[215]. Viewing the BSK as primarily stemming from ion-ion correlations, the correlation length was related to the Bjerrum length. A closed form analytical formula was obtained by solving for the BSK equation around a charged sphere. The formula was proven to describe well experimental data for several compounds, with a single fitting parameter. All other parameters of the model were taken from the literature: including the the dielectric decrement term, first suggested by Huckel.

In this work we remain the BSK framework, but extend upon Schlumpberger work in several ways. After shortly reviewing the BSK model (Section I), we explicitly incorporate non-local electrostatics, showing that finite size effects naturally lead to a correlation length proportional to  $a^2/\lambda$ , where  $a$  is the ionic size, and  $\lambda$  is the Debye screening length (Section II). We then derive the activity coefficients by solving the BSK equation in Fourier space for a charged sphere immersed in an ionic solution and obtain simple analytical expressions. In this way we avoid the question of choosing a boundary conditions, and get the correct limiting behavior for small ionic radii (Section III). In Section IV we examine our model on a much wider range of experimental data than the previously done, and find that the correlation effect present is stronger than would be expected just from finite-size considerations. We conclude (section V) by taking a closer look at the correlation length. Using the experimental data, we derive an empirical relation between the correlation length and the ionic concentration, and relate it to microscopic parameters of the system.

## 5.1 Model

The BSK equation is a phenomenological equation which successfully captures the correlations between ions in a solution, and produces qualitatively correct behaviors in high concentrated electrolytes or ionic liquids. Following [21] we start with a Ginsberg-Landau type free energy, restricted only by the rotation/inversion symmetry of the system. Assuming we have a mixture of  $N$  different ionic species immersed in a dielectric continuum of permittivity  $\varepsilon$ , the free energy functional reads:

$$\begin{aligned}
G &= \int d\mathbf{r} \left\{ g + \rho_{\text{eq}}\phi - \frac{\varepsilon}{2} [|\nabla\phi|^2 + l_c^2|\nabla^2\phi|^2] \right\} \\
g &= k_B T \sum_{i=1}^N [c_i^{\text{eq}}(\mathbf{r}) \log(c_i^{\text{eq}}(\mathbf{r})) - c_i^{\text{eq}}(\mathbf{r})]
\end{aligned} \tag{5.3}$$

where  $c_i^{\text{eq}}(\mathbf{r})$  is the local equilibrium (bulk) ionic concentration of the  $i^{\text{th}}$  specie,  $\phi(\mathbf{r})$  is the electrostatic potential,  $\rho_{\text{eq}}(\mathbf{r})$  is the charge density in the system and  $l_c$  is a phenomenological constant of the theory. The overall all charge density of point like ions with charge  $q_i$  equals  $\rho_{\text{eq}} = \sum_i q_i c_i^{\text{eq}}(\mathbf{r}) + \rho_f(\mathbf{r})$ , where  $\rho_f(\mathbf{r})$  is a fixed charged distribution. We note that in the original BSK equation crowding effects were also considered by placing the ions on a lattice [39, 21]. The lattice model prevents the accumulation of charges around charged surfaces, but can be neglected for the calculation of bulk properties, such as the activity coefficient.

We relate the local ionic concentration,  $c_i^{\text{eq}}(\mathbf{r})$ , to the overall concentrations,  $c_i^0(\mathbf{r})$ , by looking at the chemical potential of the different species in the system:

$$\begin{aligned}
\mu_i &= \frac{\delta G}{\delta c_i^{\text{eq}}(\mathbf{r})} = k_B T \log(c_i^{\text{eq}}) + \frac{\delta(\rho\phi)}{\delta c_i} = k_B \log(c_i^{\text{eq}}) + q_i\phi(\mathbf{r}) \\
c_i^{\text{eq}}(\mathbf{r}) &= \exp(\mu_i - \beta q_i\phi(\mathbf{r})) = c_i^0 \exp(-q_i\beta\phi(\mathbf{r})),
\end{aligned} \tag{5.4}$$

where  $\beta$  is the inverse temperature. Equating the functional derivative with respect  $\phi(\mathbf{r})$  to zero, leads to a generalized PB equation, also known as the BSK equation:

$$\frac{\delta G}{\delta \phi} = -\varepsilon \nabla^2 \phi(\mathbf{r}) + \varepsilon l_c^2 \nabla^4 \phi(\mathbf{r}) - \sum_i c_i^0 \exp(-\beta q_i \phi(\mathbf{r})) - \rho_f = 0 \tag{5.5}$$

Linearizing Eq. 5.5, and assuming electroneutrality,  $\sum_i c_i^0 q_i = 0$ , we get the familiar DH equation, with an extra 4<sup>th</sup> order term:

$$\nabla^2 \phi(\mathbf{r}) - l_c^2 \nabla^4 \phi(\mathbf{r}) - \lambda^2 \phi(\mathbf{r}) = \frac{\rho_f}{\varepsilon}, \tag{5.6}$$

where  $\lambda = [\varepsilon/\beta \sum_i (c_i^0 q_i^2)]^{1/2}$  is the Debye screening length.

## 5.2 Origins of the 4th Order Term: Correlation Vs. Screening

We started our discussion in the previous section with the assumption that a 4th order term is needed to improve the Poisson-Boltzmann equation. This term is associated with a new length-scale, denoted by  $l_c$ . There are three typical length-scales we relate to the bulk: the ion size, the ion-ion distance and the Bjerrum length,  $l_B$ , the length at which the electrostatic energy is comparable with the thermal one. The Debye screening length emerges as a combination of the Bjerrum length and the ion-ion distance. The correlation length is a phenomenological term, so it is not clear to how to relate it to the other physical parameters. Bazant et al [18] assumed a direct proportionality to the Bjerrum length, while Schlumpberger [215] argued it should be the harmonic mean of  $l_B$  and the average distance between ions. Liu and Eisenberg, also working in the BSK framework, assumed it is exactly proportional to the ionic radius [168]. In Section VI we compare the different choices with experimental data, but first let us introduce an analytic contribution a 4th order term that we can account for exactly: non-local electrostatic interactions.

Finite-size non-local screening effects induce a complicated dielectric response  $\epsilon(\mathbf{k})$ . A general formula for the dielectric function incorporating the non-local effects was previously derived to account both water molecules inner structure and as an ion size effect [142, 36]. Moreover, as recently argued, one can think of a more general formalism in which the correlations between the ions are expressed as an effective 'dressed ions' with more complicated structure [137]. In all cases the dielectric constant becomes a specially dependent function,  $\epsilon(|\mathbf{r} - \mathbf{r}'|)$ , or equivalently in Fourier space,  $\epsilon(\mathbf{k})$ . In the following section we show how such behavior plays out in the BSK equation.

For point-like charges the overall charge density is  $\rho_{\text{eq}}(\mathbf{r}) = \sum_i q_i c_i^{\text{eq}}(\mathbf{r})$ . More generally, we can associate each ion with an internal charge distribution  $\rho_i(\mathbf{r})$ . In that case, the overall charge density is given by the convolution of the local ionic

density and the internal charge distribution:

$$\rho(\mathbf{r}) = \rho_f + \sum_i \int d\mathbf{r}' \rho_i(\mathbf{r}' - \mathbf{r}) c_i^{\text{eq}}(\mathbf{r}). \quad (5.7)$$

Consequently, the chemical potential (Eq. 5.4) is modified:

$$\begin{aligned} \mu_i &= k_B T \log(c_i) - \frac{\delta[\rho(\mathbf{r})\phi(\mathbf{r})]}{\delta c_i^{\text{eq}}(\mathbf{r})} = k_B T \log(c_i^{\text{eq}}) - \int d\mathbf{r}' \rho_i(\mathbf{r}' - \mathbf{r}) \phi(\mathbf{r}) \\ c_i^{\text{eq}}(\mathbf{r}) &= c_i^0 \exp \left[ -\beta \int d\mathbf{r}' \rho_i(\mathbf{r}' - \mathbf{r}) \phi(\mathbf{r}) \right] \end{aligned} \quad (5.8)$$

The total charge density (Eq. 5.7) then reads:

$$\rho(\mathbf{r}) = \rho_f + \sum_i c_i^0 \int d\mathbf{r}' \rho_i(\mathbf{r}' - \mathbf{r}) \exp \left[ -\beta \int d\mathbf{r}'' \rho_i(\mathbf{r}' - \mathbf{r}'') \phi(\mathbf{r}'') \right], \quad (5.9)$$

leading to a non-local BSK equation:

$$-\varepsilon [l_c^2 (\nabla^2)^2 - \nabla^2] \phi(\mathbf{r}) = \sum_i c_i^0 \int d\mathbf{r}' \rho_i(\mathbf{r}' - \mathbf{r}) \exp \left[ -\beta \int d\mathbf{r}'' \rho_i(\mathbf{r}' - \mathbf{r}'') \phi(\mathbf{r}'') \right] \quad (5.10)$$

The non-local interactions are manifested through the integral over the finite volume of the internal charge distribution. Taking the size of the ions to be small but finite, we can Taylor expand the integral and take only the first components. To make things even simpler, we first linearize Eq. 5.10 to first order in  $\phi(\mathbf{r})$ , and expand in the Fourier space:

$$\begin{aligned} \varepsilon (l_c^2 k^4 + k^2) \phi(\mathbf{k}) + \beta S(k) \phi(\mathbf{k}) &= \rho_f(\mathbf{k}). \\ S(k) &= \sum_i c_i^0 \left| \int d\mathbf{r} \rho_i(\mathbf{r}) \exp(i\mathbf{k} \cdot \mathbf{r}) \right|^2, \end{aligned} \quad (5.11)$$

where  $S(\mathbf{k})$  is a structure factor. The 0<sup>th</sup> order in  $k$  of  $S(k)$  vanishes due to electro-neutrality. Expanding  $S(k)$  to fourth order we recover the regular BSK equation, with modified correlation length and dielectric constant. The dielectric constant we are considering is the one measured by experiments, so it already accounts for any finite-

size dependence. To estimate the effect of non-local interactions, we can focus only on the 4th order term.

For hard sphere models of ions with radii  $a_i$  and total charge  $q_i$ , the internal charge distribution is a constant  $3q_i/4\pi a_i^3$ . The structure factor then reads :

$$\begin{aligned} S(k) &= \sum_i c_i^0 \left| \frac{3q_i}{4\pi a_i^3} \int \mathrm{d}\mathbf{r} \exp(i\mathbf{k} \cdot \mathbf{r}) \right|^2 = \sum_i c_i^0 \left| \frac{3q_i}{a_i^3} \int_0^a r^2 \mathrm{d}r \frac{\sin(kr)}{kr} \right|^2 \\ &\approx \sum_i c_i^0 \left| \frac{3q_i}{a_i^3} \int_0^a r^2 \mathrm{d}r \left( 1 - \frac{(kr)^2}{6} + \frac{(kr)^4}{120} \right) \right|^2 = \sum_i c_i^0 q_i^2 \left| 1 - \frac{(ka_i)^2}{10} + \frac{(ka_i)^4}{420} \right|^2 \end{aligned}$$

Gathering terms up to 4th we find the regular BSK equation with new effective dielectric constant and correlation length:

$$\begin{aligned} \varepsilon &\rightarrow \varepsilon - \sum_i \frac{\beta(a_i q_i)^2}{5} c_i^0 \\ l_c &\rightarrow l_c + \sqrt{\frac{31}{2100}} \frac{\langle a^2 \rangle}{\lambda}, \end{aligned} \quad (5.13)$$

where  $\langle a^2 \rangle$  is an average ionic size, weighted by ionic charges and concentrations. Assuming the  $i^{\text{th}}$  ion has valency  $z_i$  ( $q_i = z_i e$ ), and a stoichiometric coefficient  $s_i$ , the average ionic size equals :

$$\langle a^2 \rangle = \left( \frac{\sum_i s_i z_i^2 a_i^4}{\sum_i s_i z_i^2} \right)^{1/2}. \quad (5.14)$$

The finite size contribute both for the dielectric decrement as well as the correlation length. However, both effects are rather small. The dielectric decrement is mainly related to interactions between the water (dipole) molecules and the salt ions. Eventually, we use empirical data to estimate the water permittivity, and any finite-size contributions to the dielectric constant will thus be taken into account.

For typical experimental values ( $a \approx 1\text{\AA}$ ,  $\lambda \approx 3\text{\AA}$ ) the correction term is roughly the order of  $\approx 0.1\text{\AA}$ . As we describe in Section V, activity experiments suggests  $l_c$  should be an order of magnitude greater. Hence, we can also neglect the finite-size contribution for the 4th order term. Note that the prefactors are a result of the par-

ticular charge distribution we choose, but the functional behavior (linear decrement of the permittivity, and  $a^2/\lambda$  dependance of the correlation length) will remain for more realistic charge distributions.

### 5.3 Activity: Charged Shell in BSK Model

Following recent works ([215, 168]), we derive the activity coefficient based on the linearized BSK equation. One problem that naturally arises when using a 4th order model is how to choose the proper boundary conditions. As shown in [215], the solutions are very sensitive to the choice of the boundary conditions. We circumvent this problem by solving the BSK equation for a sphere immersed in a dielectric continuum, where the BSK equations holds on both sides of the sphere.

First, let us solve linearized BSK equation (Eq. 5.6) around the  $i^{\text{th}}$  ion:

$$(1 - l_c^2 \nabla^2) \nabla^2 \phi(\mathbf{r}) - \lambda^{-2} \phi(\mathbf{r}) = \frac{\rho_f(\mathbf{r})}{\varepsilon}. \quad (5.15)$$

Holding the  $i^{\text{th}}$  type ion fixed we express the fixed charge distributing,  $\rho_f$ , using the Dirac  $\delta$ -function in spherical coordinates:

$$\rho_f(\mathbf{r}) = z_i e \delta^3(|\mathbf{r}| - a_i) = q_i \frac{\delta(r - a_i)}{4\pi a_i^2}. \quad (5.16)$$

In Fourier space Eq. (5.15) becomes an algebraic equation. The Fourier transform for the sphere is  $\rho_f(\mathbf{k}) = z_i e \sin(ka_i)/(2\pi^3 ka_i)$ , leading to the following solution:

$$\phi(\mathbf{k}) = \frac{z_i e \sin(ka_i)}{2\varepsilon\pi^3 z (k^2 + l_c^2 k^4 + \lambda^{-2})} \quad (5.17)$$

We recall that the excess chemical potential of the  $i^{\text{th}}$  ionic specie is given by the electrostatic energy of the ion, and is related to the overall charge density  $\rho(\mathbf{r}) = \sum_j q_j c_j(\mathbf{r})$ :

$$\mu_i^{\text{excess}} = \frac{1}{2} \sum_j \int c_j(\mathbf{r}) \frac{z_i z_j e^2}{4\pi\varepsilon r} \mathrm{d}\mathbf{r} \quad (5.18)$$

In the linearized regime expand Eq. 5.4 to find that  $c^j(\mathbf{r}) \approx c_j^0(1 + z_j e \beta \phi)$ , and along with the electro-neutrality and spherical symmetry of the problem we write the excess potential in terms of the Debye screening length:

$$\mu_i^{\text{excess}} = \frac{1}{2} \sum_i \int c_j^0 \frac{z_i (z_j)^2 \beta e^3}{4\pi \epsilon r} \phi(\mathbf{r}) d\mathbf{r} = \frac{e}{8\pi \lambda^2} \int_0^\infty r \phi(r) dr. \quad (5.19)$$

In Fourier space the integration over the radial coordinate  $r$  is replaced with integral over the radial  $k$  coordinate:

$$\mu_i^{\text{excess}} = \frac{e}{2\lambda^2} \int_0^\infty \phi(k) dk. \quad (5.20)$$

Plugging in our solution for the BSK equation yields:

$$\mu_i^{\text{excess}} = -\frac{(z_i e)^2}{4\pi^2 \epsilon(\lambda)} \int_0^\infty \frac{\sin(ka_i)}{ka_i} \frac{dk}{l_c^2 k^4 + k^2 + \lambda^{-2}} \quad (5.21)$$

There are three length-scales in the problem: the Debye screening length, the correlation length and the ionic radius. Defining  $\delta_c = l_c/\lambda$  and  $\alpha_i = a_i/\lambda$  we find a modification for the classical Debye-Huckel activity:

$$\mu_i^{\text{excess}} = -\frac{(z_i e)^2}{4\pi^2 \epsilon \lambda} \int_0^\infty \frac{\sin(k\alpha_i)}{k\alpha_i} \frac{dk}{\delta_c^2 k^4 + k^2 + 1} \quad (5.22)$$

The integral in Eq. 5.22 can be evaluated in the complex plane, though it easier to identify the roles of the ionic radius and correlation length directly from the above integral form. Both effectively limit the boundaries of the integration, and reduce the overall all magnitude of the excess chemical potential. The term  $\sin(k\alpha_i)/k\alpha_i$  limits the integration to  $k < 1/a_i$ , as expected from the effect of finite radius. On the other hand, the term  $\delta_c^2 k^4$  starts to dominate for values of  $k$  comparable to  $\delta_c^{-1}$ , again effectively trimming the integration.

The analytical result, obtained from evaluating the integral, yields:

$$\mu_i^{\text{excess}} = -\frac{(z_i e)^2}{4\pi^2 \varepsilon (\lambda l_c)^2} \left[ \frac{(e^{-ab_1} - 1)b_2^2 - (e^{-ab_2} - 1)b_1^2}{ab_1^2 b_2^2 (b_1^2 - b_2^2)} \right], \quad (5.23)$$

where  $b_{1,2} = \frac{1}{\sqrt{2}l_c} \left[ 1 \pm \sqrt{1 - 4 \left(\frac{l_c}{\lambda}\right)^2} \right]^{1/2}$  are the solutions of the characteristic equation. For  $l_c < (2\lambda)$  both solutions are purely real, while higher correlation length generates oscillations in the electric potential. For small ionic radii we can expand Eq. (5.23) to second order:

$$\mu_i^{\text{excess}} \approx -\frac{(z_i e)^2}{8\pi\lambda} \frac{1 - \alpha_i^2/(6\delta)}{\sqrt{1 + 2\delta}} \quad (5.24)$$

It is useful to express the new activity coefficient as the original DH formula, with an effective screening length:

$$\lambda_{\text{eff}} = \lambda \left[ \frac{(e^{-ab_1} - 1)b_2^2 - (e^{-ab_2} - 1)b_1^2}{ab_1^2 b_2^2 (b_1^2 - b_2^2)} \right]^{-1} \approx \lambda \sqrt{1 + 2\delta} [1 + \alpha_i^2/(6\delta)]. \quad (5.25)$$

Note that the radius is required to be small compare to both  $l_c$  and  $\lambda$ . In the limit of  $l_c, a \ll \lambda$ , we get  $\lambda_{\text{eff}} \rightarrow \lambda + \frac{a}{2}$ , which is **different** from the Debye-Huckel theory by a factor of 1/2. This factors comes from allowing charges to be present inside the shell, leading to a larger charge overall. In the opposite limit, if  $l_c$  is very large ( $l_c \gg \lambda$ ), the effective screening length scales as  $\sqrt{\lambda l_c}$ .

### 5.3.1 Returning to the Boundary Condition Problem

The fourth order BSK model poses a difficult question on the nature of the boundary conditions. Different choices lead to very different results. Solving BSK equation in all space, including the inside the particle, was our way to circumvent this difficulty. However, this is not physical, and effectively yields an additional charge inside the ion. A more realistic model would set the BSK equation only outside of the particle and setting the boundary condition according to Gauss law ( $\hat{n} \cdot \mathbf{D}(\mathbf{r})|_{r=a} = q_s$ ). The BSK is a 4th order equation, so an extra boundary condition is required. Schlumpberger[215]

showed that by choosing the boundary condition that sets the **first** derivative of the potential to zero, we get the following formula for the activity:

$$\mu_i^{\text{excess}} = \frac{z_i^2 e^2}{8\pi\epsilon_c l_c^2 (b_2^2 - b_1^2)} \left[ \frac{1}{b_1(b_1 a + 1)} - \frac{1}{b_2(b_2 a + 1)} \right], \quad (5.26)$$

which corresponds to a different effective Debye screening length:

$$\tilde{\lambda}_{\text{eff}} = \lambda \left[ \frac{\delta_c^2 (b_2^2 - b_1^2)}{\lambda} \right] \cdot \left[ \frac{1}{b_1(b_1 a + 1)} - \frac{1}{b_2(b_2 a + 1)} \right]^{-1} \quad (5.27)$$

On the face of it, Eq. 5.27 looks very different from the effective screening length predicted by our model in Eq. 5.25. However, expanding Eq. 5.27 in small ionic radii, we find they are quite similar:

$$\tilde{\lambda}_{\text{eff}} \approx \lambda \sqrt{1 + 2\delta} [1 - \alpha^2/\delta] \quad (5.28)$$

To lowest order, the effective screening length is exactly what we would expect for a point like particle. Note that this is a result of choosing the right boundary conditions. Different boundary conditions would not yield this expected result, and are thus less physical (for this problem). The next order is different by a pre-factor of 1/6, but still share the same functional dependence. It turns out that in the high concentration regime of our interest, the second order correction is quite small. For typical values ( $a \approx 1\text{\AA}$ ,  $l_c \approx 3\text{\AA}$  and  $\lambda \approx 3\text{\AA}$ ) it contributes to less than 10% of the effective screening length.

To conclude, finding the activity in the Fourier space had two advantages: First, we were able to easily extract the correct small-ion limit of the activity, which turns out to be a good approximation for high concentrations. Moreover, it sets an additional constraint on the boundary conditions required for solving the real-space BSK equation. The main drawback of this method is in its limitation to small radii: for large ions, or highly concentrated electrolytes the effect of size is important. Our model is thus limited for small ions only, and other models (such as Schlumpberger's model) might describe more accurately salt-in-solvent or ionic liquids for example.

This reasoning is applicable for any fixed charge distributions, and holds for other geometries, as in Santangelo one-component plasma model [211]. If the surface is of constant potential, we can neglect correlation effects on the surface, in which case the Gauss law becomes  $\epsilon \hat{n} \cdot \nabla \phi = q_s$ , and the third derivative should go to zero. A more general approach was previously described by Bazant [18], by arguing that for a metal, the Stern layer can be modeled as a thin dielectric layer with uniform electric field, which leads, again, to the vanishing of the third derivative.

## 5.4 Comparing Results with Experiments

Two key modifications for the activity formula are required before comparing Eq. 5.23 to experimental data: adding the Born energy contribution, as well as accounting for the decrement in the dielectric constant. The excess chemical potential then reads:

$$\mu_i^{\text{ex}} = k_B T \ln \gamma_i = \frac{(z_i e)^2}{8\pi \epsilon_0 \epsilon_c \lambda_{\text{eff}}} + \frac{(z_i e)^2}{8\pi \epsilon_0 a} \left( \frac{1}{\epsilon_c} - \frac{1}{\epsilon_w} \right), \quad (5.29)$$

where  $\lambda_{\text{eff}}$  is defined in Eq. 5.25, and is a function of the correlation length  $l_c$ ,  $\epsilon_w$  is the water permittivity,  $\epsilon_c$  is the dielectric constant at concentration  $c$ . For a binary solution with stoichiometric coefficients  $s_+$  and  $s_-$  solution, the activity coefficients equals:

$$\gamma_{\pm} = (\gamma_+^{s_+} \gamma_-^{s_-})^{1/(s_+ + s_-)}. \quad (5.30)$$

We compare Eq. 5.30 to an experimental data fitted to Bromley formula [42]. Permittivity data was taken from [108], [105] and [258]. In order to evaluate the dielectric constant for concentrations that were not explicitly measured in the permittivity experiments, the data was fitted according to Zuber empirical formula [258]:

$$\epsilon_c = \frac{\epsilon_w}{1 - \alpha c}. \quad (5.31)$$

Values for densities and ionic radii were taken from the literature as well ([193] and [177] respectively). Following [18], we assume the correlation length proportional to

the Bjerrum length:

$$l_c = \beta l_B, \quad (5.32)$$

leaving the only parameter in the model to be the  $\beta$  factor.

We tested our model on 47 solutions, and were able to produce a reasonable fit for 44 of them. Fig. 5-1 shows the results for a random subset, including 6 1:1 solutions, one 1:2, one 2:2 and finally one 1:3 solution. In addition to the Eq. 5.30, the activity coefficients according to the classical Debye-Huckel equation, including the Born correction, are presented for comparison. To test the predictive power of our theory, we fit each graph in two ways: by using the entire range of concentrations, and by extrapolating high concentrations from relatively low ones (smaller than 1.5M). In most cases the limited data underestimates the activity coefficient by a small amount, resulting in larger errors. However, it seems that even with partial information, we are able capture the trend in many of the solutions we examined, and in some cases to a very good precision.

The average values of  $l_c$  remain quite close, at least for the 1 : 1 ionic solution, with an overall average correlation length around 3Å. This value is similar to the suggested correlation length in Liu and Eisenberg model [168], that claimed the correlation length should roughly be twice the ionic radius. In the next section we examine more closely the behavior of the correlation length with concentration.

### 5.4.1 Temperature Dependence

It is interesting to examine the temperature dependence of the correlation length. The available permittivity data for a wide range of temperature is rather scarce, and we could only find data for potassium iodide [138] and sodium chloride [108]. Though we don't have any available activity data for KI or NaCl in different temperatures, we use Meissner Formula [183] to extrapolate the 25C data. The results suggests that the correlation length is increasing with temperature, as shown in Table. 1. This is somewhat counter intuitive from the microscopic perspective. Naively, we would expect interactions to decrease with temperature, in the same way the Bjerrum length does.

Table 5.1: Correlation length and Fitting Errors

salt	$\beta^1$	STD <sup>2</sup>	salt	$\beta$	STD	salt	$\beta$	STD
<b>1:1 Electrolytes</b>			LiOH	-0.03	31.9	CaBr2	0.53	15.74
CsBr	0.14	1.43	MgSO4	0.33	1.3	CaNO32	0.27	3.14
CsCl	0.18	1.36	NaBr	0.28	0.67	Mg(NO3)2	0.15	13.04
CsF	0.81	5.82	NaCl	0.19	1.23	MgBr2	-0.19	119.54
CsI	0.08	1.66	NaCl	0.13	0.27	MgCl2	-0.13	154.27
CsNO3	0	20.25	NaClO4	0.13	0.62	MgI2	0.36	660.6
KBr	0.23	0.58	NaF	0.07	1.43	<b>1:3 Electrolytes</b>		
KCl	0.21	0.96	NaI	0.35	3.44	LiCl3	1.61	162.85
KClO4	0	26.98	NaNO3	0.04	0.77	<b>2:2 Electrolytes</b>		
KF	0.39	0.33	RbBr	0.18	1.13	Li2SO4	0.18	4.92
KI	0.31	1.09	RbCl	0.19	1.11	Na2SO4	0.2	3.12
KNO3	-0.09	18.67	RbF	0.43	0.99	Rb2SO4	0.39	1.61
KOH	0.23	0.67	RbI	0.18	0.96	<b>2:3 Electrolytes</b>		
LiBr	0.23	3.38	<b>1:2 Electrolytes</b>			Al2(SO4)3	0.51	0.25
LiCl	0.21	1.11	BaCl2	0.69	25.04			
LiClO4	0.33	13.44	BaI2	7.23	434.52			
LiI	0.41	12.14	BaNO32	0.06	2.57			

1.  $\beta$  is related to the correlation length by Eq. 5.32.

2.  $\times 10^{-3}$ .

Table 5.2: Correlation length as a function of temperatures

Salt	Temperature[C]	$l_c$ [ $\text{\AA}$ ]
NaCl	1.5	1.3
NaCl	25	1.91
KI	25	3.02
KI	40	3.6
KI	50	4.49

Even the non-local contribution to the correlation length decreases with temperature, since it is inversely proportional to the Debye screening length that increases. This is another example for the difficulty to simply relate the phenomenological constant  $l_c$  to microscopic variables.

## 5.4.2 Nitrate, Sulfate and Hydroxide: Adding Short-Range Interactions

Compared to the original Debye-Huckel equation, the measured activity coefficient is usually higher than predicted. Two effects that contribute to higher chemical potential were discussed in the previous sections: correlations leading to a 4th order term in the BSK equation, and the Born energy. Both effects make it less favorable for the system to add an extra charged particle. For the majority of substances we indeed

see a rise in the activity coefficient, but for several classes of electrolytes the activity remain low. In these materials a stronger effect is present, and one simple way of accounting for it is by including short range interactions, and **explicitly** make it favorable for new ions to join the party.

Adding specific interactions contributes to the overall chemical potential in two ways: directly, with a linear dependence in concentration, and indirectly, by changing the Poisson-Boltzmann equation. A simple free-energy short-range interaction term reads:

$$\Delta G = \sum_{ij} \int d\mathbf{r} \alpha_{i,j} c_i(\mathbf{r}) c_j(\mathbf{r}), \quad (5.33)$$

where  $\alpha_{ij}$  are the interaction parameters between the  $i$  and  $j^{\text{th}}$  species. The direct contribution is given by:

$$\Delta \mu_i^{\text{excess,direct}} = \sum_j \alpha_{i,j} c_j(\mathbf{r}). \quad (5.34)$$

In Appendix. 1 we derive the indirect contribution, and find it is comparable in strength to the direct one. Generally, incorporating specific interactions lead to a change in the Debye screening length:

$$\lambda = \left[ \sum_{ij} \frac{(\mathbf{I} + \mathbf{A})_{ij}^{-1} c_j^0 q_i q_j}{\epsilon k_B T} \right]^{-1/2}. \quad (5.35)$$

where  $\mathbf{I}$  is the unit matrix, and  $\mathbf{A}$  is a matrix whose elements are related to the interaction parameters:  $A_{i,j} = \beta c_i^0 \alpha_{ij}$ . For a binary solution there are, in principle, 3 additional fitting parameters. However, since much of the behavior is already captured, we consider only a weak interaction between the two different species ( $\alpha_{11} = \alpha_{22} = 0$ ). In this limit, for  $s_+ : s_-$  stoichiometry and concentration  $c_0$ , the resulting screening length reads:

$$\lambda^{-2} \approx \frac{\beta e^2 c_0 (s_1 z_1^2 + s_2 z_2^2)}{\epsilon} \left[ 1 - \frac{2\alpha_{12} s_1 z_1}{z_1 - z_2} \beta c_0 \right] \quad (5.36)$$

Fig. 5-3 shows results for 6 solutions that were not properly described by the BSK model. It is clear that introducing the extra fitting allows for an almost exact fit. Results are shown compared to both DH equation and the BSK.

From the given data we can not properly distinguish between different types of interactions. Even solvent-solute interactions can lead to changes in the activity: Eq. 5.35 is in general true, even for neutral (solvent) species. In this case, there is no direct contribution for the chemical potential (the solvent concentration is constant), but the indirect one can be important.

## 5.5 A closer Look at the Correlation Length

In the previous section we showed that the BSK equation produces a reasonable agreement with experimental data, using a single free parameter. Moreover, we showed that in many cases, we are able to successfully extrapolate the activity of high concentration based on low concentration data. We would like now to address the question first raised in Section II: how does the correlation length depends on concentration?

We can view Eq. 5.30 as an equation for  $l_c(c)$ : assuming the activity model is correct, we find the correlation length as a function of concentration. Fig. 5-2 shows the calculated correlation length length for the different solutions displayed in the previous section. We first note that, as expected, the correlation length goes to 0 in the dilute limit. The transition between the dilute regime to the correlated one happens for concentrations in which the distance between the ions is comparable with the Bjerrum length.

For most compounds, the correlation length is slowly increasing across a wide range of concentrations. This behavior resembles the Bjerrum length, which slowly increases as the dielectric constant decreases. By choosing a suitable  $\beta$  to multiply the Bjerrum length, the estimated correlation length, marked in lashed line in Fig. 5-2, fits many of the salts. It is interesting to note that a single parameter catches both the mean correlation length and the slope.

Other plausible relations for the correlation length do not work so well. The 'finite-

size' contribution, which goes as  $1/\lambda$ , overestimates the concentration dependence. A the constant model underestimates it. Moreover, to the best of our ability, we were not able to correlate the different  $l_c$ 's to any other microscopic parameter of the system, including the ionic size.

There are two obvious drawbacks to the suggested form. First, it is only applicable for large concentrations. In the dilute limit the Bjerrum length is a constant (about  $7\text{\AA}$ ), and does not vanishes. However, even for large concentrations, there are many cases where it fails. The sulfate solutions for example exhibits a decrease in the empirical correlation length, while other high valance solutions (such as  $\text{LaCl}_3$ ) depends more strongly on the concentration. Nevertheless, it is still surprising that the BSK equation along with a simple assumption on the correlation length, is able to fit well many of solutions, even if not all.

## 5.6 Conclusions

We derived the activity coefficient of an aqueous solutions based on the BSK equation, and showed it was able to match a wide range of experimental data with only single fitting parameter: the correlation length. This was achieved by linearizing the BSK equation, and solving it for charged sphere immersed in a solution. Another key ingredient was to take into account the Born energy associated with the decrement of the dielectric constant with the increase of concentrations.

Without explicit solving the complicated differential equation, we used the Fourier space analysis to obtain a simple formula for the activity coefficient. In the limit of small ionic radius, it reduced to renormalization of the Debye screening by a factor of  $\sqrt{1 + 2l_c/\lambda}$ . Corrections that take into account the the finite size of the ions increase the effective screening length even further.

The origins of the correlations length have also been discussed. In general, a BSK-like equation can be a result of ion-ion interactions beyond mean field, or a finite-size effect associated with non-local electrostatic interactions. We derived a BSK equation stemming from non-local electrostatics, and noticed that the correlation length is too

small to account for the large effect seen in experiments.

Finally, we tried to estimate the correct concentration dependence of the correlation length. With several plausible suggestion from the literature in mind, we extracted an empirical function based on activity experiments. For most compounds we observed a nearly constant behavior, with a small increase for high concentrations. A natural candidate to describe this behavior is the Bjerrum length, which was first suggested by Bazant et al in Ref. [18].

There are several extension one can consider to improve upon the the model presented. The maximal concentration we considered was of 5M, but even in lower concentrations we found two effects to be significant: the concentration dependence of the dielectric constant and ion-ion correlations. In the ionic liquid regime we expect these effect to be more pronounced, adding to other effects that were neglected in our derivation. In particular, as the screening length decreases, the ionic radii becomes the most relevant length scale, making a lattice or hard sphere considerations important.

Nevertheless, even in relatively low concentrations, it is instructive to have a simple model that relates known physical parameters to the activity coefficients. In the emerging field of Li-air batteries, for example, the solubility of the intermediate species involved is important for the battery's capacity[127, 43, 7]. A recent paper by Schutter et al [217] suggested a way to screen compounds to find ones with good solvation properties by using several descriptors: solvation energy, kPa, viscosity and HOMO levels. Computational methods, such as DFT are used to estimate these parameters, but they should apply mainly to the dilute limit. Our model can shed light on higher concentrations.

## 5.A Modified BSK: Short-Range Interaction

In section V we argued that the BSK model is not a sufficient description for some materials, for which specific short-range interactions play an important role. A simple yet powerful way to exted the BSK equation, is to add contact interaction terms to the free energy functional (Eq. 5.3):

$$\begin{aligned}
G &= \int d\mathbf{r} \left\{ g + \rho\phi - \frac{\varepsilon}{2} \left[ |\nabla\phi|^2 + l_c^2 |\nabla^2\phi|^2 + \sum_{ij} \alpha_{ij} c_i(\mathbf{r}) c_j(\mathbf{r}) \right] \right\} \\
g &= k_B T \sum_{i=1}^N [c_i(\mathbf{r}) \log(c_i(\mathbf{r})) - c_i(\mathbf{r})], \tag{5.37}
\end{aligned}$$

where  $\alpha_{i,j}$  is the interaction between the  $i^{\text{th}}$  and  $j^{\text{th}}$  ionic species. We derive the relation between the local ionic concentration,  $c_i(\mathbf{r})$ , and the bulk concentrations,  $c_i^0(\mathbf{r})$  the same as before, but now we find that  $c_i^0(\mathbf{r})$  is expressed in an implicit form:

$$\begin{aligned}
\mu_i &= \frac{\delta G}{\delta c(\mathbf{r})} = k_B \log(c_i) + q_i \phi(\mathbf{r}) + \sum_j \alpha_{ij} c_j(\mathbf{r}) \\
c_i(\mathbf{r}) &= \exp(\beta\mu_i - \beta q_i \phi(\mathbf{r}) - \beta \sum_j \alpha_{ij} c_j(\mathbf{r})) \\
&= c_i^0 \exp \left[ -q_i \beta \phi(\mathbf{r}) - \beta \sum_j \alpha_{ij} (c_j - c_j^0(\mathbf{r})) \right], \tag{5.38}
\end{aligned}$$

Define  $\delta c_i(\mathbf{r}) = c_i - c_i^0(\mathbf{r})$  as the deviation from bulk concentrations, we expand Eq. 5.38 to first order in  $\alpha$  and  $\phi$  to get a set of linear equations:

$$\begin{aligned}
\delta c_i(\mathbf{r}) &= -q_i c_i^0 \beta \phi(\mathbf{r}) - c_i^0 \beta \sum_j \alpha_{ij} \delta c_j(\mathbf{r}). \\
\delta c_i(\mathbf{r}) &= -\beta \phi \sum_j (\mathbf{I} + \mathbf{A})_{ij}^{-1} c_j^0 q_j, \tag{5.39}
\end{aligned}$$

where  $\mathbf{I}$  is the unit matrix, and  $\mathbf{A}$  is:  $A_{i,j} = \beta c_i^0 \alpha_{ij}$ . We note that for weak potentials, the first order approximation is justified even for strong interactions and large concentrations, as long as the deviations from the bulk concentrations are small enough.

The overall charge density is then given by:

$$\rho(\mathbf{r}) = \sum_i q_i c_i(\mathbf{r}) = \sum_i q_i \delta c_i(\mathbf{r}) = -\beta \phi \sum_{ij} (\mathbf{I} + \mathbf{A})_{ij}^{-1} c_j^0 q_i q_j. \tag{5.40}$$

The charge density is still linear in  $\phi$ , so the BSK equation remains exact, with a new definition of  $\lambda$ :

$$\lambda = \left[ \sum_{ij} \frac{(\mathbf{I} + \mathbf{A})_{ij}^{-1} c_j^0 q_i q_j}{\epsilon k_B T} \right]^{-1/2}. \quad (5.41)$$

In a binary solution with stoichiometry  $S_+ : S_-$  and concentration  $c_0$ , the screening length reads:

$$\begin{aligned} \lambda^{-2} &= \frac{\beta e^2 c_0}{\epsilon} \begin{bmatrix} z_1 & z_2 \end{bmatrix} \cdot \begin{bmatrix} 1 + \beta \alpha_{11} c_0 s_1 & \beta \alpha_{12} c_0 s_1 \\ \beta \alpha_{12} c_0 s_2 & 1 + \beta \alpha_{22} c_0 s_2 \end{bmatrix}^{-1} \cdot \begin{bmatrix} s_1 z_1 \\ s_2 z_2 \end{bmatrix} \\ &= \frac{\beta e^2 c_0}{\epsilon} \begin{bmatrix} z_1 & z_2 \end{bmatrix} \cdot \begin{bmatrix} 1 + \beta \alpha_{22} c_0 s_2 & -\beta \alpha_{12} c_0 s_1 \\ -\beta \alpha_{12} c_0 s_2 & 1 + \beta \alpha_{11} c_0 s_1 \end{bmatrix} \cdot \begin{bmatrix} s_1 z_1 \\ s_2 z_2 \end{bmatrix} \\ &= \frac{\beta e^2 c_0}{\epsilon} \frac{(1 + \beta \alpha_{11} c_0 s_1)(1 + \beta \alpha_{22} c_0 s_2) - (\beta \alpha_{12} c_0)^2 s_1 s_2}{(1 + \beta \alpha_{11} c_0 s_1)(1 + \beta \alpha_{22} c_0 s_2) - (\beta \alpha_{12} c_0)^2 s_1 s_2} \\ &= \frac{\beta e^2 c_0}{\epsilon} \frac{s_2 z_2^2 (1 + \beta \alpha_{11} c_0 s_1) + s_1 z_1^2 (1 + \beta \alpha_{22} c_0 s_2) - 2 \beta c_0 \alpha_{12} z_1 z_2 s_1 s_2}{(1 + \beta \alpha_{11} c_0 s_1)(1 + \beta \alpha_{22} c_0 s_2) - (\beta \alpha_{12} c_0)^2 s_1 s_2} \\ &= \frac{\beta e^2 c_0}{\epsilon} \frac{s_1 z_1^2 + s_2 z_2^2 + \beta c_0 s_1 s_2 (\alpha_{11} z_2^2 + \alpha_{22} z_1^2 - 2 \alpha_{12} z_1 z_2)}{1 + \beta c_0 (s_1 \alpha_{11} + s_2 \alpha_{22}) + (\beta c_0)^2 (\alpha_{11} \alpha_{22} - \alpha_{12}^2)} \end{aligned} \quad (5.42)$$

To leading order in  $\alpha$ :

$$\begin{aligned} \lambda^{-2} &\approx \frac{\beta e^2 c_0 (s_1 z_1^2 + s_2 z_2^2)}{\epsilon} (1 + \beta c_0 \xi) \\ \xi &= \frac{s_1 s_2 (\alpha_{11} z_2^2 + \alpha_{22} z_1^2 - 2 \alpha_{12} z_1 z_2)}{s_1 z_1^2 + s_2 z_2^2} - s_1 \alpha_{11} - s_2 \alpha_{22}. \end{aligned} \quad (5.43)$$

If we consider only interactions between the different species, that is  $\alpha_{11} = \alpha_{22} = 0$ , we get a simple expression for  $\xi$ :

$$\xi = -2 \alpha_{12} \frac{s_1 z_1}{z_1 - z_2}. \quad (5.44)$$

For the 1 : 1 solutions  $\xi$  is equal to the strength of the interaction,  $\alpha_{12}$ . There, therefore, a correction for the screening length that is proportional to  $\lambda_0 \beta \alpha_{12} c_0$ . The chemical potential, in turn, will change by the order of  $e^2 / (\text{var} \epsilon \lambda_0) \beta \alpha_{12} c_0$ . We hence conclude that the contribution from this indirect effect on the activity is comparable

to the direct contribution discussed in section V:

$$\Delta\mu_i^{\text{excess, indirect}} \approx \Delta\mu^{\text{excess, direct}} (\beta e^2/\lambda) \approx (l_B/\lambda) \Delta\mu^{\text{excess, direct}}. \quad (5.45)$$

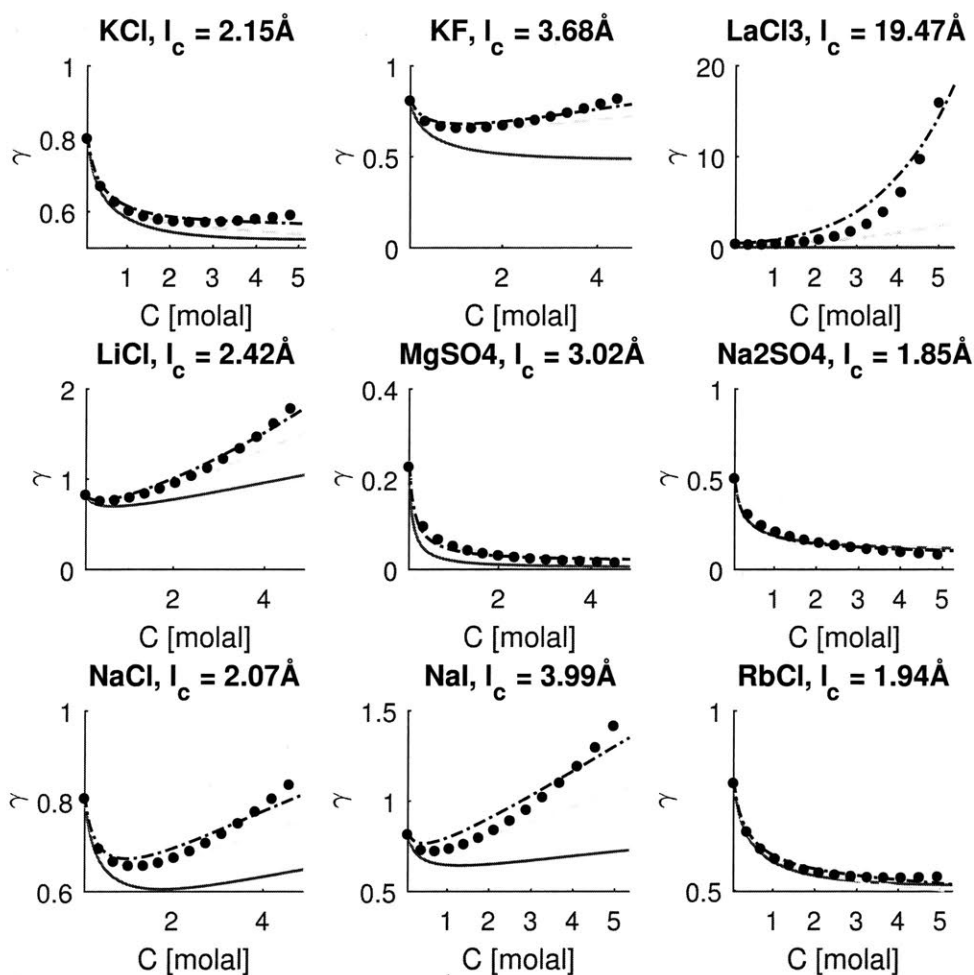


Figure 5-1: Activity coefficients for different aqueous solutions. Green lines are fitted according to Eq. 5.30 with  $l_c$  as a fitting parameter, the solid lue lines are according to Born approximation, the dashed green lines are based on our model, with  $l_c$  fitted to data  $< 1.5M$ , and the dash-dot black lines show the result of our model, fitted for the whole range. The black dots are based on experimental data fitted to Bromley formula [42]

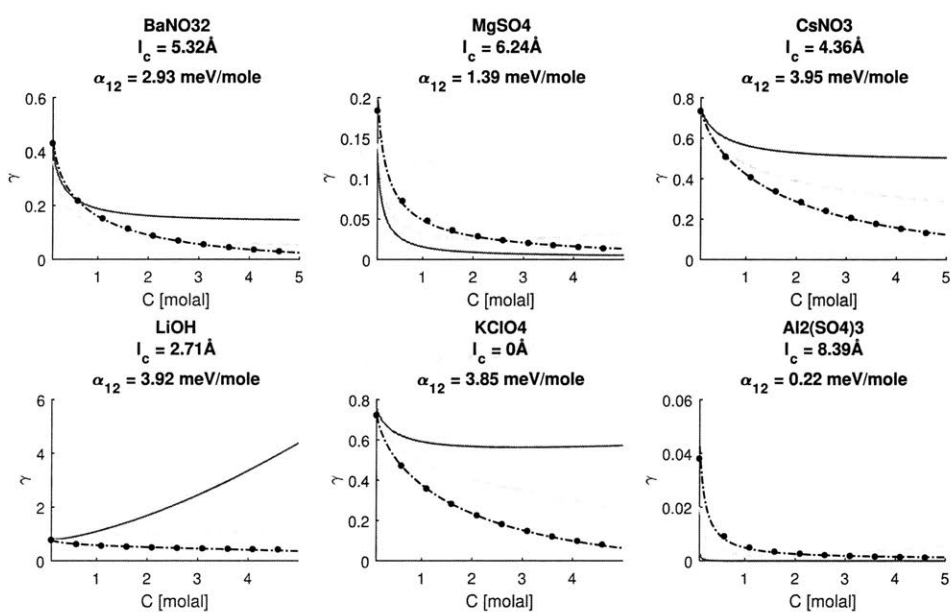


Figure 5-2: Activity coefficients for different aqueous solutions. Green lines are fitted according to Eq. 5.30 with usual definition of  $\lambda$ , the dash-dot black lines incorporate direct specific interaction term with  $\lambda$  defined by Eq. 5.36. The black dots are based on experimental data fitted to Bromley formula [42], and the blue line is according to classic DH approximation

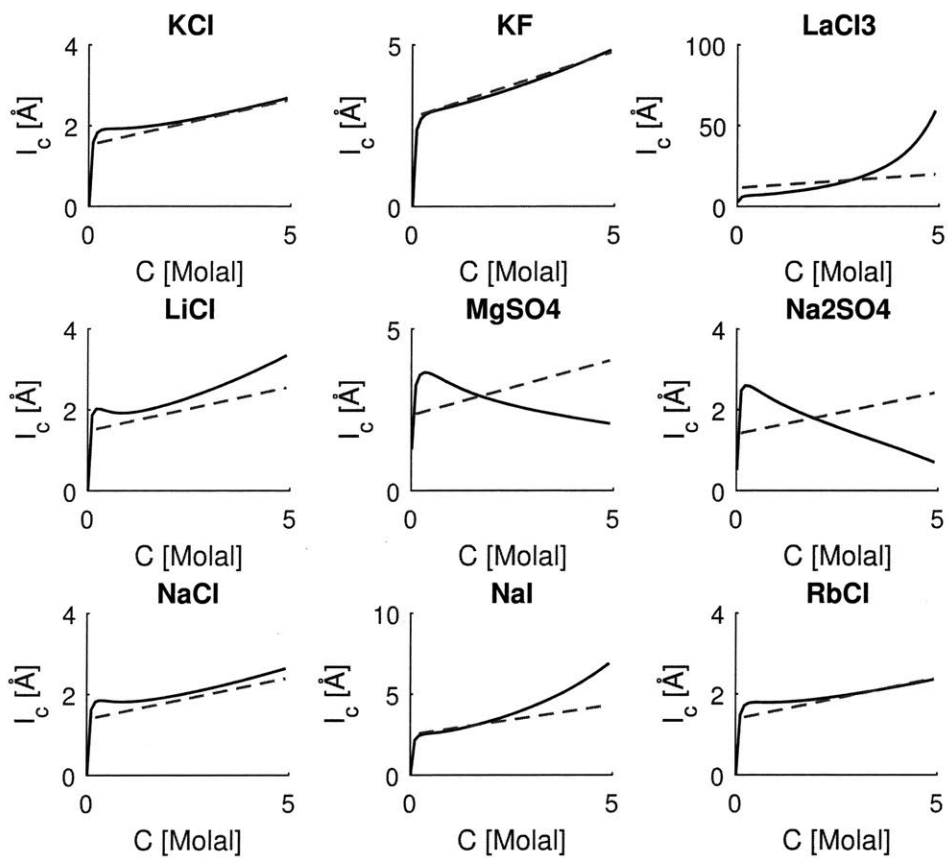


Figure 5-3: Estimated correlation length according to experimental data (solid line) and according to Eq. 5.32 (dashed line), for different ionic solutions



# Chapter 6

## Ionic activity in concentrated electrolytes: solvent structure effect revisited

Except for minor edits, the contents of this chapter have been submitted for publication and are currently under review[162].

### 6.1 Introduction

The activity coefficients of concentrated aqueous solutions play an important role in different biological and electrochemical systems[191], and indeed, many models to describe the ionic activity have been proposed over the years. In the original Debye and Hückel (DH) paper from 1923[61], the activity coefficient was calculated based on a linearized version of the Poisson-Boltzmann (PB) equation. This resulted in the well-known DH equation, which for symmetric binary electrolytes reads:

$$\ln \gamma = -\frac{A|z_+z_-|\sqrt{I}}{1 + Ba\sqrt{I}}, \quad (6.1)$$

where  $\gamma$  is the activity coefficient,  $z_{\pm}$  are the valencies of the ions,  $I = \sum_{i=\pm} c_i z_i^2$  is the ionic strength,  $c_{\pm}$  are the ionic concentrations and  $a$  is an effective distance of

closest approach, roughly equal to the ionic diameter.  $A$  and  $B$  are constant values that depend on the temperature ( $k_B T$ ), the dielectric constant of the medium ( $\epsilon$ ) and the unit charge ( $e$ ):

$$B = \sqrt{\frac{8\pi e^2}{\epsilon k_B T}}, \quad A = \frac{e^2 B}{2\epsilon k_B T}. \quad (6.2)$$

The DH equation works well for very dilute electrolytes but fails to even qualitatively capture the activity behavior at higher concentrations. In a following work[118], Huckel added an important term for the activity: the change in self-energy due to variations in the dielectric constant. Experiments measuring the static dielectric constant of ionic solutions were not available at the time, so the proposed model treated the dielectric constant as a fitting parameter. Assuming the dielectric constant of bulk water,  $\epsilon_{\text{Bulk}}$ , is decreased proportionally to the ionic concentration  $c$  ( $\epsilon \approx \epsilon_{\text{Bulk}} - \delta c$ ), the correction to the DH equation is a simple linear term in concentration. Remarkably, fitting this model to existing activity data actually estimated the dielectric decrement close to measured values, an observation first noted by Hasted et al[108] in their paper on the dielectric properties of ionic solutions.

A linear correction for the DH equation also emerges when considering short-range repulsive forces, via a virial expansion. The virial expansion offers a systematic way to include even higher order terms in concentration. First suggested by Guggenheim[104], and further developed by Pitzer[203], accounting for the second and third virial coefficients leads to a very powerful description of the activity. The Pitzer formula, which is essentially the regular Debye-Huckel with corrections to second order in the concentration, is in excellent experimental agreement for hundreds of compounds[133]. To achieve its high accuracy, the Pitzer model hence requires several fitting parameters: the virial coefficients are not derived from first principles, and the ionic radii are an empirical parameters as well. Closely related models were subsequently derived by Bromley[42], Meissner[148] and Chen[54].

In the past half a century many more models have been developed on the basis of integral equation approach to statistical theory of fluids, adapted for charged fluids. The Hyper-Netted Chain approximation (HNC) and the Mean Spherical Approxima-

tions (MSA) are examples for microscopic derivations of the activity coefficient[222, 44, 224]. Assuming a hard-sphere repulsion in addition to the Coulombic attraction, the integral equation theories give an approximated way to calculate the pair correlation function between any two ions. Usually, numerical methods are required to solve the integral equations. The activity is expressed in terms of the correlation function, without a simple closed-form formula. Another drawback of the integral equation model is that they too require some fitting parameters.

Not going into a comparison of these different approaches, we only stress that they were all derived for the primitive model of the solvent. Ions interact there via Coulomb law like they would if the solvent was a dielectric continuum, with a macroscopic dielectric constant. At the same time we know from molecular simulations that in polar solvents, water, in particular, the potential of mean-force between the ions exhibit decaying oscillations with the periodicity of the order of the diameter of the solvent molecules, with signatures of overscreening effect, and only at long distances it would approach the macroscopic Coulomb interactions, as a limiting law. How this fact would reveal itself in thermodynamics of electrolytes? One way to answer this question would be to incorporate the effects of the molecular structure of the solvent via replacing the Coulomb pair interaction potential in the above-mentioned approaches with the correspondingly modified ones. Alternatively, one could incorporate the differences from the primitive Coulomb into the short-range part of the interaction potential. Such short-range part would then extend few times farther than the average diameter of ions. In order to justify such efforts, we will do here something yet simpler: We will combine the Debye-Hueckel approach with a nonlocal electrostatic description of the solvent. Although such approach will not take into account complex correlations in a concentrated electrolyte, it will be a step towards connecting the correlations of the bound charge density of the solvent subsystem ('molecular correlations) and the ion-ion correlations in the electrolyte plasma. Such an approach will work as an interpolation. Following this root, we will result in a closed-form expression which as we will see will describe the behavior of activity coefficients very well.

Such an approach has been, actually, proposed and tried long ago [116, 146]. We revisit it below, showing that for the updated approximation of the form of nonlocal dielectric function of a pure solvent that qualitatively reproduces the simulation results for water [36, 37] we can obtain very reasonable results for the activity coefficients and explore certain trends in their dependence on electrolyte concentration.

## 6.2 Model

Our goal is to build a phenomenological description of the dielectric function of ionic solutions, that accounts for both the solvent molecules and the ions and would enable us to calculate the ionic activity coefficient. In a constant dielectric medium (the so-called "primitive" model), one can derive the dielectric response directly from the Poisson-Boltzmann equation. However, a constant dielectric medium is an approximation suitable for large ion-ion separations. At shorter separations, the molecular ordering of the water gives rise to a complicated dielectric response. Empirical formulae for the dielectric function have been suggested in the literature[146, 141], in relation with computer simulation results [36] and experimental data[227]. We will now show how we extend the pure-water empirical dielectric response for ionic solutions, by building an interpolated function that satisfies the limiting behaviors.

Within linear nonlocal electrostatics, electrical induction and electric field are related by nonlocal constitutive relation:  $D_\alpha(\mathbf{r}) = \sum_\beta \int d\mathbf{r}' \varepsilon_{\alpha\beta}(\mathbf{r} - \mathbf{r}') E_\beta(\mathbf{r}')$ , where  $\varepsilon_{\alpha\beta}(\mathbf{r} - \mathbf{r}')$  is the nonlocal dielectric tensor. In the macroscopic electrostatics  $\varepsilon_{\alpha\beta}(\mathbf{r} - \mathbf{r}') = \varepsilon \delta_{\alpha\beta} \delta(\mathbf{r} - \mathbf{r}')$  which reduces the constitutive relation to the common  $\mathbf{D}(\mathbf{r}) = \varepsilon \mathbf{E}(\mathbf{r})$ . All information about the correlations of the bound charge density in the medium are contained in the form of the tensor  $\varepsilon_{\alpha\beta}(\mathbf{r} - \mathbf{r}')$ . Referring the reader to Ref.[140] for details, we mention that in homogeneous and isotropic media, electrostatic equations will be conveniently expressed through the Fourier transform of this tensor  $\tilde{\varepsilon}_{\alpha\beta}(\mathbf{k})$ , and more precisely through its longitudinal component  $\tilde{\varepsilon}_{\parallel}(k) = \sum_{\alpha\beta} \frac{k_\alpha k_\beta}{k^2} \tilde{\varepsilon}_{\alpha\beta}(\mathbf{k})$ , often called simply  $\tilde{\varepsilon}(k)$ . Long wave-length limit (small  $k$ ) recovers macroscopic behaviour, large  $k$ , probes short range correlations. For instance, speaking about pure solvent

$k \sim 2\pi/d$ , where  $d$  is diameter of water molecule, would characterize the molecular packing effects. For much larger,  $\tilde{\epsilon}(k)$  will approach short range dielectric constant due to electronic polarizability of the molecules. We denote the corresponding dielectric constant in that limit  $\epsilon_*$ .

In the long wavelength limit, the Poisson-Boltzmann equation for a binary monovalent solution reads:

$$\epsilon_{\text{Bulk}} \nabla^2 \phi(\mathbf{r}) = 8\pi e c \sinh[e\beta\phi(\mathbf{r})] - 4\pi\rho_{\text{ext}}(\mathbf{r}), \quad (6.3)$$

where  $c$  is the bulk ionic concentration,  $\beta = 1/k_{\text{B}}T$  is the inverse temperature and  $\rho_{\text{ext}}$  is an external charge distribution. In the linear (Debye-Huckel) regime, the PB equation is a second order differential equation, or an algebraic equation in Fourier space:

$$\epsilon_{\text{Bulk}} k^2 \left[ 1 + \frac{8\pi c e^2 \beta}{\epsilon_{\text{Bulk}} k^2} \right] \tilde{\phi}(\mathbf{k}) = 4\pi \tilde{\rho}_{\text{ext}}(\mathbf{k}). \quad (6.4)$$

Comparing Eq. 6.4 to the Poisson equation, we can immediately write the dielectric response of ionic solutions in the limit of large wavelengths:

$$\tilde{\epsilon}_{\text{c,bulk}}(\mathbf{k}) = \epsilon_{\text{Bulk}} \left[ 1 + \frac{1}{(k\lambda_{\text{D}})^2} \right], \quad (6.5)$$

where  $\lambda_{\text{D}} = (8\pi c e^2 \beta / \epsilon_{\text{Bulk}})^{-1/2}$  is the Debye screening length. The divergence at small wave-numbers corresponds to the screening of the potential at distances larger than the Debye screening length. At smaller distances the screening effect is negligible, and dielectric response is only influenced by the water. This will remain true even if we consider a more complicated expression for the water dielectric response, rather than  $\epsilon_{\text{Bulk}}$ . Hence, we can write a simple interpolated formula for the dielectric response by replacing  $\epsilon_{\text{Bulk}}$  with the full  $\tilde{\epsilon}_w(k)$ :

$$\tilde{\epsilon}_c(\mathbf{k}) = \tilde{\epsilon}_w(k) \left[ 1 + \frac{1}{k^2 \lambda_{\text{D}}^2} \right] \quad (6.6)$$

This approach is similar to interpolation implemented in Refs.[140, 143] in terms of the limiting cases covered, but its form is slightly different, reflecting stronger coupling between the solvent structure and the ionic screening. Note that this interpolated response satisfies both the long and short wavelength limits. In the long-wavelength  $\tilde{\epsilon}_w(k) \rightarrow \epsilon_{\text{Bulk}}$  and we recover Eq. 6.5. In the short-wavelength, the ionic contribution is neglected as we recover the pure-water response.

By design, the interpolated formula is expected to work well if there is a separation of length-scales, and the Debye length is much larger than the molecular size of the solvent. In this limit, however, the predicted ionic activity will coincide with classical Debye-Huckel theory. Interesting physics emerges as we increase the concentration, and enter a regime where both ions and water molecules play a major role.

Within the linear approximation, this interpolation formula for the dielectric constant provides all the necessary information required to derive the activity coefficient. Let us now, following Ref.17 (first time derived in [116]), use the charging process to evaluate the activity of ions, by considering a spherical particle immersed in a dielectric medium. By slowly turning on the charge, the energy is determined by the potential on the surface of the ion:

$$u = \int_0^e dq \phi_q(r = a), \quad (6.7)$$

where  $\phi_q(r)$  is the electrostatic potential around a charged particle with charge  $q$ , and  $a$  is the effective radius of the sphere, related to the distance of closest approach to the ion. A simple way of estimating the electrostatic potential is by letting water to permeate the ion, and solving the Poisson equation in k-space:

$$\phi_q(r) = \int \frac{d\mathbf{k}}{(2\pi)^3} \frac{4\pi q \tilde{\rho}(\mathbf{k})}{\tilde{\epsilon}_c(\mathbf{k}) k^2} e^{i\mathbf{k}\cdot\mathbf{r}} = \frac{2}{\pi} \int_0^\infty dk \frac{\sin(kr)}{kr} \frac{q \tilde{\rho}(k)}{\tilde{\epsilon}_c(k)}, \quad (6.8)$$

where  $\tilde{\rho}(\mathbf{k})$  is the Fourier transform of the charge distribution, called also an ionic form-factor:

$$\tilde{\rho}(k) = \int d\mathbf{r} \rho(\mathbf{r}) e^{-i\mathbf{k}\cdot\mathbf{r}}. \quad (6.9)$$

Following Ref. [146], we use a smeared charge distribution, defined as follows:

$$\tilde{\rho}(k) = \frac{1}{\eta(a^2 + \eta^2(2 - e^{-a/\eta}))} \cdot \left\{ \frac{\eta a \sin ka}{k(1 + \eta^2 k^2)} + \frac{\eta^3(2 \cos ka - e^{-a/\eta})}{(1 + \eta^2 k^2)^2} \right\}, \quad (6.10)$$

where  $\eta$  is the smearing parameter, which describes the width of the ionic charge shell; for  $\eta \rightarrow 0$  the form-factor reduces to the Ascroft form:  $\tilde{\rho}(k) = \sin(ka)/ka$ . Combining Eqs. (6.7) and (6.8) we obtain:

$$u = \frac{e^2}{\pi} \int_0^\infty dk \frac{\tilde{\rho}(k) \sin(ak)}{\tilde{\epsilon}_c(k) ak}. \quad (6.11)$$

The excess chemical potential of moving an ion for bulk water to ionic solution with concentration  $c$ , is given by (in units of thermal energy,  $k_B T$ ):

$$\begin{aligned} \ln \gamma &= \beta [u(c) - u(c=0)] \\ &= \frac{l_B}{\pi} \int_0^\infty dk \frac{\sin^2(ak)}{(ak)^2} \left[ \frac{\tilde{\rho}(k)}{\tilde{\epsilon}_c(k)} - \frac{\tilde{\rho}(k)}{\tilde{\epsilon}_{c=0}(k)} \right], \end{aligned} \quad (6.12)$$

where  $l_B = \beta e^2$  is the vacuum Bjerrum length. Using the interpolated formula for  $\epsilon_c(k)$  (Eq. 6.6), we can write the chemical potential in terms of the water dielectric constant and relate it to the Debye Huckel limiting law:

$$\frac{\ln \gamma}{\ln \gamma^{\text{DH}}} = \frac{2}{\pi} \int_0^\infty dk \frac{\sin(ak)}{\lambda_D} \frac{\epsilon_{\text{bulk}}}{ak} \frac{\tilde{\rho}(k)}{\tilde{\epsilon}_w(k) k^2 + \lambda_D^{-2}}, \quad (6.13)$$

where  $\ln \gamma$  is the classical Debye activity formula (in the limit of  $a \rightarrow 0$ ):

$$\ln \gamma^{\text{DH}} = -\frac{l_B}{2\epsilon_{\text{bulk}}\lambda_D}. \quad (6.14)$$

Finally, we need to suggest a model for the solvent dielectric function. So far we have only specified the limits it must hold: it equals bulk values ( $\epsilon \approx 80$ ) at small

wave-vectors and some small value  $\varepsilon_*$  at large ones. It is instructive to introduce a weighting function  $f(k)$ , that equals 1 at the large wavelength limit, and 0 for short wavelengths, so we can write a general dielectric function as:

$$\tilde{\varepsilon}_w(k) = [(\varepsilon_*)^{-1} + (\varepsilon_{\text{bulk}}^{-1} - (\varepsilon_*)^{-1}) f(k)]^{-1}. \quad (6.15)$$

A simple  $f(k)$  that satisfies the correct limits is a Lorentzian shape:

$$f(k) = \frac{1}{1 + k^2 \Lambda^2}. \quad (6.16)$$

The Lorentzian shape captures some effects of solvent structure at long wavelength, implying that water molecules are correlated, and their correlation is exponentially decreasing with a decay length  $\Lambda$ . But it misses to correctly describe the short range behaviour: molecular dynamics simulations of water molecule reveal a much more complicated structures with  $k$ -dependence reflecting resonance effects of over-screening [36, 147, 80]. In the spirit of work [146] we could account for over-screening by the following formula for  $f(k)$ :

$$f(k) = \frac{(1 + (\Lambda^2 Q^2))^2}{(1 + (k\Lambda - Q\Lambda)^2)(1 + (k\Lambda + Q\Lambda)^2)}, \quad (6.17)$$

where  $\Lambda$  describes the correlation length as before, and  $Q = 2\pi/d_w$  is the wavelength for oscillations, which is determined by the molecular size of water. In this work, however, we propose a more general form to better describe the permittivity in the intermediate wave-numbers range:

$$f(k) = \frac{\alpha}{(1 + \Lambda^2 k^2)^2} + \frac{(1 - \alpha)(1 + (\Lambda^2 Q^2))^2}{(1 + (k\Lambda - Q\Lambda)^2)(1 + (k\Lambda + Q\Lambda)^2)}. \quad (6.18)$$

It mimics the basic features of the response function as found in [36], approved by experimental data ([227]). Our hybrid model is illustrated in Fig. 6-1 by looking at the response function  $\chi(k) = 1/\varepsilon_* - 1/\tilde{\varepsilon}_w(k)$ . The large peak around  $k = 3^{-1}$  is related

to overscreening and will lead to oscillations with a period just below the molecular diameter. The hybrid model corrects the longer range behavior of the overscreening model, where the dielectric function is expected to be slightly reduced, similar to the Lorentzian model as obtained in Ref. [36].

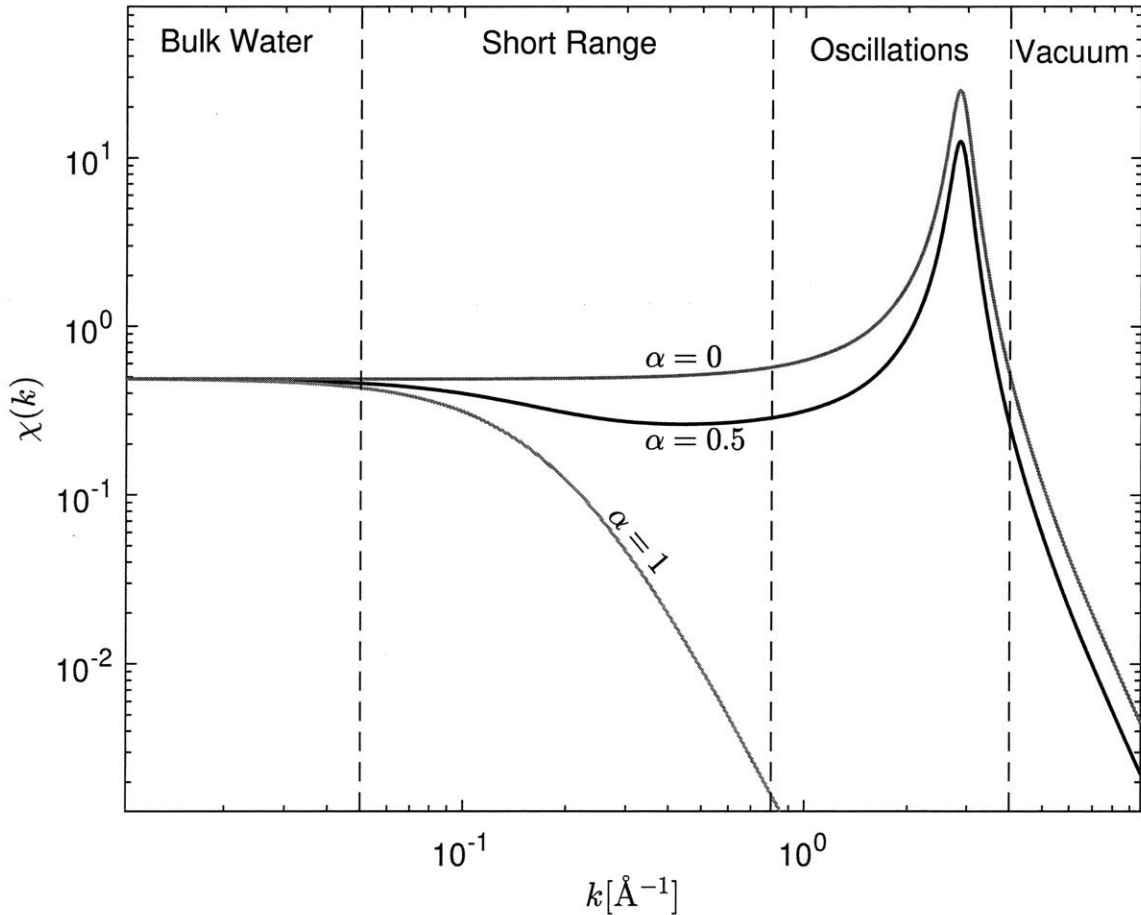


Figure 6-1: The response function  $\chi(k)$  as a function of wavenumber, for three models of dielectric functions: simple Lorentzian model, over-screening model and a hybrid model.

## 6.3 Results

Let us now calculate the activity coefficient for a typical ionic solution, for concentrations ranging from the very dilute to moderately concentrated, using Eq. 6.12. The parameters for the water dielectric response that we adopt here are summarized in Table. 1. Most of them were determined according to previous studies of pure water,

parameter	symbol	value
Short wavelength permittivity	$\epsilon_*$	2
Solvent bulk permittivity	$\epsilon_{\text{Bulk}}$	80
Solvent oscillation wavelength	$Q$	$\frac{2\pi}{2.2} \text{\AA}^{-1}$
Solvent correlation length	$\Lambda$	5\AA
Weight parameter	$\alpha$	0.03

Table 6.1: Parameters for our hybrid model of pure-water dielectric response (Eq. 6.18).

however the hybrid-model weighting function  $\alpha$  was fitted to experimental activity data.

To better understand the activity coefficient, we first examine the potential profile around a spherical ion. Fig. 6-2 shows the potential for increasing ionic concentrations, compared with standard DH approximation (Fig. 6-2 inset). The results are based on a distance of closest approach (ionic diameter,  $a$ ) of 3.5\AA, and exemplify how the non-local permittivity completely changes the potential profile and leads to a non-linear concentration dependence. In the dilute limit, the ionic screening is manifested either by a stronger exponential decay in classical DH screened potential or reduced amplitude of the decaying oscillations in the case of the non-local dielectric function. However, as we increase the concentration, the DH screening cloud gets narrower, and the potential is strongly screened. In contrast, the oscillating structure, predicted by the non-local dielectric model, persists even in high molalities.

From the charging process, we know that the activity is related to the potential on the surface of the charged ion. Two competing effects determine this potential for non-local dielectrics. For small ionic concentrations, the potential is lowered, as a result of the interaction with the screening cloud. This change allows us to recover the DH limiting law, as expected. We note, however, that in contrast to a constant-dielectric picture, the potential itself is negative, and increases in magnitude. As the ionic concentration increases, the amplitude of the oscillations is reduced, which leads to an opposite trend: the screening of the oscillations results in a smaller magnitude potential, i.e., it becomes less negative.

The resulting activity profiles are shown in Fig. 6-3, for three ionic diameters ( $a = 2\text{\AA}$ , 3 and 4\AA). For comparison, three experimental measurements of activity

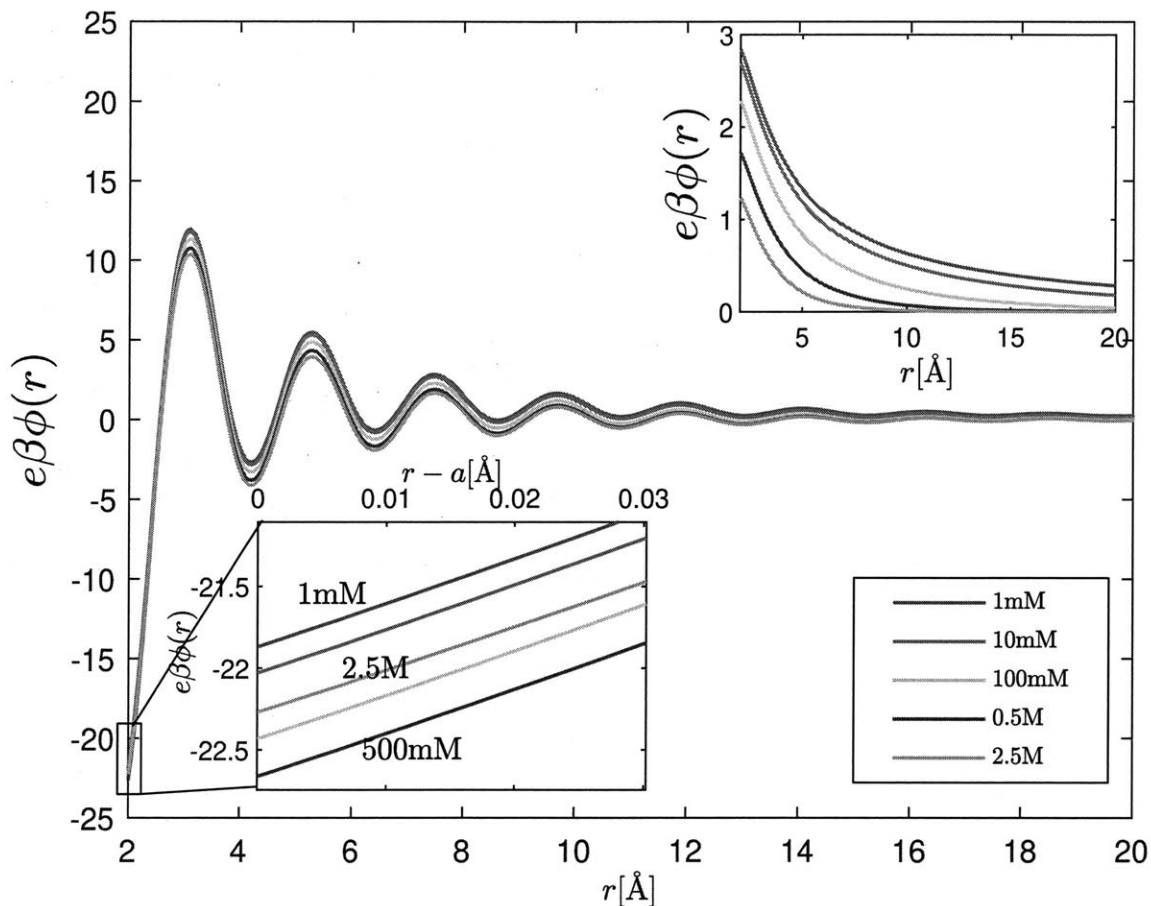


Figure 6-2: The dimensionless electrostatic potential,  $e\beta\phi(r)$ , around a spherical ion, for ionic concentrations 1mM, 10mM, 100mM, 0.5M and 2.5M, based on a the non-local dielectric function described by Eq. 6.6. Parameters of the non-local function are given in Table. 1. The ionic diameter used is 3.5Å. Right inset- the dimensionless electrostatic potential in a constant dielectric medium. Left inset- the dimensionless electrostatic potential profile near the surface of the sphere. At larger distances from the ion, as well as at any distances for the case of constant permittivity, the potential decreases with electrolyte concentration, but in the vicinity of the ion the effect is non-monotonic.

coefficients are shown as well. The experimental data were taken from ref [42] and corresponds to three monovalent ionic solutions: KCl, NaCl, and LiCl, representing three different cation sizes. Qualitatively we see that our model is able to capture the correct trend, including the increased activity at high concentrations, as well as some size dependence of the activity coefficient. The bare cation diameters for the potassium, chloride and lithium are 1.4Å, 1.94Å and 2.82Å, respectively, which are only slightly lower than the values we consider here. Hence, while we are not claiming this is a complete model, we show that with reasonable parameters, the water structure alone can explain much of the overall shape of the activity vs concentra-

tion for different ions, without resorting to correlations or concentration-dependent permittivity.

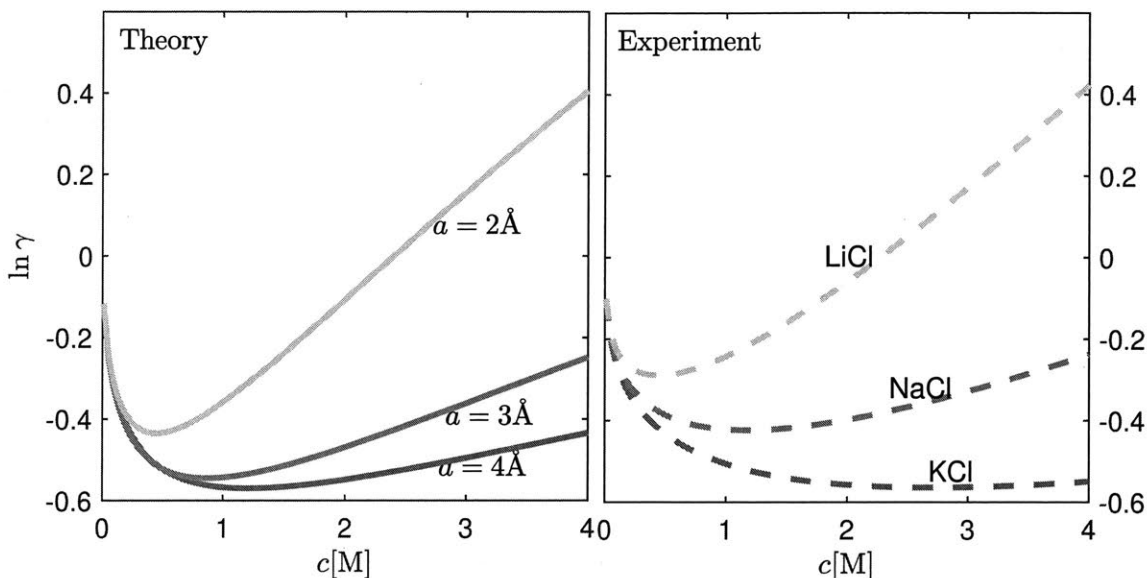


Figure 6-3: Activity coefficients as a function of ionic concentrations. Left- The activity coefficient for monovalent binary solutions, based on the non-local permittivity model, Eq. 6.12. Three different activity curves are shown, corresponding to three ionic diameters (from bottom to top): 4 Å, 3 Å and 2 Å. The parameters of the pure water dielectric function are summarized in Table. 1, and the smearing parameter was taken to be  $\eta = 0.5 \text{ \AA}$ . Left- Experimental data of activity coefficients for three ionic solutions (from bottom to top): KCl, NaCl and LiCl. Data is taken from [42].

## 6.4 Discussion

The match between the experimental activity coefficient and our model illustrates the importance of the local water structure on ionic activity. Our theory supports the original argument of Huckel himself, as well as several recent papers, that differences in the solvation energy play a central role in determining the activity coefficient. In fact, it is the main source of increasing activity at moderate salt concentrations, reversing the decreasing trend of DH theory for screening at low concentration, even before ion-ion correlations become important at high concentrations. Yet, the interplay between solvent molecules and ions is usually either ignored altogether or artificially added as an additional contribution, based on a concentration-dependent bulk dielectric constant. It is therefore significant that we use independently validated dielectric

response of the solvent.

It is important to note that we neglected several other important effects that are known to play a role in determining the activity coefficient. First, our dielectric function is based on a linearization of the Poisson-Boltzmann equation and, thus, non-linear effects in the polarization of ionic atmosphere are neglected. Moreover, extensions to the PB equation, such as ones that account for finite size ions[18, 40, 26, 130, 144], are not considered. Size and packing constraints will rapidly increase the activity coefficient when the packing fraction becomes significant. Theories of primitive models in a constant dielectric medium, supported by Monte-Carlo simulations, have shown that both size effects and non-linear contribution can be significant [48]. Another necessary contribution to the activity comes from ion-ion correlations and is especially pronounced at high concentrations. Such contributions can naturally fit into a non-local dielectric response framework by introducing a correlation length,  $l_c$ , describing the lowest order correction to the bulk dielectric constant as results of ion-ion interactions:  $\varepsilon(k) \approx_{\text{Bulk}} (r + l_c^2 k^2)$ [21]. Interestingly, ion-ion correlations has an opposite compared with water-related correlations, as the second order expansion of the pure water permittivity is negative (and proportional to  $\Lambda$ , as expected).

Last but not least, the effects of the electric field of ions on water structure have been neglected, as well as disturbance of the structure by their mere presence, which was both shown to be potentially important [147, 80]. Indeed, the detailed studies of Ref. [80], based on integral equation approach to the description of molecular correlations in water and molecular dynamic simulations, reveals a complicated dielectric response, with a strong non-linear component at high electric fields and sensitivity to the polarity of the ions. These limitations, as well as other non-electrostatic interactions that were omitted, limit the adequacy of our model. It is therefore expected that with virtually no ion-specific fitting parameters, apart from the effective 'diameter' of the closest approach, our model would only predict the correct trends, and not exact values. Our formula for the dielectric response, Eq. 6.6, is only a first step in the right direction. It is the simplest form that recovers the correct behaviors in both the very short and very long wavelength limits. To improve the results, and get

a quantitative agreement with experiments, more elaborate models are required.

# Chapter 7

## Future prospects

In this thesis, we reported several new results on the behavior of electrolytes in extreme conditions. At the end of each chapter, we discussed the limitations and simplifying assumptions of our models, and possible ways of extending the theory presented. In this chapter, we would like to briefly outline four concrete examples of possible extensions, with preliminary results.

### 7.1 Linear Electrokinetics of Concentrated Multicomponent Systems in Nanopores

In chapters 2 and 3 we considered the transport of ions through a small channel and saw how extreme confinement leads to a surprising breakdown of electroneutrality. We restricted our discussion to a channel that connects to reservoirs with equal ionic concentrations and focused on the equilibrium properties of the channel. While this approach allowed us to consider some experimental setups, in the general case we have to include pressure and chemical gradients as well[201]. A natural extension of the theory presented is to build a general linear theory of electrokinetics.

The derivation is similar to the one presented in Chapter 3, where we followed Ref. [201]. One surprising consequence of electroneutrality breakdown is that we find a non-zero charge profile in the channel even without any surface charge. In Fig. 7-1

we have an example of the concentration profile of an uncharged pore under both concentration gradient and applied electric field[123].

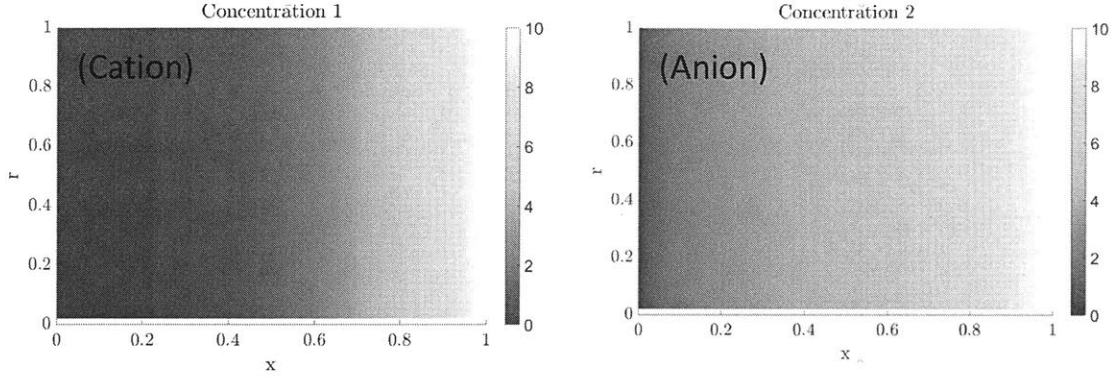


Figure 7-1: Charge density in uncharged pores. The concentration profile of anions and cations in a pore connecting reservoirs with different concentrations (1mM and 10mM)

## 7.2 Electroneutrality Breakdown for Interacting Pores

The theories of nanopores and membranes are usually interchangeable. A membrane is often thought of as a simple collection of pores. This is, however, an over-simplified picture. If the surface charge of the pores is not fully screened, the net charge of each pore can be very high, which gives rise to strong pore-pore coupling. A collection of pores has a very different behavior compared with the single pore case.

Interestingly, membranes maintain electroneutrality much better than single channels. While breaking electroneutrality can be favorable for a one-dimensional narrow channel, ions in a membrane occupy a 3d volume and hence are expected to fully screen external charges, especially in dense membranes. The transition from the 1d structure to 3d structure depends on the ratio of the pore length ( $L$ ) to pore separation ( $l$ ). This can either be studied using numerical solver (such as COMSOL) or by generalizing the "electric leakage" boundary condition we found in Chapter 33.18. Following the same derivation, but requiring the electric fields to vanish at half the distance between pores, we find the following boundary condition to hold[124]:

$$\frac{\partial \phi_{\text{in}}}{\partial r} = \frac{q_s}{\epsilon_{\text{in}}} - \frac{\epsilon_{\text{out}}}{\epsilon_{\text{in}}} \frac{\phi_{\text{in}}}{RM_{L/R}} M_{L/R} = \log \left( \frac{2L}{\pi R} \right) - \gamma + \frac{K_1 \left( \frac{\pi \ell}{2L} \right)}{I_1 \left( \frac{\pi \ell}{2L} \right)},$$

In Fig. 7-2 we compare this approximation with the full numerical solution and find an excellent match. Note that this condition is identical in its form to the "electric leakage" boundary condition, with a different  $M_{L/R}$  coefficient.

### 7.3 Validating Electroneutrality Breakdown: Experiments and Simulations

The conductance of nanochannels is determined by the number of charge carriers that reside inside the channels. Experiments show that there is a peculiar scaling relation between the concentrations of ions in the bulk and the conductivity[219]. In Chapter 2 we argued that electroneutrality breakdown is a potential mechanism for such curves. However, this required several fitting parameters, and we could not definitively rule out other interpretations.

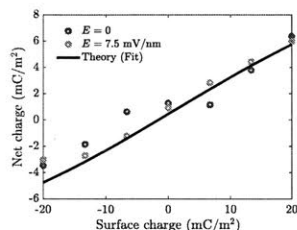
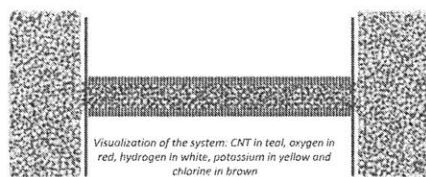
A promising way to directly measure the effect of electroneutrality breakdown exploits the pore-pore interactions in membranes, as described in the previous section. Our theory predicts that the behavior of a dense membrane is markedly different from a diluted one. By carefully choosing the parameters of the membrane, a conductance experiment can be used to verify our theory our predictions with essentially no other known competing interpretations. A promising candidate that can be controlled to high precision is Anodic Aluminum Oxide (AAO) membranes where the spacing of the channels can be designed[245, 22], as shown in Fig. 7-2.

Our predictions can also be directly observed in molecular dynamics simulations (Fig. 7-2). In the left panel of Fig. 7-2 we see the results of a small simulation, clearly showing electroneutrality breakdown. These preliminary results fit well with our predictions but still require some fitting.

### 7.4 The Hidden Order of Ionic Liquids

In Chapter 4 we found that the charge configuration in ionic liquids maximizes the charge ordering, given positional configuration. In some cases this created long-ranged

## Molecular Dynamics validation



## Proposed Experimental Validation

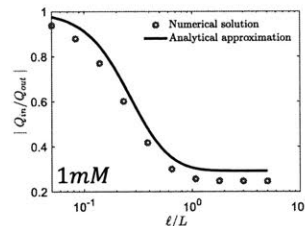
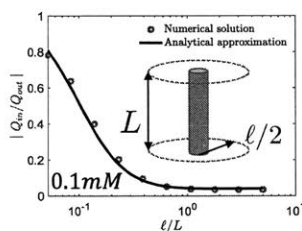
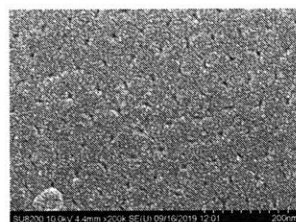
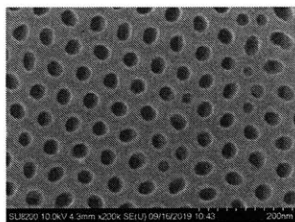


Figure 7-2: Proposed validation of electroneutrality breakdown in experiment and simulation. (a) An illustration of molecular dynamics simulation to test the breakdown of electroneutrality. (b) The net charge of the membrane changes with surface charge in agreement without theory. (c-d) Examples of AAO membranes with different pore density, figures are courtesy of the Elimelech group at Yale. (e-f) Numerical and analytical results of electroneutrality breakdown as a function of pore-pore separation.

structures EMIM-TFSI ionic liquid), but for aqueous LiTFSI the ordering was short-ranged. We attributed this behavior to a "hidden" positional ordering that existed in ionic liquids but was missing in LiTFSI. In the lack of positional order, we showed that geometric frustrations limit the correlation to a handful of neighbors. We coined it a "hidden" order, because the standard way of quantifying positional order, via the pair-correlation function, did not show any apparent structure.

An interesting extension of this work is to quantify and directly observe the positional ordering. While radial distribution functions are not a good starting point, other measures can be more successful. Particularly, the orientational order parameter in 2d and ring statistics have promising potential.

### 7.4.1 Orientational Order in 2D

The melting of a 2-dimensional ionic crystal into an ionic liquid can be characterized by the orientational order parameter[187]:

$$\psi_4 = \frac{1}{N} \sum_n \left| \sum_m \exp(4i\alpha_{m,n}) \right|, \quad (7.1)$$

where  $N$  is the number of ions in the system, and  $\alpha_{m,n}$  is the angle between  $\mathbf{r}_{m,n}$  and the  $x$ -axis, and the summation is on 4 nearest neighbors. If the system is completely ordered, all bond angles are  $\pi/4$ , and  $\psi_4 = 1$ . As disorder increases, the angles become more random. At complete disorder, the value of  $\psi_4$ , for 4 nearest neighbors is around 0.4. Note that this is a local measure of positional order that is useful. Increasing the number of nearest neighbors in the summation will reduce the value of the order parameter to 0 in complete disorder.

We performed a small Monte-Carlo simulation of melting in 2D, to see if there is a correlation between the electrostatic ground state configuration and the value of  $\psi_4$ . Starting from a square lattice and increasing the temperature, we measured for each simulation both the order parameter and the amount of over-screening. Preliminary results are shown in fig. 7-3(b), where we see that for a large range of temperatures charge ordering perfectly follows the orientational order parameter. As the temperature increase, the system is completely disordered, and the charge configuration is no longer optimal.

### 7.4.2 Ring Statistics in 3D

While  $\psi_4$  is a useful order parameter in 2d, ordering in 3d the ordering is more subtle. The generalized orientational order parameter[230] do not explain charge ordering in a significant way, at least to the best of our efforts. Alas, a different measure is required. One particularly useful measure is called "ring statistics", and was first introduced in the context of amorphous silicon[178, 255, 10]. In a solid, where all atoms are connected by chemical bonds and form a graph, a ring is the shortest path

from an atom back to itself. In crystal silicon, for example, all atoms have a ring of size 12, while amorphous silicon has smaller rings of size 8 and 10.

The concept of a ring naturally captures geometric frustrations, which occur for any ring of an uneven number. We applied this measure to simulation data and calculated the ratio of 3-rings to 4-rings. Our graph was defined by connected each ion to its two nearest neighbors, and the results are shown in Fig. 7-2(a). The transition from complete disorder, to ionic crystal, matches the charge ordering pattern.

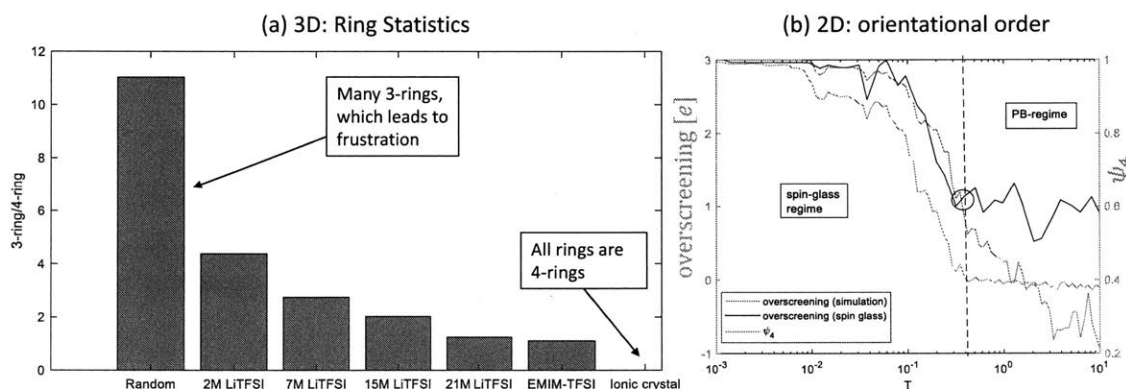


Figure 7-3: The hidden order in ionic liquids. (a) The ratio of 3-rings to 4-rings for different systems with increasing degree of charge ordering. (b) 2d example: the orientational order parameter  $\psi_4$  as a function of temperature in a MC simulation of melting.

# Chapter 8

## Concluding Remarks

In this thesis, we looked at the two regimes where classical "Poisson-Boltzmann" theory fails: strong correlations and extreme confinement. A common theme throughout this work is our attempt of finding basic guiding principles to explain complicated behaviors. This allowed us in Chapter 2 to discover the surprising "electroneutrality breakdown" in nanopores, offer a startling interpretation for the long-ranged charge ordering in ionic liquids in Chapter 4, and incorporate complex ion-solvent interactions in Chapter 6. We intentionally sought the simplest model that was able to explain an interesting feature or capture an intriguing phenomenon. Yet, it also limits the predictive power of our results, and further exploration and development are required.

We started by examining nanopores and the behavior of ions confined to long and narrow channels. Comparing the scaling of entropy and the electrostatic interactions in the pore, we found that the screening length in the axial direction increases exponentially with the mean ionic separation. When the screening length exceeds the physical length of the pore, the pore is only partially screened and gains a net charge. We then derived an algebraic mean-field equation for the accumulated charge in nanopores, under the assumption of uniformly charged pores, and used it to fit experimental data of ionic conductance. The breakdown of electroneutrality played a key role in the dilute limit, since it captures the decrease in the number of mobile ions, as seen in the experiment.

In the following Chapter, we relaxed the uniform pore assumption and adapted the standard Poisson-Boltzmann equation to account for neutrality breakdown. We did so by constructing an approximated Robin-type boundary condition that enables for electric fields to spill into the outer dielectric matrix. Once we obtained exact charge profiles, we were able to calculate a general expression for the conductance and consider two additional effects: electroosmotic flow and a Stefan-Maxwell coupling between ionic fluxes.

We neglected in our analysis many important physical mechanisms, including entrance and edge effects, ion-ion correlations, specific ion-pore interactions, and dehydration. While our theory is far from complete, we expect our qualitative argument to hold in the general case: Electric fields leak out of narrow pores. This effect should be incorporated regardless of the specific model one wishes to use, and our approximated boundary condition offers an especially convenient way of extending different models.

In Chapter 4 we considered the regime of strong ion-ion interactions by utilizing Molecular Dynamics (MD) simulations of ionic liquids. We found that the seemingly complicated patterns of charge ordering obey a basic rule: it is the optimal configuration of charges in presence of positional disorder. For a given positional configuration, ionic liquids try to extend their charge ordering as much as possible, creating the longest possible patterns of alternating signs. However, in order to maintain a long-ranged structure, ions have to be placed in a way that prevents geometric frustrations. Ionic crystals, with NaCl or CsCl structures, are examples of such frustration-free structures. In the liquid phase, however, frustrations are abundant, and charge oscillations are therefore limited.

To prove that ions are in their optimal charge configuration, we performed an atomistic MD simulation and optimized each positional configuration for best charge distribution. This artificial decoupling of positions and charges might make the reader might feel uncomfortable. The positions are, after all, determined by the interaction between charges. Admittedly, this is the main drawback of our approach, which has limited predictive power. Nevertheless, it allowed us to reveal several interesting

observations that shed new light on the behavior of ionic liquids.

Most importantly, we now identify an underlying partial partial positional ordering in ionic liquids that manifests itself in long-ranged oscillations. This ordering is much less pronounced in concentrated LiTFSI aqueous solution, where the strong disorder limits the correlation range to a handful of neighboring ions. Second, we can definitively attribute the observed charge ordering to the bare electrostatic interactions, as our theory neglects all other complexities of the full simulations. Finally, we demonstrated that when an ionic liquid is placed near an electrified surface, it creates an ordered layering structure, which explains the observed "over-screening" phenomenon.

These observations fundamentally differ from the standard interpretations of charge ordering. It is tempting to describe decaying oscillations (in ionic liquids or otherwise), as a solution of linear partial differential equations (PDEs). Qualitatively, linear PDEs predict a similar behavior. Furthermore, by considering additional physical processes, such as non-local electrostatics or specific interactions, we do obtain high order PDEs within the mean-field approximation. Yet, a linear mean-field theory has a key flaw: it neglects the ordering of ionic positions. Our analysis shows that long-range charge oscillations require an underlying positional order that relieves geometric frustrations; it is impossible to have more than a few oscillations otherwise.

Giving up continuum modeling, however, may not be necessary. One takeaway from our analysis is that we should rethink the way we build coarse-grained models in ionic liquids. In the dilute limit, charge ordering characterizes the competition between entropic forces and electrostatic interactions and determines the thermodynamic properties of the system. Conversely, in ionic liquids, charge ordering only represents the underlying positional order. It is therefore might be instructive to devise a continuum theory that directly addresses this order parameter.

The final two chapters of the thesis focus on ion-ion and ion-solvent correlations in concentrated electrolytes. This intermediate range of electrostatic interactions requires modifications beyond Poisson-Boltzmann, but does not exhibit the long-ranged charge ordering of ionic liquids. We showed that a non-local permittivity

operator is a powerful tool in incorporating complex behavior, with only handful of phenomenological parameters. We studied in these chapters the activity coefficient of an ionic solution, and in particular its departure from the Debye-Huckel theory.

In Chapter 5 we used a 4-th order extension of the Poisson-Boltzmann theory, known as the BSK theory. With essentially just one fitting parameter, related to the correlation length, we were able to fit a wide range of ionic solutions with remarkable accuracy. In Chapter 6, we revisited the role of the solvent structure on the activity coefficients by introducing an interpolated formula for the non-local dielectric function. At high concentrations the ordering of the water molecules contributes significantly to the activity coefficients and can not be neglected (in Chapter 5 we circumvent this problem by artificially adding the Born solvation term). The non-local dielectric function is motivated motivated by microscopic models, but not directly derived from first principles. We 'engineered' a form that satisfies important limiting behaviors and symmetry requirements, but one that is also tractable computationally as well. This is the main drawback of this approach: it is a good way of introducing new effects and examining their qualitative consequences, but its accuracy is limited.

In the penultimate chapter of the thesis we briefly sketched four specific examples of possible extensions to the thesis. It is our hope, however, that this thesis leaves the reader with more questions than answers. We have just begun to explore the extreme regimes of confinement and correlations and the ways it forces us to depart ways with the classical Poisson-Boltzmann theory.

# Bibliography

- [1] Theory of simple liquids. In Jean-Pierre Hansen and Ian R. McDonald, editors, *Theory of Simple Liquids (Fourth Edition)*. Academic Press, Oxford, fourth edition edition, 2013.
- [2] J R Abo-Shaer, C Raman, J M Vogels, and Wolfgang Ketterle. Observation of vortex lattices in Bose-Einstein condensates. *Science*, 292(5516):476–479, 2001.
- [3] Ariel Abrashkin, David Andelman, and Henri Orland. Dipolar Poisson-Boltzmann equation: ions and dipoles close to charge interfaces. *Physical Review Letters*, 99(7):077801, 2007.
- [4] Ram M Adar, Tomer Markovich, and David Andelman. Bjerrum pairs in ionic solutions: A Poisson-Boltzmann approach. *Journal of Chemical Physics*, 146(19):194904, 2017.
- [5] Ram M Adar, Tomer Markovich, Amir Levy, Henri Orland, and David Andelman. Dielectric constant of ionic solutions: Combined effects of correlations and excluded volume. *The Journal of chemical physics*, 149(5):054504, 2018.
- [6] David Adar, Ram, Markovich, Tomer, Andelman. Bjerrum pairs in ionic solutions: a Poisson-Boltzmann approach. *Unpublished*, pages 1–9, 2017.
- [7] Nagaphani B. Aetukuri, Bryan D. McCloskey, Jeannette M. García, Leslie E. Krupp, Venkatasubramanian Viswanathan, and Alan C. Luntz. Solvating additives drive solution-mediated electrochemistry and enhance toroid growth in non-aqueous  $\text{Li}\ddot{\text{A}}\text{So}_2$  batteries. *Nature Chemistry*, 7(January):50–56, 2015.
- [8] Kumar Varoon Agrawal, Steven Shimizu, Lee W Drahushuk, Daniel Kilcoyne, and Michael S Strano. Observation of extreme phase transition temperatures of water confined inside isolated carbon nanotubes. *Nature Nanotechnology*, 12(3):267, 2017.
- [9] Pedro H R Alij3, Frederico W Tavares, Evaristo C Biscaia Jr, and Argimiro R Secchi. Effects of electrostatic correlations on ion dynamics in alternating current voltages. *Electrochimica Acta*, 152:84–92, 2015.
- [10] Clark L Allred, Xianglong Yuan, Martin Z Bazant, and Linn W Hobbs. Elastic constants of defected and amorphous silicon with the environment-dependent interatomic potential. *Physical Review B*, 70(13):134113, 2004.

- [11] Wolfhard Almers and EW McCleskey. Non-selective conductance in calcium channels of frog muscle: calcium selectivity in a single-file pore. *The Journal of Physiology*, 353(1):585–608, 1984.
- [12] David Andelman. Electrostatic properties of membranes: the poisson-boltzmann theory. In *Handbook of biological physics*, volume 1, pages 603–642. Elsevier, 1995.
- [13] Mathias Bækbo Andersen, M Van Soestbergen, A Mani, Henrik Bruus, PM Biesheuvel, and MZ Bazant. Current-induced membrane discharge. *Physical review letters*, 109(10):108301, 2012.
- [14] Rob Atkin and Gregory G Warr. The Smallest Amphiphiles : Nanostructure in Protic Room-Temperature Ionic Liquids with Short Alkyl Groups. *Journal of Physical Chemistry B*, 112:4164–4166, 2008.
- [15] Bhavya Balu and Aditya S Khair. Role of stefan–maxwell fluxes in the dynamics of concentrated electrolytes. *Soft Matter*, 14(41):8267–8275, 2018.
- [16] Victor Barcion. Ion flow through narrow membrane channels: Part I. *SIAM Journal on Applied Mathematics*, 52(5):1391–1404, 1992.
- [17] J-L Barrat. A density functional calculation of the liquid-solid phase diagram of a charged-hard-spheres model of a salt. *Journal of Physics C: Solid State Physics*, 20(8):1031, 1987.
- [18] Martin Z Bazant, Mustafa Sabri Kilic, Brian D Storey, and Armand Ajdari. No Title. *Advances in Colloid and Interface Science*, 152(1):44—88, 2009.
- [19] Martin Z Bazant, Mustafa Sabri Kilic, Brian D Storey, and Armand Ajdari. Towards an understanding of induced-charge electrokinetics at large applied voltages in concentrated solutions. *Advances in Colloid and Interface Science*, 152(1-2):48–88, 2009.
- [20] Martin Z Bazant, Mustafa Sabri, Brian D Storey, and Armand Ajdari. Towards an understanding of induced-charge electrokinetics at large applied voltages in concentrated solutions. *Advances in Colloid and Interface Science*, 152(1-2):48–88, 2009.
- [21] Martin Z. Bazant, Brian D. Storey, and Alexei A. Kornyshev. Double layer in ionic liquids: Overscreening versus crowding. *Physical Review Letters*, 106(4):046102, 2011.
- [22] A Belwalkar, E Grasing, W Van Geertruyden, Z Huang, and WZ Misiolek. Effect of processing parameters on pore structure and thickness of anodic aluminum oxide (aao) tubular membranes. *Journal of membrane science*, 319(1-2):192–198, 2008.

- [23] HJC Berendsen, JR Grigera, and TP Straatsma. The missing term in effective pair potentials. *Journal of Physical Chemistry*, 91(24):6269–6271, 1987.
- [24] Simon Berneche and Benoit Roux. Energetics of ion conduction through the k<sup>+</sup> channel. *Nature*, 414(6859):73, 2001.
- [25] P. M. Biesheuvel and M. Z. Bazant. Analysis of ionic conductance of carbon nanotubes. *Physical Review E*, 94(5):050601(R), 2016.
- [26] J J Bikerman. XXXIX. Structure and capacity of electrical double layer. *Philosophical Magazine*, 33(220):384–397, 1942.
- [27] RB Bird, WE Stewart, and EN Lightfoot. Transport phenomena (revised second ed.) john wiley & sons. *New York*, 2007.
- [28] Niels Bjerrum. *Untersuchungen über Ionenassoziation*. AF Høst, 1926.
- [29] R Blossey, A C Maggs, and R Podgornik. Structural interactions in ionic liquids linked to higher-order Poisson-Boltzmann equations. *Physical Review E*, 95(6):060602(R), 2017.
- [30] Lydéric Bocquet and Elisabeth Charlaix. Nanofluidics, from bulk to interfaces. *Chemical Society Reviews*, 39(3):1073–1095, 2010.
- [31] Dezső Boda, David D Busath, Bob Eisenberg, Douglas Henderson, and Wolfgang Nonner. Monte carlo simulations of ion selectivity in a biological na channel: Charge–space competition. *Physical Chemistry Chemical Physics*, 4(20):5154–5160, 2002.
- [32] Dezső Boda, David D Busath, Douglas Henderson, and Stefan Sokolowski. Monte carlo simulations of the mechanism for channel selectivity: the competition between volume exclusion and charge neutrality. *Journal of Physical Chemistry B*, 104(37):8903–8910, 2000.
- [33] Dezső Boda, Wolfgang Nonner, Mónika Valiskó, Douglas Henderson, Bob Eisenberg, and Dirk Gillespie. Steric selectivity in na channels arising from protein polarization and mobile side chains. *Biophysical Journal*, 93(6):1960–1980, 2007.
- [34] Dezső Boda, Mónika Valiskó, Bob Eisenberg, Wolfgang Nonner, Douglas Henderson, and Dirk Gillespie. The effect of protein dielectric coefficient on the ionic selectivity of a calcium channel. *Journal of Chemical Physics*, 125(3):034901, 2006.
- [35] Dezső Boda, Mónika Valiskó, Bob Eisenberg, Wolfgang Nonner, Douglas Henderson, and Dirk Gillespie. Combined effect of pore radius and protein dielectric coefficient on the selectivity of a calcium channel. *Physical Review Letters*, 98(16):168102, 2007.

- [36] Philippe A Bopp, Alexei A Kornyshev, and Godehard Sutmann. Static nonlocal dielectric function of liquid water. *Physical Review Letters*, 76(8):1280, 1996.
- [37] Philippe A Bopp, Alexei A Kornyshev, and Godehard Sutmann. Frequency and wave-vector dependent dielectric function of water: Collective modes and relaxation spectra. *Journal of Chemical Physics*, 109(5):1939–1958, 1998.
- [38] José Rafael Bordin, Alexandre Diehl, Marcia C Barbosa, and Yan Levin. Ion fluxes through nanopores and transmembrane channels. *Physical Review E*, 85(3):031914, 2012.
- [39] I. Borukhov, D. Andelman, and H. Orland. Adsorption of large ions from an electrolyte solution: A modified Poisson-Boltzmann equation. *Electrochimica Acta*, 46(2-3):221–229, 2000.
- [40] Itamar Borukhov, David Andelman, and Henri Orland. Steric effects in electrolytes: A modified poisson-boltzmann equation. *Physical Review Letters*, 79(3):435, 1997.
- [41] W Richard Bowen and Julian S Welfoot. Modelling the performance of membrane nanofiltration—critical assessment and model development. *Chemical Engineering Science*, 57(7):1121–1137, 2002.
- [42] Leroy A. Bromley. Thermodynamic properties of strong electrolytes in aqueous solutions. *AIChE Journal*, 19(2):313–320, 1973.
- [43] Colin M Burke, Vikram Pande, Abhishek Khetan, Venkatasubramanian Viswanathan, and Bryan D Mccloskey. Enhancing electrochemical intermediate solvation through electrolyte anion selection to increase nonaqueous Li  $\text{O}_2$  battery capacity. *Proceedings of the National Academy of Sciences*, 2(30):201505728, 2015.
- [44] C. Caccamo. Integral equation theory description of phase equilibria in classical fluids. *Physics Reports*, 274(1-2):1–105, 1996.
- [45] José N Canongia Lopes, Margarida F Costa Gomes, and Agílio A H Pádua. Nonpolar, polar, and associating solutes in ionic liquids. *Journal of Physical Chemistry B*, 110(34):16816–16818, 2006.
- [46] José N. Canongia Lopes and Agílio A. H. Pádua. Cl&p: A generic and systematic force field for ionic liquids modeling. *Theoretical Chemistry Accounts*, 131(3):1129, Feb 2012.
- [47] José NA Canongia Lopes and Agílio AH Pádua. Nanostructural organization in ionic liquids. *The Journal of Physical Chemistry B*, 110(7):3330–3335, 2006.
- [48] DN Card and JP Valleau. Monte carlo study of the thermodynamics of electrolyte solutions. *Journal of Chemical Physics*, 52(12):6232–6240, 1970.

- [49] Jacopo Catalano, RGH Lammertink, and PM Biesheuvel. Theory of fluid slip in charged capillary nanopores. *arXiv preprint arXiv:1603.09293*, 2016.
- [50] Wai-Fong Chan, Hang-yan Chen, Anil Surapathi, Michael G Taylor, Xiaohong Shao, Eva Marand, and J Karl Johnson. Zwitterion functionalized carbon nanotube/polyamide nanocomposite membranes for water desalination. *ACS Nano*, 7(6):5308–5319, 2013.
- [51] Samarth Chandra. Dependence of ground-state energy of classical n-vector spins on n. *Physical Review E*, 77(2):021125, 2008.
- [52] Chih-Chang Chang and Ruey-Jen Yang. Electrokinetic energy conversion efficiency in ion-selective nanopores. *Applied Physics Letters*, 99(8):083102, 2011.
- [53] David Leonard Chapman. Li. a contribution to the theory of electrocapillarity. *The London, Edinburgh, and Dublin philosophical magazine and journal of science*, 25(148):475–481, 1913.
- [54] Chau-Chyun Chen, Herbert I Britt, Joseph F Boston, and Lawrence B Evans. Extension and application of the pitzer equation for vapor-liquid equilibrium of aqueous electrolyte systems with molecular solutes. *AIChE Journal*, 25(5):820–831, 1979.
- [55] Thiago Colla, Matheus Giroto, Alexandre P dos Santos, and Yan Levin. Charge neutrality breakdown in confined aqueous electrolytes: Theory and simulation. *Journal of Chemical Physics*, 145(9):094704, 2016.
- [56] Brian E Conway. *Electrochemical supercapacitors: scientific fundamentals and technological applications*. Springer Science & Business Media, 2013.
- [57] Ben Corry. Water and ion transport through functionalised carbon nanotubes: implications for desalination technology. *Energy & Environmental Science*, 4(3):751–759, 2011.
- [58] SL Cowan, JH Schulman, T Teorell, W Wilbrandt, AV Hill, JJ Bikerman, RB Dean, and Kurt H Meyer. General discussion. *Journal of the Chemical Society, Faraday Transactions*, 33:1051–1057, 1937.
- [59] E Hawkins Cwirko and RG Carbonell. Transport of electrolytes in charged pores: analysis using the method of spatial averaging. *Journal of Colloid and Interface Science*, 129(2):513–531, 1989.
- [60] Hirofumi Daiguji, Peidong Yang, Andrew J Szeri, and Arun Majumdar. Electrochemomechanical energy conversion in nanofluidic channels. *Nano Letters*, 4(12):2315–2321, 2004.
- [61] P. Debye and E. Huckel. The theory of electrolytes I. The lowering of the freezing point and related occurrences. *Zeitschrift für Physik*, 24:185–206, 1923.

- [62] Vincent Démery, David S Dean, Thomas C Hammant, Ron R Horgan, and Rudolf Podgornik. Overscreening in a 1d lattice coulomb gas model of ionic liquids. *Europhysics Letters*, 97(2):28004, 2012.
- [63] B V Derjaguin. Theory of the stability of strongly charged lyophobic sols and the adhesion of strongly charged particles in solutions of electrolytes. *Acta physicochimica U.R.S.S.*, 14:633–662, 1941.
- [64] Aleksandar Donev, Andrew J. Nonaka, Changho Kim, Alejandro L. Garcia, and John B. Bell. Fluctuating hydrodynamics of electrolytes at electroneutral scales. *Physical Review Fluids*, 4:043701, Apr 2019.
- [65] Rachel Downing, Bjorn K Berntson, Guilherme V Bossa, and Sylvio May. Differential capacitance of ionic liquids according to lattice-gas mean-field model with nearest-neighbor interactions. *The Journal of chemical physics*, 149(20):204703, 2018.
- [66] Declan A Doyle, Joao Morais Cabral, Richard A Pfuetzner, Anling Kuo, Jacqueline M Gulbis, Steven L Cohen, Brian T Chait, and Roderick MacKinnon. The structure of the potassium channel: molecular basis of k<sup>+</sup> conduction and selectivity. *Science*, 280(5360):69–77, 1998.
- [67] Chuanhua Duan and Arun Majumdar. Anomalous ion transport in 2-nm hydrophilic nanochannels. *Nature Nanotechnology*, 5(12):848, 2010.
- [68] Stanislav S Dukhin, Ralf Zimmermann, and Carsten Werner. Electrokinetic phenomena at grafted polyelectrolyte layers. *Journal of Colloid and Interface Science*, 286(2):761–773, 2005.
- [69] Jörn Dunkel, Sebastian Heidenreich, Knut Drescher, Henricus H Wensink, Markus Bär, and Raymond E Goldstein. Fluid dynamics of bacterial turbulence. *Physical Review Letters*, 110(22):228102, 2013.
- [70] E Victoria Dydek and Martin Z Bazant. Nonlinear dynamics of ion concentration polarization in porous media: The leaky membrane model. *AIChE Journal*, 59(9):3539–3555, 2013.
- [71] Samuel Frederick Edwards and Phil W Anderson. Theory of spin glasses. *Journal of Physics F: Metal Physics*, 5(5):965, 1975.
- [72] SF Edwards and Andrew Lenard. Exact statistical mechanics of a one-dimensional system with coulomb forces. ii. the method of functional integration. *Journal of Mathematical Physics*, 3(4):778–792, 1962.
- [73] Razi Epsztein, Evyatar Shaulsky, Mohan Qin, and Menachem Elimelech. Activation behavior for ion permeation in ion-exchange membranes: Role of ion dehydration in selective transport. *Journal of Membrane Science*, 2019.

- [74] A Esfandiari, B Radha, FC Wang, Q Yang, S Hu, S Garaj, RR Nair, AK Geim, and K Gopinadhan. Size effect in ion transport through angstrom-scale slits. *Science*, 358(6362):511–513, 2017.
- [75] F Evans and H Wennerstrom. The colloidal domain, where physics, chemistry, biology and technology meet, 1994.
- [76] RB Evans III, GM Watson, and EA Mason. Gaseous diffusion in porous media at uniform pressure. *Journal of Chemical Physics*, 35(6):2076–2083, 1961.
- [77] J. C. Fair and J. F. Osterle. Reverse electro dialysis in charged capillary membranes. *Journal of Chemical Physics*, 54(8):3307–3316, 1971.
- [78] Samuel J Faucher, Narayana R Aluru, Martin Z Bazant, Daniel Blankschtein, Alexandra H Brozena, John Cumings, J Pedro de Souza, Menachem Elimelech, Razi Epsztein, John T Fourkas, et al. Critical knowledge gaps in mass transport through single-digit nanopores: A review and perspective. *The Journal of Physical Chemistry C*, 2019.
- [79] Maxim V Fedorov, Nikolaj Georgi, and Alexei A Kornyshev. Double layer in ionic liquids: The nature of the camel shape of capacitance. *Electrochemistry Communications*, 12(2):296–299, 2010.
- [80] Maxim V Fedorov and Alexei A Kornyshev. Unravelling the solvent response to neutral and charged solutes. *Molecular Physics*, 105(1):1–16, 2007.
- [81] Maxim V Fedorov and Alexei A Kornyshev. Towards understanding the structure and capacitance of electrical double layer in ionic liquids. *Electrochimica Acta*, 53(23):6835–6840, 2008.
- [82] Maxim V Fedorov and Alexei A Kornyshev. Ionic Liquids at Electric Interfaces. *Chemical Reviews*, 114:2978–3036, 2014.
- [83] Alan Finkelstein and Olaf Sparre Andersen. The gramicidin A channel: a review of its permeability characteristics with special reference to the single-file aspect of transport. *Journal of Membrane Biology*, 59(3):155–171, 1981.
- [84] Michael E Fisher and Yan Levin. Criticality in ionic fluids: Debye-hückel theory, Bjerrum, and beyond. *Physical review letters*, 71(23):3826, 1993.
- [85] Elzbieta Frackowiak and Francois Beguin. Carbon materials for the electrochemical storage of energy in capacitors. *Carbon*, 39(6):937–950, 2001.
- [86] Yeqing Fu, Yi Jiang, Sophie Poizeau, Abhijit Dutta, Aravind Mohanram, John D Pietras, and Martin Z Bazant. Multicomponent gas diffusion in porous electrodes. *Journal of the Electrochemical Society*, 162(6):F613–F621, 2015.

- [87] Ryusuke Futamura, Taku Iiyama, Yuma Takasaki, Yury Gogotsi, Mark J Biggs, Mathieu Salanne, Julie Segalini, Patrice Simon, and Katsumi Kaneko. Partial breaking of the coulombic ordering of ionic liquids confined in carbon nanopores. *Nature materials*, 16(12):1225, 2017.
- [88] Béatrice Garcia, Serge Lavallée, Gérald Perron, Christophe Michot, and Michel Armand. Room temperature molten salts as lithium battery electrolyte. *Electrochimica Acta*, 49(26):4583–4588, 2004.
- [89] Michael R Garey and David S Johnson. *Computers and intractability: a guide to the theory of NP-completeness*, volume 29. Freeman, San Francisco, 1979.
- [90] Nir Gavish, Doron Elad, and Arik Yochelis. From Solvent-Free to Dilute Electrolytes: Essential Components for a Continuum Theory. *Journal of Physical Chemistry Letters*, 9:36–42, 2018.
- [91] Nir Gavish and Arik Yochelis. Theory of phase separation and polarization for pure ionic liquids. *Journal of Physical Chemistry Letters*, 7(7):1121–1126, 2016.
- [92] M A Gebbie, M Valtiner, X Banquy, E T Fox, W A Henderson, and J N Israelachvili. Ionic liquids behave as dilute electrolyte solutions. *Proceedings of the National academy of Sciences of the United States of America*, 110(24):9674–9679, 2013.
- [93] Michel X Goemans and David P Williamson. Improved approximation algorithms for maximum cut and satisfiability problems using semidefinite programming. *Journal of the ACM*, 42(6):1115–1145, 1995.
- [94] Ekaterina Gongadze, Ursula van Rienen, Veronika Kralj-Iglič, and Aleš Iglič. Spatial variation of permittivity of an electrolyte solution in contact with a charged metal surface: a mini review. *Computer Methods in Biomechanics and Biomedical Engineering*, 16(5):463–480, 2013.
- [95] Zachary A.H. Goodwin, Guang Feng, and Alexei A Kornyshev. Mean-Field Theory of Electrical Double Layer In Ionic Liquids with Account of Short-Range Correlations. *Electrochimica Acta*, 225:190–197, 2017.
- [96] M Gouy. Sur la constitution de la charge électrique à la surface d’un électrolyte. *Journal of Theoretical and Applied Physics*, 9(1):457–468, 1910.
- [97] Michael Grant and Stephen Boyd. CVX: Matlab software for disciplined convex programming, version 2.0 beta. <http://cvxr.com/cvx>, 2013.
- [98] Michael C Grant and Stephen P Boyd. Graph implementations for nonsmooth convex programs. In *Recent advances in learning and control*. Springer, London, 2008.

- [99] Simon Gravelle, Laurent Joly, François Detcheverry, Christophe Ybert, Cécile Cottin-Bizonne, and Lydéric Bocquet. Optimizing water permeability through the hourglass shape of aquaporins. *Proceedings of the National academy of Sciences of the United States of America*, 110(41):16367–16372, 2013.
- [100] Yoav Green, Ran Eshel, Sinwook Park, and Gilad Yossifon. Interplay between nanochannel and microchannel resistances. *Nano Letters*, 16(4):2744–2748, 2016.
- [101] Yoav Green, Shahar Shloush, and Gilad Yossifon. Effect of geometry on concentration polarization in realistic heterogeneous permselective systems. *Physical Review E*, 89(4):043015, 2014.
- [102] Richard J Gross and JF Osterle. Membrane transport characteristics of ultrafine capillaries. *Journal of Chemical Physics*, 49(1):228–234, 1968.
- [103] Weihua Guan and Mark A Reed. Electric field modulation of the membrane potential in solid-state ion channels. *Nano Letters*, 12(12):6441–6447, 2012.
- [104] E.a. Guggenheim. L. The specific thermodynamic properties of aqueous solutions of strong electrolytes. *Philosophical Magazine*, 19(127):588–643, 1935.
- [105] Walter J. Hamer and Y. Yung chi. Osmotic coefficients and mean activity coefficients of uni- and divalent electrolytes in water at 25°C. *Journal of Physical and Chemical Reference Data*, 1(4):1047–1100, 1972.
- [106] Jean Pierre Hansen and Ian R McDonald. Statistical mechanics of dense ionized matter. iv. density and charge fluctuations in a simple molten salt. *Physical Review A*, 11(6):2111, 1975.
- [107] Herbert Spencer Harned and Benton Brooks Owen. *The Physical Chemistry of Electrolytic Solutions... Revised and Enlarged*. Reinhold Publishing Corporation, 1950.
- [108] J. B Hasted, D. M Ritson, and C. H Collie. Dielectric Properties of Aqueous Ionic Solutions. Parts I and II. *Journal of Chemical Physics*, 16(1):1–21, 1948.
- [109] Marius M Hatlo and Leo Lue. Electrostatic interactions of charged bodies from the weak-to the strong-coupling regime. *Europhysics Letters*, 89(2):25002, 2010.
- [110] Robert Hayes, Gregory G Warr, and Rob Atkin. Structure and nanostructure in ionic liquids. *Chemical Reviews*, 115(13):6357–6426, 2015.
- [111] Peter Hess and Richard W Tsien. Mechanism of ion permeation through calcium channels. *Nature*, 309(5967):453, 1984.
- [112] Andreas Hildebrandt, Ralf Blossey, Sergej Rjasanow, Oliver Kohlbacher, and H-P Lenhof. Novel formulation of nonlocal electrostatics. *Physical Review Letters*, 93(10):108104, 2004.

- [113] Bertil Hille. *Ionic channels in excitable membranes*. sinauer associates Inc, Sunderland, MA, 2001.
- [114] Roger W Hockney and James W Eastwood. *Computer simulation using particles*. CRC Press, 1988.
- [115] Jason K Holt, Hyung Gyu Park, Yinmin Wang, Michael Stadermann, Alexander B Artyukhin, Costas P Grigoropoulos, Aleksandr Noy, and Olgica Bakajin. Fast mass transport through sub-2-nanometer carbon nanotubes. *Science*, 312(5776):1034–1037, 2006.
- [116] K Holub and AA Kornyshev. Polar solvent structure in the debye-hückel theory of strong electrolytes. *Zeitschrift für Naturforschung A*, 31(12):1601–1608, 1976.
- [117] John Hubbard. Calculation of partition functions. *Physical Review Letters*, 3(2):77, 1959.
- [118] E. Huckel. 1huckel\_e\_zur\_theorie\_konzentrierterer\_wasseriger\_losungen\_st.pdf. *Zeitschrift für Physik*, 26:93, 1925.
- [119] William Humphrey, Andrew Dalke, and Klaus Schulten. VMD – Visual Molecular Dynamics. *Journal of Molecular Graphics*, 14:33–38, 1996.
- [120] Jacob N Israelachvili. *Intermolecular and surface forces*. Academic press, 2015.
- [121] V Ivaništšev, Kathleen Kirchner, Tom Kirchner, and Maxim V Fedorov. Restructuring of the electrical double layer in ionic liquids upon charging. *Journal of Physics: Condensed Matter*, 27(10):102101, 2015.
- [122] V Ivaništšev, S O’Connor, and M V Fedorov. Poly (a) morphic portrait of the electrical double layer in ionic liquids. *Electrochemistry Communications*, 48:61–64, 2014.
- [123] Amir Levy Nathanael Assefa Martin Z. Bazant J. Pedro de Souza, Mohammad Mirzadeh. Linear electrokinetics of concentrated multicomponent systems in nanopores. In preparation.
- [124] Martin Z. Bazant J. Pedro de Souza, Amir Levy. Electroneutrality breakdown for interacting pores. In preparation.
- [125] X Jiang, J Huang, H Zhao, B G Sumpter, and R Qiao. Dynamics of electrical double layer formation in room-temperature ionic liquids under constant-current charging conditions. *Journal of Physics: Condensed Matter*, 26(28):284109, 2014.
- [126] Xikai Jiang, Ying Liu, and Rui Qiao. Current rectification for transport of room-temperature ionic liquids through conical nanopores. *Journal of Physical Chemistry C*, 120(8):4629–4637, 2016.

- [127] Lee Johnson, Chunmei Li, Zheng Liu, Yuhui Chen, Stefan a Freunberger, Praveen C Ashok, Bavishna B Praveen, Kishan Dholakia, Jean-Marie Tarascon, and Peter G Bruce. The role of LiO<sub>2</sub> solubility in O<sub>2</sub> reduction in aprotic solvents and its consequences for Li-O<sub>2</sub> batteries. *Nature chemistry*, 6(12):1091–9, 2014.
- [128] PC Jordan, RJ Bacquet, JA McCammon, and P Tran. How electrolyte shielding influences the electrical potential in transmembrane ion channels. *Biophysical Journal*, 55(6):1041–1052, 1989.
- [129] A Kamenev, J Zhang, AI Larkin, and B. I. Shklovskii. Transport in one-dimensional coulomb gases: From ion channels to nanopores. *Physica A: Statistical Mechanics and its Applications*, 359:129–161, 2006.
- [130] Mustafa Sabri Kilic, Martin Z Bazant, and Armand Ajdari. Steric effects in the dynamics of electrolytes at large applied voltages. i. double-layer charging. *Physical Review E*, 75(2):021502, Feb 2007.
- [131] Dong-Kwon Kim, Chuanhua Duan, Yu-Feng Chen, and Arun Majumdar. Power generation from concentration gradient by reverse electrodialysis in ion-selective nanochannels. *Microfluidics Nanofluidics*, 9(6):1215–1224, 2010.
- [132] G-T Kim, S S Jeong, M-Z Xue, A Balducci, M Winter, S Passerini, F Alessandrini, and G B Appetecchi. Development of ionic liquid-based lithium battery prototypes. *Journal of Power Sources*, 199:239–246, 2012.
- [133] Hee-talk Kim and William J Frederick. Evaluation of Pitzer Ion Interaction Parameters of Aqueous Electrolytes at 25ÅrC . 1 . Single Salt Parameters. *Journal of Chemical and Engineering Data*, 33(2):177–184, 1988.
- [134] Sung Jae Kim, Sung Hee Ko, Kwan Hyoung Kang, and Jongyoon Han. Direct seawater desalination by ion concentration polarization. *Nature Nanotechnology*, 5(4):297, 2010.
- [135] Sung Jae Kim, Yong-Ak Song, and Jongyoon Han. Nanofluidic concentration devices for biomolecules utilizing ion concentration polarization: theory, fabrication, and applications. *Chemical Society Reviews*, 39(3):912–922, 2010.
- [136] Sung Jae Kim, Ying-Chih Wang, Jeong Hoon Lee, Hongchul Jang, and Jongyoon Han. Concentration polarization and nonlinear electrokinetic flow near a nanofluidic channel. *Physical review letters*, 99(4):044501, 2007.
- [137] Roland Kjellander. Nonlocal electrostatics in ionic liquids: The key to an understanding of the screening decay length and screened interactions. *Journal of Chemical Physics*, 145(12), 2016.
- [138] A. V. Kobelev, A. S. Lileev, and A. K. Lyashchenko. Microwave dielectric properties of aqueous potassium iodide solutions as a function of temperature. *Russian Journal of Inorganic Chemistry*, 56(4):652–659, 2011.

- [139] A A Kornyshev, A I Rubinshtein, and M A Vorotyntsev. Model nonlocal electrostatics. I. *Journal of Physics C: Solid State Physics*, 11(15):3307, 1978.
- [140] AA Kornyshev. Nonlocal screening of ions in a structured polar liquid—New aspects of solvent description in electrolyte theory. *Electrochimica Acta*, 26(1):1–20, 1981.
- [141] AA Kornyshev, S Leikin, and G Sutmann. Overscreening in a polar liquid as a result of coupling between polarization and density fluctuations. *Electrochimica Acta*, 42(5):849–865, 1997.
- [142] A.A. Kornyshev, M.A. Vorotyntsev, H. Nielsen, and J. Ulstrup. Non-local screening effects in the long-range interionic interaction in a polar solvent. *Journal of the Chemical Society, Faraday Transactions 2: Molecular and Chemical Physics*, 78(2), 1982.
- [143] Alexei A Kornyshev. Non-local dielectric response of a polar solvent and Debye screening in ionic solution. *Journal of the Chemical Society, Faraday Transactions*, 79(5):651–661, 1983.
- [144] Alexei A. Kornyshev. Double-layer in ionic liquids: Paradigm change? *Journal of Physical Chemistry B*, 111(20):5545–5557, 2007.
- [145] Alexei A Kornyshev and Rui Qiao. Three-dimensional double layers. *Journal of Physical Chemistry C*, 118(32):18285–18290, 2014.
- [146] Alexei A Kornyshev and Godehard Sutmann. The shape of the nonlocal dielectric function of polar liquids and the implications for thermodynamic properties of electrolytes: A comparative study. *Journal of Chemical Physics*, 104(4):1524–1544, 1996.
- [147] Alexei A Kornyshev and Godehard Sutmann. Nonlocal dielectric saturation in liquid water. *Physical Review Letters*, 79(18):3435, 1997.
- [148] C. L. Kusik and H. P. Meissner. Electrolyte activity coefficients in inorganic processing. *AIChE Symposium Series*, 173(74):14, 1978.
- [149] Celine Largeot, Cristelle Portet, John Chmiola, Pierre-Louis Taberna, Yury Gogotsi, and Patrice Simon. Relation between the ion size and pore size for an electric double-layer capacitor. *Journal of the American Chemical Society*, 130(9):2730–2731, 2008.
- [150] JL Lebowitz and JK Percus. Mean spherical model for lattice gases with extended hard cores and continuum fluids. *Physical Review*, 144(1):251, 1966.
- [151] Alpha A. Lee, Svyatoslav Kondrat, Dominic Vella, and Alain Goriely. Dynamics of Ion Transport in Ionic Liquids. *Physical Review Letters*, 115(10):106101, 2015.

- [152] Alpha A. Lee, Carla S. Perez-Martinez, Alexander M. Smith, and Susan Perkin. Scaling analysis of the screening length in concentrated electrolytes. *Physical Review Letters*, 119:026002, Jul 2017.
- [153] Alpha A. Lee, Dominic Vella, Susan Perkin, and Alain Goriely. Are room-temperature ionic liquids dilute electrolytes? *Journal of Physical Chemistry Letters*, 6(1):159–163, 2015.
- [154] Chang Young Lee, Wonjoon Choi, Jae-Hee Han, and Michael S Strano. Coherence resonance in a single-walled carbon nanotube ion channel. *Science*, 329(5997):1320–1324, 2010.
- [155] D W Lee, D J Im, and I S Kang. Electric double layer at the interface of ionic liquid–dielectric liquid under electric field. *Langmuir*, 29(6):1875–1884, 2013.
- [156] Ming Lee and Kwong-Yu Chan. Non-neutrality in a charged slit pore. *Chemical Physics Letters*, 275(1-2):56–62, 1997.
- [157] Ming Lee, Kwong-Yu Chan, David Nicholson, and Stephen Zara. Deviation from electroneutrality in cylindrical pores. *Chemical Physics Letters*, 307(1-2):89–94, 1999.
- [158] A Lenard. Exact statistical mechanics of a one-dimensional system with coulomb forces. *Journal of Mathematical Physics*, 2(5):682–693, 1961.
- [159] Yan Levin. Electrostatics of ions inside the nanopores and trans-membrane channels. *Europhysics Letters*, 76(1):163, 2006.
- [160] Amir Levy, David Andelman, and Henri Orland. Dielectric constant of ionic solutions: A field-theory approach. *Physical review letters*, 108(22):227801, 2012.
- [161] Amir Levy, David Andelman, and Henri Orland. Dipolar poisson-boltzmann approach to ionic solutions: A mean field and loop expansion analysis. *The Journal of chemical physics*, 139(16):164909, 2013.
- [162] Amir Levy, Martin Z Bazant, and Alexei A Kornyshev. Ionic activity in concentrated electrolytes: solvent structure effect revisited. *arXiv preprint arXiv:1905.12076*, 2019.
- [163] Amir Levy, J. Pedro de Souza, and Martin Z Bazant. Electroneutrality breakdown in nanopores. Submitted, 2019.
- [164] Amir Levy, Michael McEldrew, and Martin Z Bazant. Spin-glass charge ordering in ionic liquids. *Physical Review Materials*, 3(5):055606, 2019.
- [165] David R Lide. *CRC handbook of chemistry and physics*, volume 85. CRC press, 2004.

- [166] EN Lightfoot, EL Cussler, and RL Rettig. Applicability of the stefan-maxwell equations to multicomponent diffusion in liquids. *AIChE Journal*, 8(5):708–710, 1962.
- [167] Jinn-Liang Liu and Bob Eisenberg. Correlated ions in a calcium channel model: a Poisson–Fermi theory. *Journal of Physical Chemistry B*, 117(40):12051–12058, 2013.
- [168] Jinn-Liang Liu and Bob Eisenberg. Numerical methods for a Poisson-Nernst-Planck-Fermi model of biological ion channels. *Physical Review E*, 92(1):12711, 2015.
- [169] Jinn-Liang Liu and Bob Eisenberg. Poisson–Fermi model of single ion activities in aqueous solutions. *Chemical Physics Letters*, 637:1–6, 2015.
- [170] Wai Yin Lo and Kwong-Yu Chan. Non-neutrality in a charged capillary. *Molecular Physics*, 86(4):745–758, 1995.
- [171] Marcelo Lozada-Cassou, Wilmer Olivares, and Belky Sulbarán. Violation of the electroneutrality condition in confined charged fluids. *Physical Review E*, 53(1):522, 1996.
- [172] Marcelo Lozada-Cassou, Wilmer Olivares, Belky Sulbarán, and Yu Jiang. Violation of the electroneutrality condition in confined unsymmetrical electrolytes. *Physica A: Statistical Mechanics and its Applications*, 231(1-3):197–206, 1996.
- [173] Zhi-Xiang Luo, Yun-Zhao Xing, Yan-Chun Ling, Alfred Kleinhammes, and Yue Wu. Electroneutrality breakdown and specific ion effects in nanoconfined aqueous electrolytes observed by nmr. *Nature Communications*, 6:6358, 2015.
- [174] Mainak Majumder, Nitin Chopra, Rodney Andrews, and Bruce J Hinds. Nanoscale hydrodynamics: enhanced flow in carbon nanotubes. *Nature*, 438(7064):44, 2005.
- [175] Manoel Manghi, John Palmeri, Khadija Yazda, François Henn, and Vincent Jourdain. Role of charge regulation and flow slip in the ionic conductance of nanopores: An analytical approach. *Physical Review E*, 98(1):012605, 2018.
- [176] Ali Mani and Martin Z Bazant. Deionization shocks in microstructures. *Physical Review E*, 84(6):061504, 2011.
- [177] Y. Marcus. *Ions In Solution And Their Solvation*. Wiley, New Jersey, 2015.
- [178] Carol S Mariani and Linn W Hobbs. Network properties of crystalline polymorphs of silica. *Journal of non-crystalline solids*, 124(2-3):242–253, 1990.
- [179] Leandro Martínez, Ricardo Andrade, Ernesto G Birgin, and José Mario Martínez. Packmol: a package for building initial configurations for molecular dynamics simulations. *Journal of Computational Chemistry*, 30(13):2157–2164, 2009.

- [180] Hajime Matsumoto, Hikari Sakaebe, and Kuniaki Tatsumi. Preparation of room temperature ionic liquids based on aliphatic onium cations and asymmetric amide anions and their electrochemical properties as a lithium battery electrolyte. *Journal of Power Sources*, 146(1-2):45–50, 2005.
- [181] Michael McEldrew, Zachary Anthony Holmes Goodwin, Alexei A Kornyshev, and Martin Z Bazant. Theory of the double layer in water-in-salt electrolytes. *Journal of Physical Chemistry Letters*, 9(19):5840–5846, 2018.
- [182] Duncan McLaren-Young-Sommerville. An introduction to the geometry of  $n$  dimensions. 1958.
- [183] H P MEISSNER. *Prediction of Activity Coefficients of Strong Electrolytes in Aqueous Systems*, chapter 25, pages 495–511. AMERICAN CHEMICAL SOCIETY, WASHINGTON, D. C., 1980.
- [184] Kurt H Meyer and J-F Sievers. La perméabilité des membranes i. théorie de la perméabilité ionique. *Helvetica Chimica Acta*, 19(1):649–664, 1936.
- [185] Christopher Miller. Ionic hopping defended. *Journal of General Physiology*, 113(6):783–787, 1999.
- [186] Gi Jong Moon, Myung Mo Ahn, and In Seok Kang. Osmotic pressure of ionic liquids in an electric double layer: Prediction based on a continuum model. *Physical Review E*, 92(6):063020, 2015.
- [187] David R Nelson and BI Halperin. Dislocation-mediated melting in two dimensions. *Physical Review B*, 19(5):2457, 1979.
- [188] Roland R Netz and David Andelman. Neutral and charged polymers at interfaces. *Physics reports*, 380(1-2):1–95, 2003.
- [189] Roland R Netz and Henri Orland. Beyond poisson-boltzmann: Fluctuation effects and correlation functions. *The European Physical Journal E*, 1(2-3):203–214, 2000.
- [190] Roland R Netz and Henri Orland. Beyond Poisson-Boltzmann: Fluctuation effects and correlation functions. *European Physical Journal E: Soft Matter*, 1(2-3):203–214, 2000.
- [191] John Newman and Karen E Thomas-Alyea. *Electrochemical systems*. John Wiley & Sons, Inc., Hoboken, New Jersey, 2012.
- [192] Wolfgang Nonner and Bob Eisenberg. Ion permeation and glutamate residues linked by poisson-nernst-planck theory in l-type calcium channels. *Biophysical Journal*, 75(3):1287–1305, 1998.
- [193] P. Novotny and O. Sohnel. Densities of binary aqueous solutions of 306 inorganic substances. *Journal of Chemical & Engineering Data*, 33(1):49–55, 1988.

- [194] L So Ornstein and F Zernike. Integral equation in liquid state theory. In *Proceedings of the royal netherlands academy of arts and science*, volume 17, page 793, 1914.
- [195] R Palm, H Kurig, K Tõnurist, A Jänes, and E Lust. Is the mixture of 1-ethyl-3-methylimidazolium tetrafluoroborate and 1-butyl-3-methylimidazolium tetrafluoroborate applicable as electrolyte in electrical double layer capacitors? *Electrochemistry Communications*, 22:203–206, 2012.
- [196] O Patsahan and A Ciach. Correlation functions in an ionic liquid at coexistence with an ionic crystal: results of the brazovskii-type field theory. *Journal of Physics: Condensed Matter*, 19(23):236203, 2007.
- [197] Jerome K Percus and George J Yevick. Analysis of classical statistical mechanics by means of collective coordinates. *Physical Review*, 110(1):1, 1958.
- [198] Aurélien Perera. Charge ordering and scattering pre-peaks in ionic liquids and alcohols. *Physical Chemistry Chemical Physics*, 19(2):1062–1073, 2017.
- [199] Aurelien Perera and Redha Mazighi. Simple and complex forms of disorder in ionic liquids. *Journal of Molecular Liquids*, 210:243–251, 2015.
- [200] Carla S Perez-Martinez, Alexander M Smith, and Susan Perkin. Underscreening in concentrated electrolytes. *Discussions of the Faraday Society*, 199:239–259, 2017.
- [201] P. B. Peters, R. van Roij, M. Z. Bazant, and P. M. Biesheuvel. Analysis of electrolyte transport through charged nanopores. *Physical Review E*, 93:053108, May 2016.
- [202] Dimiter N Petsev and Gabriel P Lopez. Electrostatic potential and electroosmotic flow in a cylindrical capillary filled with symmetric electrolyte: Analytic solutions in thin double layer approximation. *Journal of Colloid and Interface Science*, 294(2):492–498, 2006.
- [203] Kenneth S Pitzer. Thermodytriarnics of Electrolytes. I. Theoretical Basis and General Equations. *Journal of Physical Chemistry*, 77(2):268–277, 1973.
- [204] Steve Plimpton. Fast parallel algorithms for short-range molecular dynamics. *Journal of Computational Physics*, 117(1):1 – 19, 1995.
- [205] Rudi Podgornik and Boštjan Žekš. Inhomogeneous coulomb fluid. a functional integral approach. *Journal of the Chemical Society, Faraday Transactions 2: Molecular and Chemical Physics*, 84(6):611–631, 1988.
- [206] STP Psaltis and Troy W Farrell. Comparing charge transport predictions for a ternary electrolyte using the maxwell–stefan and nernst–planck equations. *Journal of The Electrochemical Society*, 158(1):A33–A42, 2011.

- [207] Sergio Roberto Rivera and Torben Smith Sørensen. Grand canonical ensemble monte carlo simulations of donnan potentials, nonelectroneutrality, activity coefficients and excess energy in spherical charged or uncharged pores with restricted primitive model electrolytes. *Molecular Simulation*, 13(2):115–160, 1994.
- [208] Robert Anthony Robinson and Robert Harold Stokes. *Electrolyte solutions*. Courier Corporation, 2002.
- [209] Benjamin Rotenberg and Mathieu Salanne. Structural transitions at ionic liquid interfaces. *Journal of Physical Chemistry Letters*, 6(24):4978–4985, 2015.
- [210] Subin Sahu and Michael Zwolak. Ionic selectivity and filtration from fragmented dehydration in multilayer graphene nanopores. *Nanoscale*, 9(32):11424–11428, 2017.
- [211] Christian D. Santangelo. Computing counterion densities at intermediate coupling. *Physical Review E*, 73(4):041512, 2006.
- [212] Varanasi Sasidhar and Eli Ruckenstein. Electrolyte osmosis through capillaries. *Journal of Colloid and Interface Science*, 82(2):439–457, 1981.
- [213] William A Sather and Edwin W McCleskey. Permeation and selectivity in calcium channels. *Annual Review of Physiology*, 65(1):133–159, 2003.
- [214] R Schlögl. Zur theorie der anomalen osmose. *Zeitschrift für Physikalische Chemie*, 3:73–102, 1955.
- [215] Sven Schlumberger. *Shock Electrodialysis for Water Purification and Electrostatic Correlations in Electrolytes*. PhD thesis, Massachusetts Institute of Technology, 2016.
- [216] Markus Schmuck and Martin Z Bazant. Homogenization of the poisson–nernst–planck equations for ion transport in charged porous media. *SIAM Journal on Applied Mathematics*, 75(3):1369–1401, 2015.
- [217] Christoph Schutter, Tamara Husch, Venkatasubramanian Viswanathan, Stefano Passerini, Andrea Balducci, and Martin Korth. Rational design of new electrolyte materials for electrochemical double layer capacitors. *Journal of Power Sources*, 326:541–548, 2016.
- [218] Bruno Scrosati and Jürgen Garche. Lithium batteries: Status, prospects and future. *Journal of Power Sources*, 195(9):2419–2430, 2010.
- [219] Eleonora Secchi, Antoine Niguès, Laetitia Jubin, Alessandro Siria, and Lydéric Bocquet. Scaling behavior for ionic transport and its fluctuations in individual carbon nanotubes. *Physical Review Letters*, 116(15):154501, 2016.

- [220] Shiro Seki, Yo Kobayashi, Hajime Miyashiro, Yasutaka Ohno, Akira Usami, Yuichi Mita, Nobuo Kihira, Masayoshi Watanabe, and Nobuyuki Terada. Lithium secondary batteries using modified-imidazolium room-temperature ionic liquid. *Journal of Physical Chemistry B*, 110(21):10228–10230, 2006.
- [221] Patrice Simon and Yury Gogotsi. Materials for electrochemical capacitors. *Nature Materials*, 7(11):845, 2008.
- [222] Jean-Pierre Simonin, Olivier Bernard, and L Blum. Real ionic solutions in the mean spherical approximation. 3. Osmotic and activity coefficients for associating electrolytes in the primitive model. *Journal of Physical Chemistry B*, 102(97):4411–4417, 1998.
- [223] Alessandro Siria, Philippe Poncharal, Anne-Laure Biance, Rémy Fulcrand, Xavier Blase, Stephen T Purcell, and Lydéric Bocquet. Giant osmotic energy conversion measured in a single transmembrane boron nitride nanotube. *Nature*, 494(7438):455, 2013.
- [224] Sloth, Peter and Torben S. Soerensen. Model of Electrolyte Solutions. *Journal of Physical Chemistry*, 94(c):2116–2123, 1990.
- [225] Alexander M. Smith, Alpha A. Lee, and Susan Perkin. Switching the structural force in ionic liquid-solvent mixtures by varying composition. *Physical Review Letters*, 118(9):096002, 2017.
- [226] Ain A Sonin. Osmosis and ion transport in charged porous membranes: a macroscopic, mechanistic model. In *Charged Gels and Membranes*, pages 255–265. Springer, 1976.
- [227] AK Soper. Orientational correlation function for molecular liquids: the case of liquid water. *Journal of Chemical Physics*, 101(8):6888–6901, 1994.
- [228] Torben Smith Sørensen and Peter Sloth. Ion and potential distributions in charged and non-charged primitive spherical pores in equilibrium with primitive electrolyte solution calculated by grand canonical ensemble monte carlo simulation. comparison with generalized debye–hückel and donnan theory. *Journal of the Chemical Society, Faraday Transactions*, 88(4):571–589, 1992.
- [229] A. J. Staverman. Non-equilibrium thermodynamics of membrane processes. *Journal of the Chemical Society, Faraday Transactions*, 48:176–185, 1952.
- [230] Paul J Steinhardt, David R Nelson, and Marco Ronchetti. Icosahedral bond orientational order in supercooled liquids. *Physical Review Letters*, 47(18):1297, 1981.
- [231] Brian D. Storey and Martin Z. Bazant. Effects of electrostatic correlations on electrokinetic phenomena. *Physical Review E*, 86(5):1–11, 2012.

- [232] Robert F. Stout and Aditya S. Khair. A continuum approach to predicting electrophoretic mobility reversals. *Journal of Fluid Mechanics*, 752:R1–R12, 2014.
- [233] RL Stratonovich. On a method of calculating quantum distribution functions. In *Soviet Physics Doklady*, volume 2, page 416, 1957.
- [234] Liumin Suo, Oleg Borodin, Tao Gao, Marco Olguin, Janet Ho, Xiulin Fan, Chao Luo, Chunsheng Wang, and Kang Xu. "Water-in-salt" electrolyte enables high-voltage aqueous lithium-ion chemistries. *Science*, 350(6263):938–943, 2015.
- [235] Liumin Suo, Yong-sheng Hu, Hong Li, Michel Armand, and Liquan Chen. high-energy rechargeable metallic lithium batteries. *Nature Communications*, 4:1–9, 2013.
- [236] M Tedesco, H. V. M. Hamelers, and P. M. Biesheuvel. Nernst-planck transport theory for (reverse) electro dialysis: I. effect of co-ion transport through the membranes. *Journal of Membrane Science*, 510:370–381, 2016.
- [237] Torsten Teorell. Transport processes in ionic membranes. *Progress in Biophysics and Molecular Biology*, 3:305, 1953.
- [238] Alessandro Triolo, Olga Russina, Hans-Jurgen Bleif, and Emanuela Di Cola. Nanoscale Segregation in Room Temperature Ionic Liquids. *Journal of Physical Chemistry B*, 118(11):4641–4644, 2007.
- [239] Ramya H Tunuguntla, Robert Y Henley, Yun-Chiao Yao, Tuan Anh Pham, Meni Wanunu, and Aleksandr Noy. Enhanced water permeability and tunable ion selectivity in subnanometer carbon nanotube porins. *Science*, 357(6353):792–796, 2017.
- [240] Frank HJ van der Heyden, Derek Stein, and Cees Dekker. Streaming currents in a single nanofluidic channel. *Physical review letters*, 95(11):116104, 2005.
- [241] Mark W Verbrugge and Robert F Hill. Ion and solvent transport in ion-exchange membranes i. a macrohomogeneous mathematical model. *Journal of the Electrochemical Society*, 137(3):886–893, 1990.
- [242] Evert Johannes Willem Verwey and Jan Theodoor Gerard Overbeek. *Theory of the stability of lyophobic colloids*. Elsevier, New York, 1948.
- [243] Juan J Vilatela and Rebeca Marcilla. Tough electrodes: carbon nanotube fibers as the ultimate current collectors/active material for energy management devices. *Chemistry of Materials*, 27(20):6901–6917, 2015.
- [244] Eduardo Waisman and Joel L Lebowitz. Mean spherical model integral equation for charged hard spheres i. method of solution. *The Journal of Chemical Physics*, 56(6):3086–3093, 1972.

- [245] Xin Wang and Gao-Rong Han. Fabrication and characterization of anodic aluminum oxide template. *Microelectronic Engineering*, 66(1-4):166–170, 2003.
- [246] Zhen-Gang Wang. Fluctuation in electrolyte solutions: The self energy. *Physical Review E*, 81(2):021501, 2010.
- [247] Carsten Werner, Ralf Zimmermann, and Thomas Kratzmüller. Streaming potential and streaming current measurements at planar solid/liquid interfaces for simultaneous determination of zeta potential and surface conductivity. *Colloids and Surfaces A: Physicochemical and Engineering Aspects*, 192(1-3):205–213, 2001.
- [248] Max Whitby, Laurent Cagnon, Maya Thanou, and Nick Quirke. Enhanced fluid flow through nanoscale carbon pipes. *Nano Letters*, 8(9):2632–2637, 2008.
- [249] Hugo Wioland, Francis G Woodhouse, Jörn Dunkel, and Raymond E Goldstein. Ferromagnetic and antiferromagnetic order in bacterial vortex lattices. *Nature Physics*, 12(4):341, 2016.
- [250] Yu Yan, Qian Sheng, Ceming Wang, Jianming Xue, and Hsueh-Chia Chang. Energy conversion efficiency of nanofluidic batteries: hydrodynamic slip and access resistance. *Journal of Physical Chemistry C*, 117(16):8050–8061, 2013.
- [251] Jun Yang, Fuzhi Lu, Larry W Kostiuk, and Daniel Y Kwok. Electrokinetic microchannel battery by means of electrokinetic and microfluidic phenomena. *Journal of Micromechanics and Microengineering*, 13(6):963, 2003.
- [252] Shuhuai Yao and Juan G Santiago. Porous glass electroosmotic pumps: theory. *Journal of Colloid and Interface Science*, 268(1):133–142, 2003.
- [253] Andriy Yaroshchuk. What makes a nano-channel? a limiting-current criterion. *Microfluid Nanofluidics*, 12(1-4):615–624, 2012.
- [254] Arik Yochelis. Spatial structure of electrical diffuse layers in highly concentrated electrolytes: A modified poisson–nernst–planck approach. *Journal of Physical Chemistry C*, 118(11):5716, 2014.
- [255] Xianglong Yuan and AN Cormack. Efficient algorithm for primitive ring statistics in topological networks. *Computational Materials Science*, 24(3):343–360, 2002.
- [256] J Zhang, A Kamenev, and B. I. Shklovskii. Conductance of ion channels and nanopores with charged walls: a toy model. *Physical Review Letters*, 95(14):148101, 2005.
- [257] J Zhang, A Kamenev, and B. I. Shklovskii. Ion exchange phase transitions in water-filled channels with charged walls. *Physical Review E*, 73(5):051205, 2006.

- [258] André Zuber, Lúcio Cardozo-Filho, Vladimir Ferreira Cabral, Ricardo Figueiredo Checoni, and Marcelo Castier. An empirical equation for the dielectric constant in aqueous and nonaqueous electrolyte mixtures. *Fluid Phase Equilibria*, 376:116–123, 2014.
- [259] Bruno J Zwolinski, Henry Eyring, and Cecil E Reese. Diffusion and membrane permeability. *Journal of Physical Chemistry*, 53(9):1426–1453, 1949.